MILD WEAR IN DRY AND LUBRICATED SLIDING SYSTEMS

By

STUART GREGORY HODGSON

A thesis submitted for the degree of Doctor of Philosophy

UNIVERSITY OF ASTON

March 1988

THE UNIVERSITY OF ASTON

MILD WEAR IN DRY AND LUBRICATED SLIDING SYSTEMS

BY

STUART GREGORY HODGSON

A thesis submitted for the degree of:
DOCTOR OF PHILOSOPHY - 1988

SUMMARY

A vertical pin on horizontal disc machine has been used to conduct a series of experiments in air under dry and lubricating sliding conditions. For dry sliding low load and speed combinations were chosen to correspond to the mild wear region below the Welsh T_1 transition. Lubricated tests were conducted under flooded conditions using Esso Technical White Oil alone and with a 0.1% stearic acid additive, for load and speed ranges that produced substantial amounts of asperity contact and thus a boundary lubricated regime of wear. The test material in all cases was AISI 52100 steel, for unlubricated sliding subjected to loads from 5 to 50 N and a range of speeds from 10^{-3} to 1.0 ms^{-1}, and for lubricated sliding loads of 50 to 123 N and for speeds of 10^{-2} to 1.0 ms^{-1}.

Unlubricated wear debris was found to be a mixture of α-Fe_2O_3 and α-Fe. Unlubricated wear was found to occur via a thin film logarithmic oxide growth followed by agglomeration into thicker oxide plateaux 2 to 10 µm in thickness. Lubricated wear occurred via a thick film diffusion controlled oxide growth producing homogeneous oxide plateaux 0.1 to 0.2 µm in thickness. X-ray photoelectron spectroscopy identified the presence of a surface film on pins worn in White Oil with stearic acid, which is thought to be iron stearate.

A model has been developed for unlubricated wear based upon the postulated growth of thin film oxides by a logarithmic rate law. The importance of sliding geometry and environment to the dominant wear mechanism has been illustrated.

ACKNOWLEDGEMENTS

I should like to especially thank my supervisor, mentor and friend Dr. J. L. Sullivan, for his patience, help and direction throughout this project. I should also like to thank Dr. C. Bovington and Dr. M. Sexton and Exxon Chemicals for their advice and financial support during the work. Thanks also to Mr. H. Arrowsmith for his mechanical genius and particular thanks to Mr. A. Abbot for his expertise and professionalism in the face of adversity.

Finally, I would like to thank my family; my mother, sister and especially my brother, Robert, for helping me to my present position, and lastly thanks to my fiancee and future wife for her support, encouragement and advice over the last two years.

CONTENTS

LIST OF FIGURES

Page

LIST OF TABLES

CHAPTER ONE

INTRODUCTION

1.1 Purpose of the Investigation

Wear is the damage, or deterioration due to rubbing of materials leading to the removal of part or all of the rubbing surface. The prevention or reduction of this process has become of great importance in recent decades with the increasing use of mechanised labour saving devices. Spurred by the economic advantages of reducing wear, much work has been done into surface coatings or implantation, however, in the normal course of wear it is often a reaction product of the surface and environment which causes the most dramatic reduction of wear, namely oxides.

Fink[1] in 1930 was the first to identify oxidation as a mechanism of wear reduction, followed by Rosenberg and Jordan[2] in 1935 who found that steel exhibited a wear rate in hydrogen which was 50 times that in air. Since this early work extensive study has been directed to determine the mechanisms of oxide formation, growth and removal.

Early on in the study of wear, Lancaster[3] and Welsh[4,5] clearly demonstrated that under dry sliding conditions large changes in wear rate could result from small changes in applied load and/or sliding speed. Welsh produced a series of curves, the general pattern of which now bears his name, from which three transitions T_1, T_2 and T_3, were defined. These transitions were originally defined in terms of applied load at a fixed sliding speed, but subsequent work has shown that sliding speed at a fixed load is an equally valid definition.

Since this early work, extensive study has been conducted into wear above the T_2 transition and into the transition phenomena itself. There is, however, little published work specifically aimed at the region of oxidational wear below the Welsh T_1 transition, where loads and/or speeds are low and frictional heating negligible. This is to be regretted since, apart from the need to characterise dry wear in this region, such a study could lead to a better understanding of important problems associated with oxide film formation under lubricated conditions, particularly in boundary lubrication[6].

Prutten et al.[7] showed that the corrosion of metals by solutions or organic acids in hydrocarbons took place via an oxide film. Tingle[8] went on to show that a 1% solution of lauric acid was no more effective in lubricating a freshly cut metal surface in paraffin than was the paraffin

itself. However if an oxide film had been generated beforehand on exposure to oxygen and water vapour, the additive acted as an effective boundary lubricant.

It was to attempt to elucidate the mechanisms of oxide growth below the T_1 transition along with those during boundary lubrication that this investigation was initiated. It was thought that a study of oxide formation under low load and speed combinations in air, and similar studies performed under flooded lubricated conditions, for the same sliding geometry, would afford a valuable insight to the mechanism of wear reduction, and provide useful information on the overlooked region of wear below the T_1 transition.

1.2 Characterisation of the Wear of Metals

The classification of the wear of metals has been subject to several alternate interpretations in the past with the terminology of one being interchangeable with another, leading to confusing or even contradictory statements. In view of this a clear definition of the several distinct forms of wear is a necessary prerequisite to any study.

Archard and Hirst[9] produced the most basic classification of wear, that is two components mild and severe, while Burwell and Strang[10] preferred seven distinct classes: adhesive, corrosive, surface fatigue or pitting, abrasive, fretting, cavitation and erosive wear. The Archard and Hirst classification is the easiest to apply to any wear situation, since it is entirely phenomenological with severe wear being characterised by low contact resistance and large, ~ 10^{-2} mm diameter, metallic wear particles, and mild wear being characterised by small, ~ 10^{-4} mm diameter, oxidised debris. The Burwell and Strang usage is based upon the mechanism of removal of wear particles which is a more definitive classification, but one which requires more specific explanation of each mode of wear. Burwell[11] and Quinn[12] provide good explanations of this wear terminology, the major observations of which are listed below.

1.2.1 Adhesive Wear

Adhesive wear occurs when surfaces slide against each other, and the pressure between the contacting asperities is high enough to cause local plastic deformation and adhesion[13]. Adhesive forces between surfaces arise from atomic attraction and result in local cold welding of

neighbouring asperities. Adhesion is favoured by clean surfaces and non-oxidising conditions[14]. Adhesion occurs between a few junctions which increase in size as motion continues. Eventually thejunctions rupture at their weakest point, usually resulting in metal transfer from one surface to another[15]. These transferred particles may be transferred back to the original surface, or else come off the surface to form loose wear particles. Very severe adhesive wear resulting in gross surface damage is known as gouging.

Adhesive wear decreases if the asperity is harder, because the contact area is lower, increases if the asperity is chemically clean due to bonding and welding being more likely and increases if the wear couple is mutually soluble.

1.2.2 Corrosive Wear

Corrosive wear is a form of chemical wear which results from the interaction of the environment with the sliding surfaces, producing some corrosion product, followed by the removal of this product via some other mechanism due to the sliding, fatigue for example. If the environment is hostile, liquid sodium say, then one has a form of wear which proceeds rapidly and is truly corrosive.

If however, the environment is the normal atmosphere, or a lubricant exposed to normal atmosphere, it is possible to obtain a mild form of corrosive wear called oxidational wear[16].

In oxidational wear the reaction products and thus wear debris are oxides. For a wide range of material combinations and environments the oxide films present on the surface are sufficient to prevent intermetallic contact and hence reduce friction and inhibit further wear. In these circumstances the rate of removal of oxide achieves an equilibrium with the rate of regeneration of the film by oxidation at the surface. Thus, oxidational wear will occur when the oxidation rate at the surface is sufficient to maintain a protective oxide film between the interacting asperities.

1.2.3 Abrasive Wear

Abrasive wear may be subdivided into two distinct categories. The first is two body abrasion where a rough hard surface slides against a softer surface[17], and the second is a three body abrasion where loose hard particles are responsible for the surface damage[18]. During abrasive wear smooth surfaces become roughened with fairly regular grooves. This type of damage is usually described

as scratching, scoring or gauging depending on the degree of severity. A reduction in third body particle size would reduce three body abrasion, since there is a critical size below which rolling becomes more likely than abrasion[18], and Burwell[11] suggested that sharp particles contribute more to abrasive wear than do rounded ones.

1.2.4 Surface Fatigue Wear

This form of wear is observed during repeated sliding or rolling over a track. The repeated loading and unloading cycles to which the materials are exposed may induce the formation of surface and subsurface cracks, which eventually will result in a break-up of the surface with the formation of large fragments, ~ 100 μm diameter, leaving large pits in the surface[19]. Further to this, Archard and Hirst[9] have suggested that material initially transferred by adhesion may finally be removed by fatigue processes. Also large oxide plateaux are also likely to be broken up and removed by a fatigue process.

1.2.5 Fretting Wear

Fretting can be considered as a form of wear which occurs when wear mechanisms act together under conditions of small oscillatory displacement[20]. This is common since most machinery is subject to vibration both in transit and during operation. Because of the oscillating small amplitude motion the surfaces are never brought out of contact and therefore there is little opportunity for the wear debris to escape. Most commonly, fretting is combined with corrosion in which case the wear is known as fretting corrosion[21]. In air the corrosion product is oxide.

1.2.6 Transfer Wear

Transfer involves the removal of material from one surface and redeposition of that material on another, or from one surface, to another position on that surface. An attempt to follow the general wear process was made in 1951 by Rabinowicz and Tabor[15] using radioactive tracers. They showed that transfer consisted of discrete particles and that the volume of the transferred material per unit distance of sliding was approximately proportional to the

load. Rabinowicz[22] went on to estimate the size distribution of transferred particles and found them to be comparable to the actual areas from which they were formed, ~ 10^{-5} m diameter, as deduced by Holm[23], and Bowden and Tabor[13] using contact resistance measurements.

Kerridge[24] has shown that information about detailed mechanisms in wear can be obtained by combining tracer techniques with conventional methods of wear measurement. He found that with a soft-steel pin rubbing unlubricated on a hard steel ring, the metallic transfer from a soft pin to a hard ring could be the first stage in the wear process. With steels, however, it was suggested that subsequent stages of the wear mechanism were the slow oxidation of the transferred layer and its removal as loose oxidised debris. The material worn away was then replaced by new transferred material. The transferred material was found to be in a hardened condition. Further tests in an inert atmosphere showed a decrease in wear rate so Kerridge concluded that the oxidation and removal of the transferred material was the rate-determining process. This work reveals the important fact that wear particles may be produced directly when localised regions of the surface come into contact.

Kerridge and Lancaster[25] developed the radiographic method of Kerridge[24] to study the severe wear of a 60/40 brass pin rubbing on a hardened steel ring, a material combination which gives very reproductive wear rates and a wear rate proportional to the load. It was found that

during the initial stages of sliding, no wear particles were produced, but a transferred film of brass builds up on the steel surface. As the film thickness approached a steady value, wear particles started to appear until an equilibrium condition was reached. When the brass pin was replaced by an otherwise similar irradiated pin and sliding continued it was found that wear continued as before but initially these wear particles were not radioactive. Thus they could not have originated from the pin, but must have been detached from the inactive transfer film on the steel ring. As sliding continued with an active pin, the inactive film was gradually replaced by active brass and the wear debris therefore eventually became active. By a similar technique it was established that the material in the transferred film remained there until it was removed as debris. In other words, there was no back transfer from the film to the pin. Further experiments showed that the wear was a two stage process starting from the transfer of the material from the pin to the ring followed by the removal of transferred material as wear particles. The transfer from the pin occurred as discrete particles, and the material that was removed from the ring was aggregated from many such particles. Archard and Hirst[26] in a study of mild wear, using hardened steel on hardened steel, showed that back transfer was possible.

1.3 The Severity of Wear and Severe/Mild Wear Transitions

Following the initial work conducted by Fink[1] in identifying oxidation as a factor leading to reduced wear, Mailander and Dies[27] and Siebel and Kobitzch[28] attempted to explain the behaviour of steels for a number of sliding conditions with respect to changes in load and speed, and again identified oxidation and oxide formation as a factor in wear reduction. Dies[29] also recognised the importance of dissolved oxygen in fluids. The relationship between load and wear rate was investigated by Burwell and Strang[10] who found that in general the wear rate was proportional to the load and independent of the apparent area of contact. This was supported by Holm[23] who showed that when wear rate is expressed as volume removed per unit sliding distance, the severity of the wear rate might be assessed by comparison with the real area of contact. This work then led Archard[30] in 1961 to define his wear law as:

$$w = KA \qquad (1.1)$$

where w is the wear rate in m^3/m and A is the real area of contact. K, the Archard wear factor, is dimensionless and represents the probability of producing a wear particle at

each asperity encounter. It is this variation in K, for a given real area of contact, which determines the mode and severity of the wear rate.

There exists, however, periodic changes in wear mode, dependent upon speed and load, which also influences the severity of the wear rate. Hirst and Lancaster[31] have described some of the factors influencing the magnitudes of the transition loads and in agreement with Moore and Tegart[32] showed that wearing-in is a process which alters the surface layers such that with continued rubbing the wear rate is dependent upon the new properties of these surface layers.

When observed these generated layers have been referred to as "hard", "white" or "non-etching" and have been reported to form in most ferrous metals under a wide range of conditions; they are thought to be a martensitic phase of the metal produced with an extremely fine grain size by the rapidity of heating and cooling. In their review on white layers, Eyre and Baxter[33] collate much of the literature in this area, and conclude that the properties of white layers, their extreme hardness and resistance to tempering, are due to second phase particles pinning an extremely fine crystallite structure. This means that structurally white layers may appear in one of several different forms depending on material and operating conditions, but that there remains a basic similarity in methods of production and that differences are superficial.

The influence of temperature on the severe wear of 60/40 brass rubbing on hardened steel has been investigated by Lancaster[34]. Low sliding speed was used to minimise frictional heating and temperatures were raised by external heating. Two regimes of wear were found. At light loads protective surface films were generated during sliding and there was little intermetallic contact, at higher loads the wear rate increased by several orders of magnitude and there was extensive intermetallic contact. At the transition load between these two regimes it was suggested that there was an equilibrium between the rate of formation of a protective surface film and its rate of destruction. The magnitude of the transition load was found to increase with temperature, that is an increase in temperature of the sliding metals facilitates the formation of a protective film.

The previously mentioned Welsh curves probably represent the most definitive method of separating these modes of wear for steels and the terms T_1 , T_2 and T_3 representing transition points are common terminology. Below T_1 , mild wear occurs by the removal of oxide debris from an oxidised surface supported on a work-hardened substrate. T_1 is a transition to severe wear initiated by the protective surface oxide produced at lower loads. Plastic deformation of the substrate occurs, caused by higher bulk temperature, and the wear rate increases

dramatically with the production of metallic debris. Between T_1 and T_2 severe wear occurs. At the T_2 transition the surface temperature is high enough for phase hardening to produce a hard "white layer" structure which prevents deformation and helps to establish an oxidised surface once more. The wear rate is reduced considerably but is not as low as the wear rate below the T_1 transition. At loads above the T_2 transition a third transition T_3 has been reported by Welsh[35]. Above T_3 permanent phase hardening occurs so that oxide formation is no longer necessary for the mild wear behaviour to be sustained. These regions of the Welsh curve are shown in Figure 1.1.

During running-in the hardness of the metal surfaces increases until a critical hardness, dependent on the material composition, is exceeded. This hardness, usually in the range 340 to 425 VPN[35], indicates that the substrate is now capable of supporting an oxide, such that fracture will occur within the oxide. Since mild wear is dependent on formation of an oxide layer, altering the bulk composition to reduce oxidation has been found to prolong running-in. It has been found[9,36] that a 3% chromium steel has twice the running-in time of a 1% chromium steel under the same test conditions. Independent oxidation rates have shown at a 3% chromium steel oxidises at a significantly slower rate.

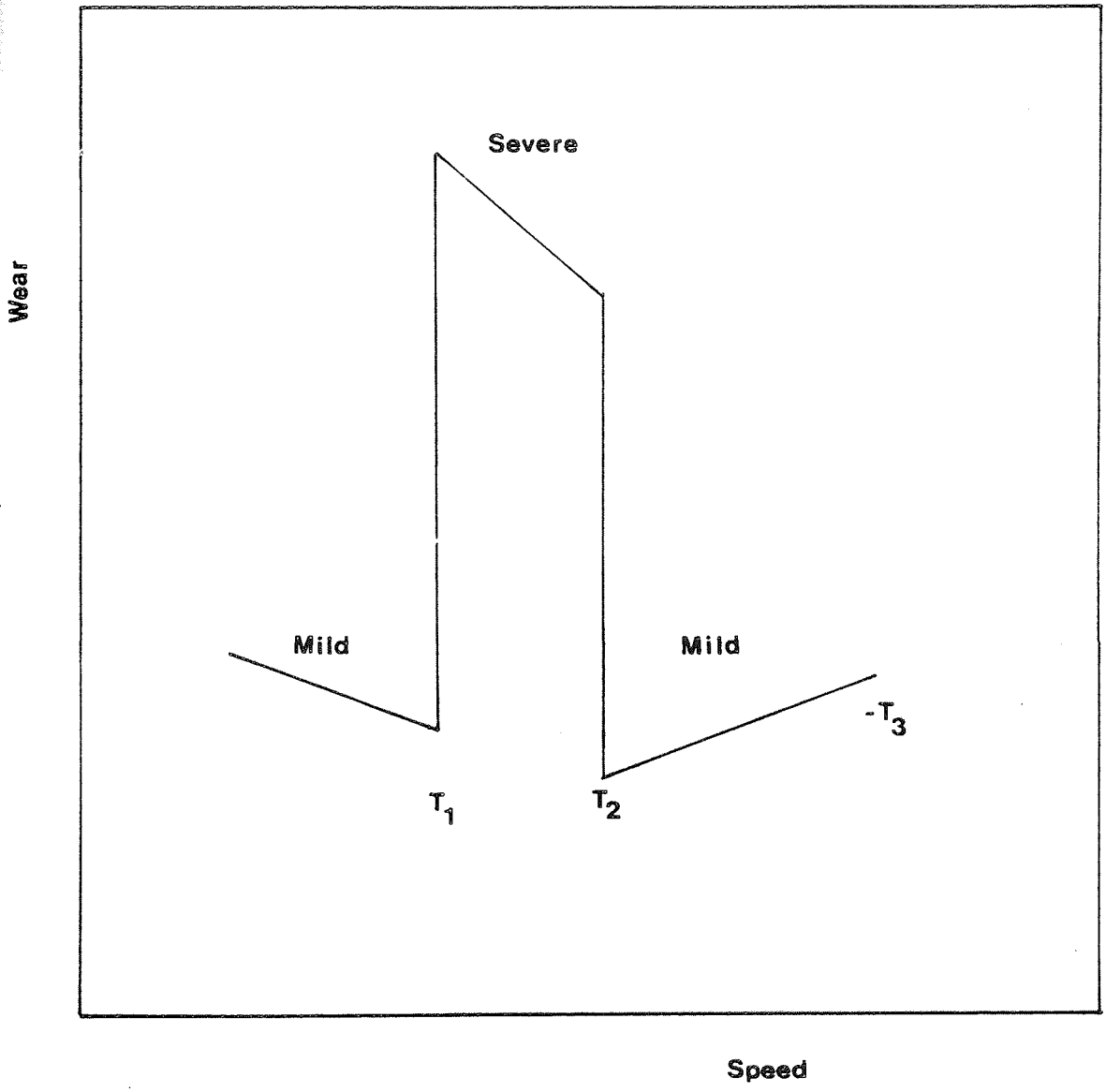

Figure 1.1

Classical Welsh curve showing wear rate against speed for constant load. The three major wear regions are shown along with the Welsh T_1, T_2 and T_3 transitions

A review of earlier studies on the sliding wear mechanisms of metals has been made by Childs[37]. He concluded that, in general, the influence of sliding speed and load on the wear mechanisms observed during the dry wear of soft steels is as follows: at low loads and speeds surface work hardening and smoothing can occur under a protective oxide film, wear occurring either by removal of the film or by metal fatigue. At slightly higher loads and speeds oxide protection may break down leading to severe metallic wear and transfer, but at higher speeds still, enhanced oxidation caused by frictional heating coupled with the possibility of surface transformation hardening of steels can restore oxide protectiveness. In hotter conditions still, gross surface softening can cause a reversion to severe wear but in even hotter conditions a further regime of oxide domination exists. This effectively summarises the three major modes distinguished in the Welsh curve; below T_1 , between T_1 and T_2 , and above T_2 . To understand further the mechanisms of wear the highly important factor of temperature must be examined.

1.4 Temperature in Unlubricated Wear

The growth of oxides under unlubricated sliding conditions occurs at some oxidational temperature, T_0 , generated by sliding friction. There is still controversy, however, over whether it is the general surface temperature or "hot-spot" or contact temperature which govern oxide growth.

The major obstruction to the resolution of this controversy is the determination of those temperatures under practical experimental conditions. Attempts have been made to measure those temperatures directly using dynamic thermocouple techniques, by measuring the thermoelectric voltage produced at the sliding interface of a pair of dissimilar metals[38]. Other direct measurements using infra-red photographic methods have been employed by Winer et al[39,40]. All these direct methods are disadvantageous either by limiting sliding pairs to dissimilar metals or demanding that one partner be transparent.

Other methods such as imbedded thermocouples[41,42], and the use of wearing pins contained within a calorimeter[43,44,51,52], have been used to monitor heat flow during wear. These forms of measurement suffer due to their indirect nature, and reliance upon extensive

theoretical heat flow analysis to deduce surface and contact temperatures.

Blok[45,46] in 1937 was probably one of the first researchers to realise the importance of flash temperatures in the study of wear. He worked with lubricants under an extreme pressure regime and performed a rather complicated mathematical treatment to support his work. The flash temperature seen in Blok's work is probably very similar, although not identical, to the hot-spot temperatures postulated under dry-wear conditions. This work initiated the other path open to investigators when attempting to determine oxidational temperatures: that of the theoretical, empirical analysis.

A theoretical study similar to Blok's was performed by Jaeger[47] who provided mathematical solutions to equations describing moving uniform plane sources of heat, thus deducing hot-spot temperatures. Holm[48] and Bowden and Tabor[13] have each performed similar, although simpler, analyses of these temperatures. Jaeger's findings have been developed without their mathematical complexity by Archard[49] who considered both elastic and plastic deformation in his surface modelling of contact temperatures, and showed that most oxidation must have taken place at or near the contact temperature.

The work of Archard[49], Jaeger[47] and Holm[48] has been drawn together, in an extension of an approach by Grosberg and Molgaard[50], to form a complex heat flow analysis which yields the values of several surface parameters, including contact temperatures, achieved during wear[51,52]. The model inherent in the above heat flow analysis will be discussed in section 1.5.

The crucial observation accompanying these investigations is that oxides which could not be generated at general surface temperatures are often present in collected debris[53] indicating that oxidation occurs at some higher temperature. The view that contact rather than surface temperature is the most important factor determining oxide growth is supported by Tao[54] and Molgaard and Srivastava[55], although in other published work Molgaard and Srivastava[56] suggested that the oxidational temperature may be somewhat lower than the contact temperature even for oxidation nominally at the contact region. This latter suggestion is possibly closer to the truth since during contact there is no free access of oxygen to the surface.

Stott, Glascott and Wood[57] produced a quantitative expression for the relative amounts of oxide generated in and out of contact and concluded that either mode could predominate. They stated that if excess contact temperature rises are significant, particularly where the

number of load bearing contacts is small, the majority of the oxide is formed at the contact temperature. Conversely if there are a large number of contacts, particularly under low speed, high temperature conditions and the excess contact temperature rise is small, then out of contact oxidation predominates[58,59].

Sullivan and Athwal[44] and Sullivan and Granville[60] have also shown that out of contact oxidation, especially at high temperatures, can become the dominant mechanism.

1.5 Quantitative Theories, and Mechanisms of Unlubricated Oxide Formation

1.5.1. Quantitative Theories

One of the earliest works which describes wear mechanisms quantitatively is that of Yoshimoto and Tsukizoe[61] who assumed a model which represented profile curves of two contacting metal surfaces and from this theoretically deduced the number and size of individual contact areas. Assuming that during an encounter the whole of the oxide, developed in a previous encounter, is removed, they expressed wear rate as:

$$w = \frac{\pi}{4}\frac{n}{\tau}\frac{1}{V}\left\{\left(\frac{3}{\pi P_m}\right)^{1/2} LW^{1/2} - \frac{3}{\pi P_m} W\right\} \qquad (1.2)$$

where w is the wear rate, n and τ are logarithmic oxidational constants, W is the load and L is a parameter relating to the length of one edge of the apparent contact area and P_m is the flow pressure of the surface. This expression is for Fe_2O_3 film wear, but they also deduced expressions for Fe_3O_4 film wear, surface contact resistance and mechanical wear. This equation is similar in form to that deduced by Uhlig[62] who described a contact model between a metal and a flat surface, where this equation describes two metal surfaces in contact. The main conclusions of Yoshimoto and Tsukizoe were (i) the wear rate is approximately proportional to the square root of the load, $W^{1/2}$, (ii) the wear rate is approximately proportional to the length of one edge of the apparent contact area and (iii) the wear rate is inversely proportional to the velocity, V. There was, however, no experimental validification of the expression, although the approach outlined by these authors is a useful guide to developing a quantitative description of an oxidation-scrape-oxidation mechanism[57].

Earles and Powell[63] adopted the model of Yoshimoto and Tsukizoe to explain a series of experiments conducted on EN1A steel. They observed initially comparatively large

friction coefficients, 0.4 to 0.8, during severe wear-in which lasted about 2 minutes where mild wear ensued and friction coefficients dropped to 0.1 to 0.5 with the formation of a near continuous oxide film. At speeds above 25 ms^{-1} they found a critical load (dependent on speed) above which periodic removals of the surface film occurred producing metallic wear and high friction. The subsequent increase in oxidation was seen then to allow conditions of mild wear to be re-established within a few seconds. Friction coefficient and wear rate were found to vary with the square root of the load, and instability in the self-generated oxide film was proposed to lead to periodic increases in these parameters.

Earles and Powell[64] later interpreted their data using Yoshimoto and Tsukizoe's equation for Fe_3O_4 film wear, erroneously adopting it for their high speed experimental results. Surprisingly the variation predicting the wear rate proportionality with square root of load was substantiated.

Tenwick and Earles[65] later advanced a modified theory based on more fundamental physical, rather than statistical, properties and considered a mechanism based on parabolic oxidation to give the expression:

$$N/_W = \frac{1}{KP_o} \frac{Ph_c}{\exp\ (-Q/_{R\theta})} \qquad (1.3)$$

where N is the applied load, w the wear rate, P the asperity strength, h_c the critical oxide film thickness, KP_o an Arrhenius constant for parabolic oxidation, Q the activation energy, R the universal gas constant and θ the oxidational temperature. This equation is much more realistic in predicting the variation of wear rate with load and incorporating temperature as an active parameter. Temperature has been further investigated by Earles and Powell[66] and Quinn[67] who then went on to develop a model for oxidational wear, again based upon parabolic oxidation.

Quinn[68] proposed two possible mechanisms. The first that the bulk of oxidation occurs at the instant that virgin metal is exposed and that further metal contact causes shearing at the metal-oxide boundary. The second is that oxidation occurs at each contact until the oxide grows to a critical thickness when it becomes detached to form a wear particle. Quinn modified the Archard wear law, equation (1.1), but re-interpreted K, by assuming that 1/K encounters are necessary to produce an oxide of critical thickness at the real areas of contact and obtained the expression:

$$w = \left\{ \frac{d\, A_p \exp\left(-Q_{p/RT_o}\right)}{\xi^2\, P_o^{\,2}\, f_o^{\,2}\, U} \right\} A \qquad (1.4)$$

where w is the wear rate, d the distance of sliding contact at an asperity (= 2a) where a is the asperity radius, A_p is the Arrhenius constant for parabolic oxidation, Q_p is the oxidational activation energy for parabolic oxidation, T_o the oxidational temperature, ξ the thickness of oxide film at the real areas of contact, P_o the average density of oxides formed at the real areas of contact, f_o the mass fraction of the oxide film which is oxygen and U the sliding speed. Where A, the real area of contact, is defined as $A = W/P_m$ where W is the applied load and P_m the material hardness, or alternatively as $A = N\pi a^2$ where N is the number of asperity contacts. This model assumes that there are N circular contacts at any one time, of mean radius a, and that there is an oxide film of thickness ξ at the time each plateaux breaks off to form a wear particle.

The oxidational temperature was deduced from an extension of an approach developed by Grosberg and Molgaard[50] and the use of an iterative computer search technique which provided suitable values of N, a, ξ and T_c, the contact temperature, by comparing experimental and theoretical values of the division of heat between the wearing pair[44,69].

An important point was made here by Sullivan et al[69] during this work by pointing out that oxidational growth constants will differ depending on the predominant oxide

types, and that growth constants measured from static oxidation experiments are not appropriate to tribological situations.

1.5.2. Further Mechanisms of Oxide Film Formation

The major mechanisms concerning unlubricated wear have already been presented along with their corresponding quantitative expressions, in the previous section. One further important mechanism, with no quantitative analysis, needs to be mentioned for completeness. This has been reported by Stott et al[70,71] in the form of oxide glazes formed on rubbing surfaces under reciprocating sliding conditions. They proposed that oxide fragments are formed by an oxidation-scrape-reoxidation mechanism, where oxide growth both during the contact and out of contact is completely removed during the next or some subsequent asperity interaction. The oxide debris may then either be swept away, or cause abrasive removal of the metal surface in which case severe wear will ensue, or become fragmented, compacted and undergo plastic deformation to form a protective oxide glaze in which case mild oxidational wear is the result.

Further experiments in this series[72,73] showed that the rate of oxide production could not account for the rate of development of the oxide glaze film. They therefore proposed[74] that under the conditions of their experiments, metal debris is produced, broken up and reduced in size until the surface to volume ratio is such that spontaneous oxidation occurs. The running-in time relates simply to the time required to reduce the metallic particles to the required critical size. The reciprocating sliding geometry in these experiments is conducive to debris entrapment which is a necessary prerequisite for this mechanism of oxide layer production.

1.6 Characterisation of Lubrication Regimes

In much the same way as in unlubricated systems, lubricated terminology describes distinct forms of surface interaction or non-interaction, whichever the case. It is again useful to clarify the nomenclature relevant to each system. Four classes are used to describe the possible surface-lubricant-surface combinations. These are hydrodynamic, elastohydrodynamic, mixed and boundary lubrication. Each of these is described below, and shown diagrammatically in a Stribeck variation in figure 1.2.

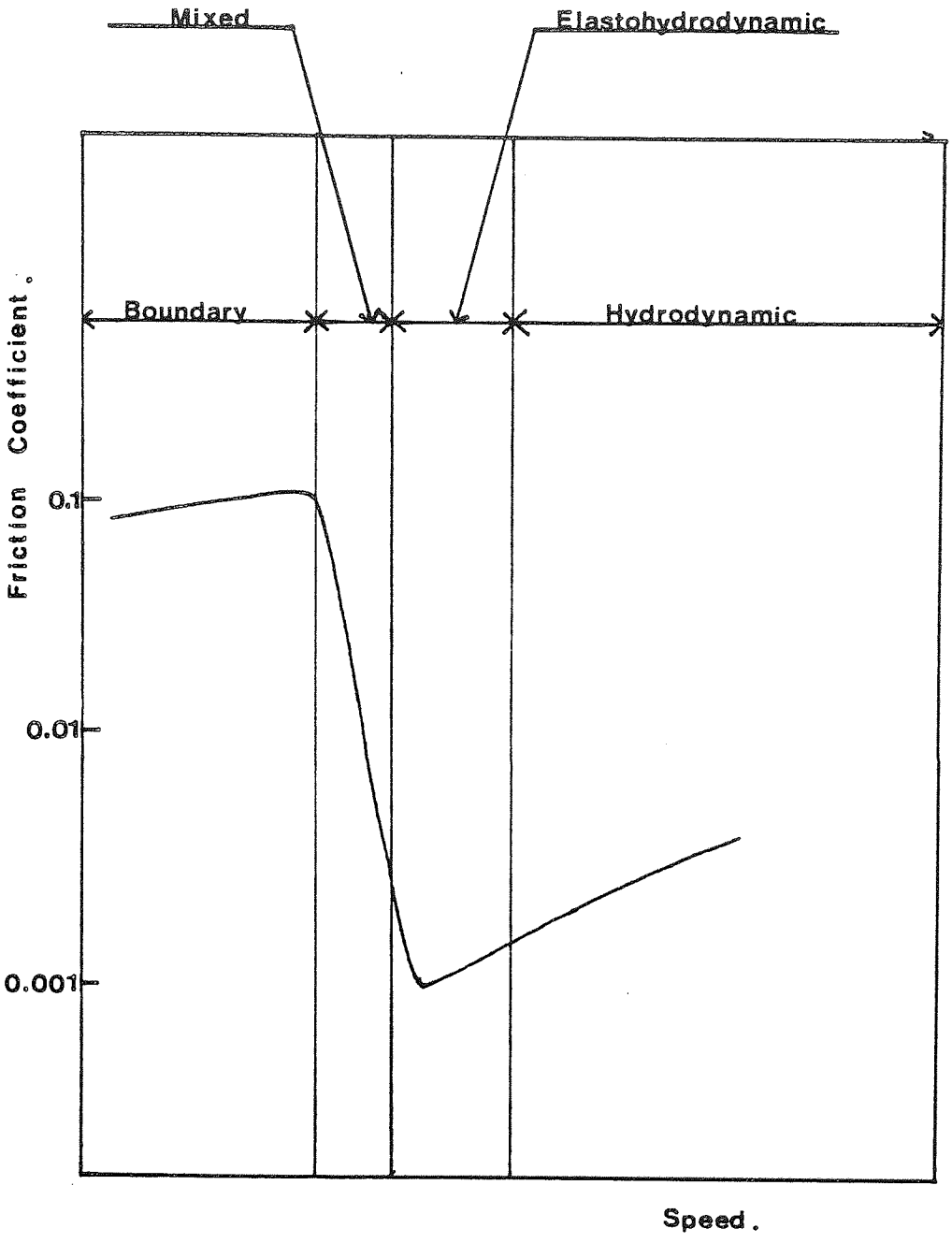

Figure 1.2

Classical Stribeck curve showing the four classifications of lubricated wear

1.6.1 Hydrodynamic Lubrication

In hydrodynamic lubrication the moving surfaces are completely separated by a continuous film of lubricant and the resistance to motion and friction coefficient is due solely to the viscosity of the lubricant. Although for a given load a speed suitable to provide hydrodynamic lubrication can be chosen, in most cases loads are light and speeds high. In the ideal case there will be no surface interaction and no wear. Friction coefficients are extremely low typically of the order 0.001 to 0.01. Minimum fluid film thicknesses usually exceed 10^{-7} m which is generally greater than surface roughness, which is of course essential for true hydrodynamic lubrication.

1.6.2 Elastohydrodynamic Lubrication

It has been recognised that many loaded contacts of low geometrical conformity, such as gears and cams, frequently behave as though they were hydrodynamically lubricated. This form of lubrication is achieved when surfaces are elastically deformed by loads which are carried over small areas. Crook[75] has shown that under

these conditions the viscosity of the lubricant at the surface temperature of the sliding pair is of the greatest importance, and that this, along with pressure increases leading to increases in viscosity of the fluid, and thus greater load distribution, are the reasons for elastohydrodynamic lubrication. This viscosity increase allows high hydrodynamic pressures to be generated and thus an increase in fluid film thicknesses sufficient to separate the surfaces at the leading edge of the Hertzian region.

1.6.3 Mixed Lubrication

Mixed lubrication takes place in the speed and load region between elastohydrodynamic and boundary lubrication. There are some intermittent contacts between the surfaces which result in wear but the majority of the contact is governed by a mixture of the two effects. Out of contact the surfaces are separated by films of molecular proportions as in boundary lubrication. Coefficients of friction are in the region between 0.01 and 0.1 corresponding to elastohydrodynamic and boundary lubrication values.

1.6.4 Boundary Lubrication

Boundary lubrication occurs only if a surface active agent is present in the lubricant. Boundary lubrication may be defined as a condition of lubrication in which the friction between two surfaces is determined by the properties of the surfaces and by the surfactant properties of the lubricant. This type of lubrication occurs under some combinations of high load and small apparent area of contact, low sliding speed and rough surfaces.

Wear under conditions of boundary lubrication has often been shown to be the result of oxidative attack on the metal surface[76,77,78,79]. Appledoorn et al[79] proposed that a direct reaction takes place between dissolved oxygen and the nascent metal surface to form an easily removed oxide layer. This simple mechanism cannot account, however, for the wear reducing effect of lubricant antioxidant additives demonstrated by Bose, Klaus and Tewksbury[78]. There is good evidence[76,77] that reactions take place between the oxidised lubricant and the metal surface and it has been proposed[80] that oxidation of the surface occurs by reaction with oxidised lubricant species.

In contrast, some of the products of oil oxidation have been shown to have anti-wear properties, particularly in lubricants which were initially non-polar[81]. The oxidation of white oils has been studied[82] by monitoring the build up of oxidation products and one, a peroxide, found to promote oxidational wear and another, an acid, to inhibit oxidational wear. Denison[83] and Prutton et al[84] have shown that corrosion of steel by lubricating oils containing acids will not occur to any appreciable extent unless peroxides are present in the oil. Further, the rate of corrosion is determined by the concentration of the peroxides in the oil[83], and it is postulated that the corrosive action takes place in two steps: the reaction of peroxide with the metal to form metal oxides, and the subsequent reaction of the oxide with the acid to form a salt, or metallic soap.

Frictional heating and/or metal catalysis have been suggested as the principal factors initiating these chemical reactions[85] although complex chemical interactions are undoudtedly involved. The important factor of oxygen concentration in the oil has a profound effect on wear under boundary lubrication, and is considered in the following section.

1.7 Oxidational Wear in Boundary Lubrication

In the case of boundary lubrication there is a substantial amount of asperity-asperity contact and oxidation has been identified as an important component of wear[7,8], although the mechanism is likely to be similar to that proposed by Quinn[68] rather than that of Stott et al[74] because of debris removal by the lubricant.

Bowden and Young[86] described the formation of metallic soap films by reaction between an organic acid and the surface metallic oxide. The oxide was found to be a necessary prerequisite to the production of a soap film and hence to the reduction in wear. Hirst and Lancaster[87] showed that the rate of metal oxide formation affects friction and wear during boundary lubrication, and suggested that oxide film formation complemented the protection afforded by the acid.

Severe wear is seen to ensue when oxygen is removed from the lubricant[88] which has been further substantiated by Godfrey[89,90] who observed a reduction in friction coefficient with a sulphur solution in white oil when the white oil was used in the presence of oxygen. He observed the oxides α-Fe_2O_3 and Fe_3O_4 in oxygen, but when the system was operated in nitrogen without the sulphur additive, large metallic severe wear particles resulted. Further to this Nakayma and Okamoto[91], in a study of copper under

boundary conditions, found an optimum value for the concentration of dissolved oxygen at which minimum friction and wear occurred. The increased rate of wear above this optimum value was explained in terms of the formation of thicker oxide films which are more easily sheared.

Begelinger and deGee[92] observed large decreases in both friction and wear with increased oxygen concentration in the lubricant in a steel on steel system, and this they attributed to oxidation of asperities during localised breakdown of the boundary film. The effect then is to prevent metal to metal contact during these periods. Sullivan and his extensive study of aluminium bronze on steel[93-97] identified the major protecting element to be copper oxide, Cu_2O, and oxidational wear to be the dominant mode. He deduced that the major action of the dimeric acid used in the investigations at 12 ppm was to provide the surface with sufficient protection for a protective oxide film to develop and be maintained.

Sullivan[98] has developed a quantitative wear expression based upon the parabolic oxidational wear equation developed by Quinn et al[68,69] and a relationship describing the periodic time of vibration of surface molecules by Kingsbury[99,100] to the fractional film defect of a surface, and the periodic time of vibration of that molecule as given by Frenkel[101] into a comprehensive wear expression for parabolic oxidational wear under boundary lubricated conditions:

$$w = \left\{ \frac{2a \; X \; A_p \; \exp\left(^{-E}/_{RT_d}\right) \exp\left(^{-Q_p}/_{RT_o}\right)}{U^2 \; f^2 \; P^2 \; \xi_0{}^2 \; t_o} \right\} \frac{W}{P_m}$$

where w is the wear rate, a the asperity contact radius, X the diameter of an adsorbed molecule, A_p the Arrhenius constant for parabolic oxidation, E the molecular heat of adsorption, T_d the molecular desorption temperature, Q_p the activation energy for parabolic oxidation, T_o the oxidational temperature, U the sliding speed, f the fraction of oxide which is oxygen, P the density of oxide, ξ_c the critical oxide thickness, t_o the fundamental periodic time of vibration of the molecule at the adsorbed site, W the normal load and P_m the flow pressure. The expression in brackets is the Archard wear factor, and comprises all the relevant variables from oxidational wear theories of both lubricated and unlubricated origin.

1.8 Research Programme

The initial aim of the present research was to investigate the wear of AISI 52100 steel for a range of low loads and speeds in the region below the T_1 transition. Wear rates, friction, heat flow and contact resistance measurements are considered in conjunction with the results of several analytical techniques such as microhardness testing, powder X-ray diffraction, scanning electron microscopy and Auger electron spectroscopy to deduce the mechanism of oxide production and removal in this area.

Secondly, the same system will be monitored under lubricated conditions both with and without the boundary lubricating additive stearic acid. Again the method of oxide production and removal will be investigated and this compared with the results obtained from the unlubricated tests. All results will be analysed in light of past and present investigations into similar areas.

CHAPTER TWO

EXPERIMENTAL DETAILS

2.1 Introduction

This chapter will provide details of the experimental arrangement and procedures used throughout the research, along with explanations of the various methods of analysis and their application in the study of test samples.

In section 2.2 - 2.7 the pin-on-disc machine used in this study is described. Details of the instrumentation used in collecting test data are provided. Sections 2.8 and 2.9 describe sample preparation and experimental procedures respectively. Sections 2.10 - 2.15 are dedicated to the physical methods of analysis used in the study of worn pin and disc specimens for both lubricated and unlubricated wear experiments.

The large proportion of friction and wear results presented in the next chapter were digitally recorded. At regular intervals throughout the research, however, wear rates were checked against results from mass loss, and chart recorder data to ensure that results were consistent for each method.

Section 2.16 deals with the heat flow and temperature calculations in an extended form to that presented by Rowson and Quinn[102].

2.2 The Wear Test Equipment

A Denison model T62 Tribotester, shown in Figure 2.1, was used to conduct the experiments. This machine consists essentially of a vertical 4 mm diameter pin, loaded against a flat, horizontally rotating disc. The disc was driven by a 0.5 H.P. servo-controlled d.c. motor which provided continuously variable linear speeds at the pin of 1.0×10^{-3} to 1.0 ms^{-1} and 0.2 to 20 ms^{-1}. The latter corresponding to the original 100 - 6000 rpm specifications of the Tribotester and the former to a 20:1 step down ratio via a pulley system installed for the purpose of this work. Loads of between 5 and 200 N may be applied to the pin through a gimballed load arm by means of a spring loaded weight system designed to reduce inertial loading. The entire load arm assembly may be moved back and forth parallel to the loading arm enabling the pin to be positioned at any desired track radius on the disc. The pin was held in the underside of the load arm within an electrically and thermally insulated brass housing.

Figure 2.1

T62, Denison Wear Tester

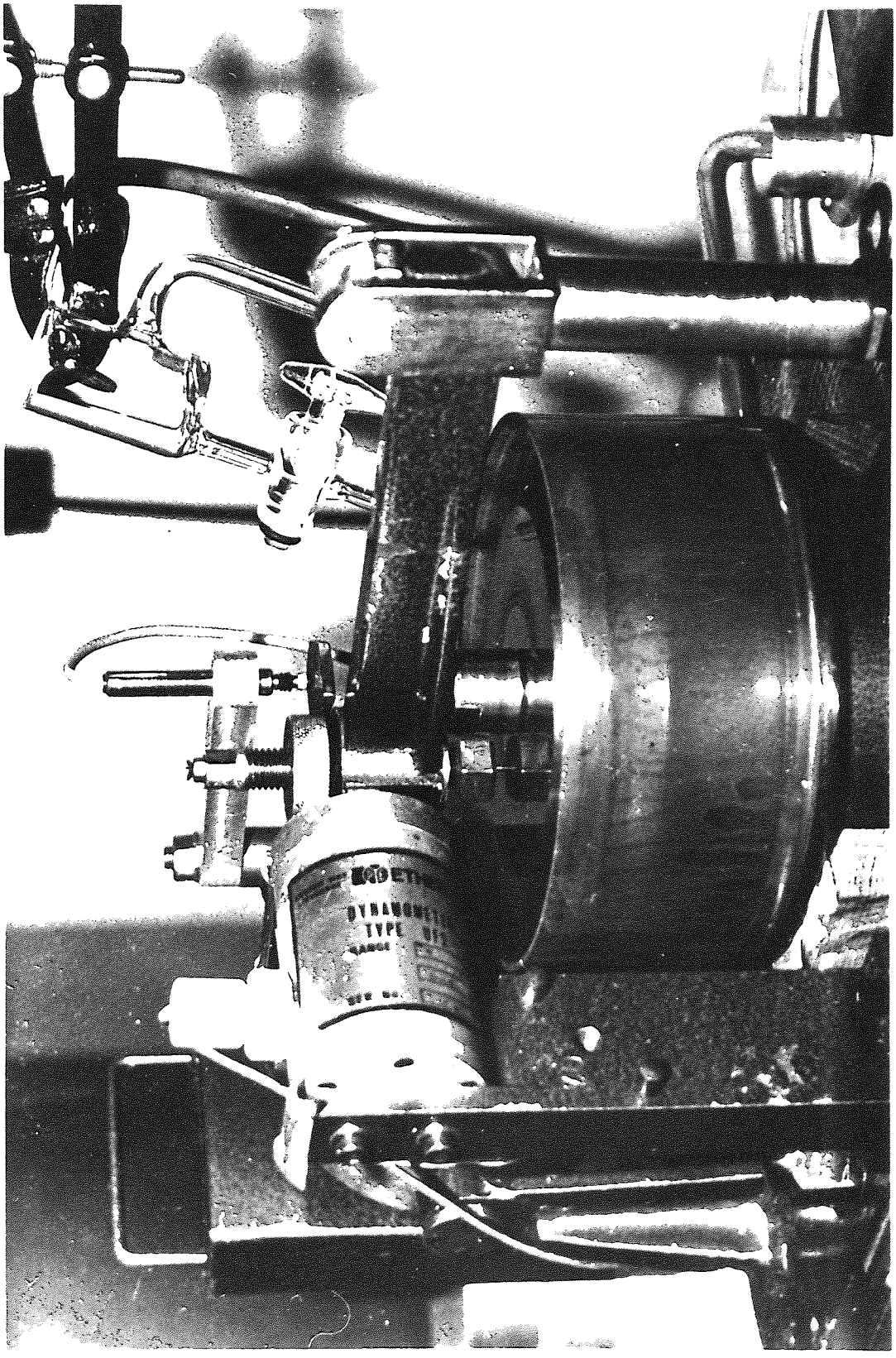

For the lubricated wear tests an oil reservior was added which surrounds the disc but which otherwise does not interfere with the experimental arrangement. Oil was supplied to the disc using a peristaltic pump via a 0.45 μm Nucleopore filter and flow adjustment reservior. Where tubing was unavoidable, Vinescol 23, a fluorinated synthetic rubber of 6 mm diameter was used. This tubing contains no plasticisors and is corrosion resistant for many materials including organic and inorganic acids. A flow rate of 4 ml min^{-1} was used to provide continuously flooded conditions on the disc. The oil collecting in the reservior surrounding the disc then overflowed into the main sump through a glass-wool prefilter, as shown in Figure 2.2. This system unavoidably leads to particle contamination of this sump as the high flow rate and flooded wearing conditions, maintained over extensive periods, required an uneconomical quantity of oil were a single pass option to be adopted. However, the Nucleopore filter provided effective screening of the oil prior to its introduction to the disc.

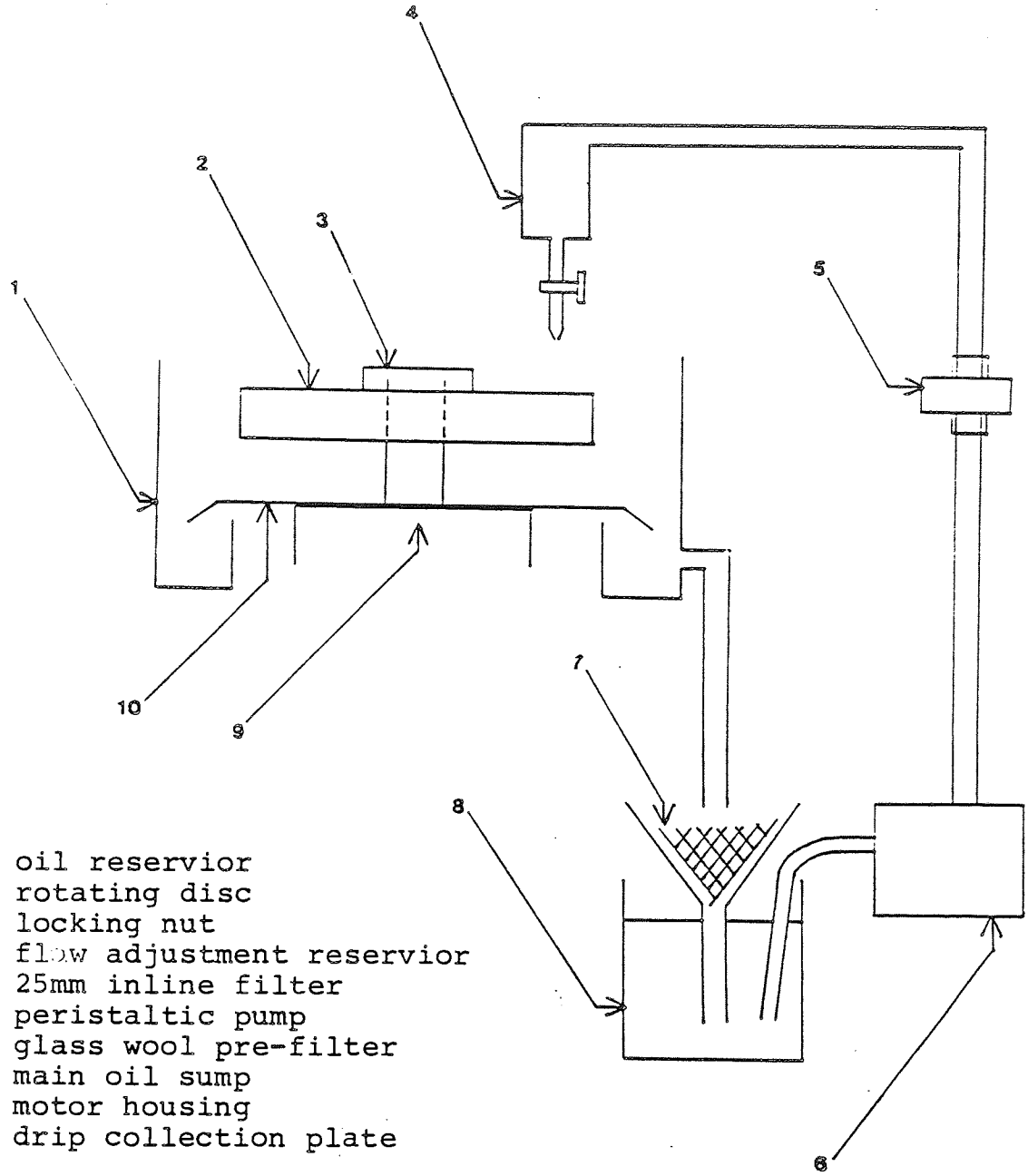

Key:

1. oil reservior
2. rotating disc
3. locking nut
4. flow adjustment reservior
5. 25mm inline filter
6. peristaltic pump
7. glass wool pre-filter
8. main oil sump
9. motor housing
10. drip collection plate

Figure 2.2

Schematic representation of the oil filter and delivery system for the Denison T62 tribotester

2.3 Friction and Wear Measurement

The wear of the pin was determined using a linear displacement transducer connected above the load arm in a vertical clamp. The transducer sensitivity is 1.05 μm mV^{-1} over a 12 kHz range and the signal output was externally amplified using an ODI oscillator demodulator.

The friction force on the pin was measured using an Ether type UF2 tensile/compressive strain gauge dynamometer incorporating a four arm fully active bridge. The sensitivity is 0.55 NmV^{-1}, the signal output being amplified within the Denison control unit.

The signals from the friction and wear transducers after amplification were fed directly into a C.I.L. Electronics TA880 A/D converter, strain gauge and thermocouple amplifier. The majority of the experimental results were taken digitally with a CBM PET microcomputer, detailed in section 2.7, via the multimonitor which was operated on a full range 0-200 mV input to take advantage of the 16 bit A/D conversion available. The wear transducer signal was zeroed within the microcomputer before each experiment, so that any displacement after the start of an experiment could be interpreted directly as a measurement of wear.

2.4 Temperature Measurement

To monitor the heat flow in this study (detailed in section 2.15) two thermocouple measurements were required. One temperature was ambient near to the wearing surfaces, the other was the temperature of the pin on its outer surface near to the pin/disc interface. To achieve this a thermocouple was spot-welded to the pin prior to each experiment, and another was positioned permanently above the disc near to the pin.

The thermocouple wire was Type K standard, output 40 $\mu V\ ^{\circ}C^{-1}$ between 0 and 400°C with an operating temperature range of -50 to 400°C. The thermocouple outputs were monitored directly by the TA880 which incorporates Type K thermocouple amplification and a continuously recalibrated internal cold junction.

2.5 Determination of Sliding Speed

The Denison wear tester provides a speed indicator which is used to initially set the disc speed. However, in view of the accuracy with which the time of reading is known when using microcomputer controlled data collection, variation in the assumed speed of sliding could introduce unnecessary error and should preferably be eliminated. To this end a digital revmeter was constructed. The sensor is a slotted opto switch comprising an infra-red source and a sensor with an infra-red filter, to minimise ambient light effects. This feeds an IVO low-medium high speed digital counter and liquid crystal display. A low current 3.6 V nickel-cadmium battery powers the counter display, and is itself on constant charge via a voltage rectifier from a 3 VA transformer. The full circuit diagram is shown in Figure 2.3. At the end of each experiment the revmeter value is used in conjunction with the computer's internal clock reading to accurately determine the speed of sliding. The only error in this system is introduced while the computer is data-logging, which pauses the internal clock. This time, however, is negligible when compared with the time of the experiment.

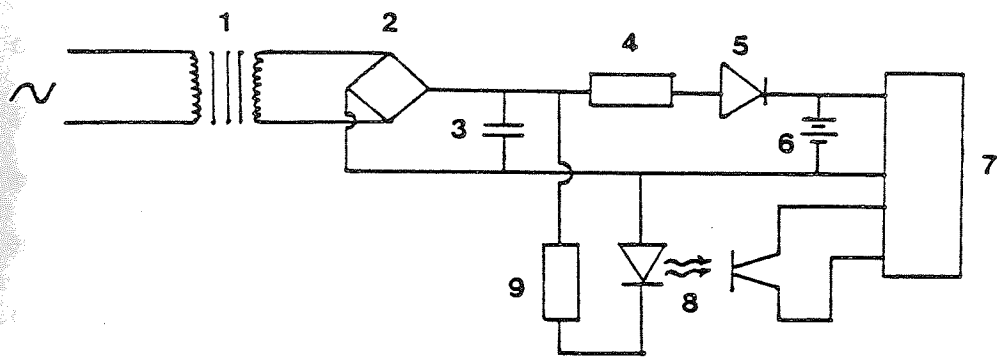

Key:

1. 6V transformer
2. bridge rectifier
3. 470 µF capacitor
4. 4.7 KΩ resistor
5. Ln 914 diode
6. 3.6V nickel cadmium battery
7. digital rev-meter and counter
8. slotted opto switch and infra red LED
9. 33 KΩ resistor

Figure 2.3

Circuit diagram representing the digital rev-meter used in these experiments

2.6 Contact Resistance Measurement

The contact resistance between pin and disc can provide useful information on the amount of oxide coverage existing at the contacting areas. This resistance may vary from 0Ω for metal-metal contact, up to MΩ for oxide-oxide contact. Conventional meters such as the AVO or DVM have proved unsuitable for this measurement due to reading errors and response time. Recently, Glascott, Stott and Wood[103] developed a device specifically to measure contact resistance, the circuit diagram of which is shown in Figure 2.4. A logarithmic compression was used since a wide ranging 10 kHz bandwidth may be achieved by exploiting the expotential voltage-current characteristic of a diode, or diode connected transistor.

The contact resistance was measured by introducing a 10 m.v. P.d. across the wearing junction. No greater voltage should be used due to potentially high current densities that might occur in the regions of contact. It has been estimated (103) that for a 10 mV P.d. the current produces less than a 2°C temperature rise at the real areas of contact.

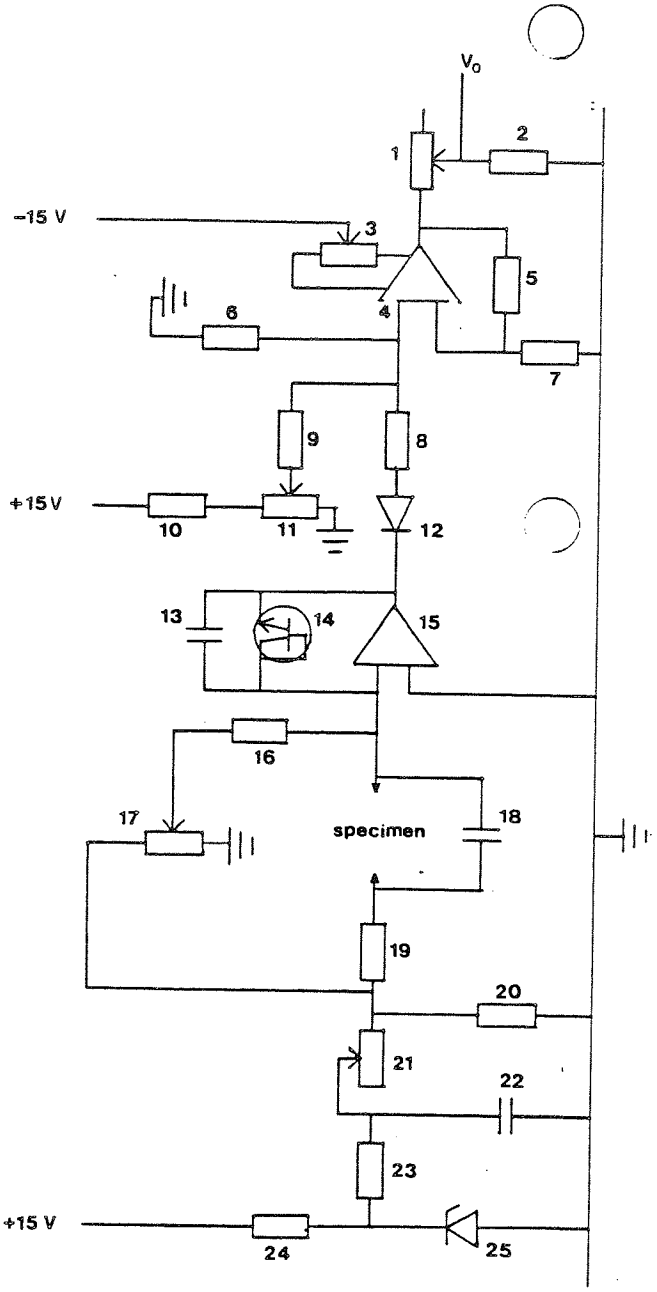

Figure 2.4

Circuit diagram representing the contact resistance device used in these experiments

Key for Figure 2.4

1. 1 kΩ potentiometer
2. 100 Ω resistor
3. 10 kΩ potentiometer
4. 741A operational amplifier
5. 22 kΩ resistor
6. 22 kΩ resistor
7. 2.2 kΩ resistor
8. 2.2 kΩ resistor
9. 2.2 kΩ resistor
10. 2.2 kΩ resistor
11. 220 kΩ resistor
12. signal diode
13. 0.1 µF capacitor
14. BC109 transistor
15. 308A operational amplifier
16. 470 kΩ resistor
17. 470 Ω potentiometer
18. 0.1 µF capacitor
19. 10 Ω resistor
20. 1.0 Ω resistor
21. 390 Ω potentiometer
22. 100 µF capacitor
23. 220 Ω resistor
24. 330 Ω resistor
25. BZY 88 (5.6V) zener diode

The device has been duplicated by the author and used in these experiments. One electrode was connected to the disc via the central drive shaft, and the other to the pin through the pin holder. Data was collected continuously on a JJ Instruments CR552 chart recorder.

2.7 Computerised Data Collection, Storage and Analysis

Data from friction, wear and thermocouple transducers were collected using a microcomputer via a CIL Electronics TA880 16 bit ADC strain gauge and thermocouple amplifier. The TA880 incorporates an internal Z80 processor which permitted direct external programming from the CBM PET microcomputer via an IEEE - 488 interface. Basic programs were written by the author which operated the data acquisition during an experiment as specified prior to the start of the experiment.

Friction and wear data were digitised with a stated error of 0.0015% and stored on flexible disc during the course of an experiment. The TA880 operating parameters for Type K thermocouple inputs are presented elsewhere (104) and along with the wear and friction data, the thermocouple signal is digitised with a 0.0015% error. Data collected through the TA880 inputs have stated errors of $\pm$ 0.006% + 1 digit for friction and wear, and $\pm$ 0.1^{0}C +

1 digit for Type K thermocouple measurement. All of these remain negligible compared to experimental scatter.

Raw and processed data were stored on flexible disc and thus utilized a medium which is concise, orderly and available for instant access.

Digital information processing greatly facilitated the analysis of results, providing almost instantaneous values of wear rate, friction coefficients and general surface temperatures.

2.8 Sample Preparation

2.8.1 Disc Preparation

The disc material was AISI 52100 semi annealed low alloy steel of mean bulk hardness 280 $\pm$ 10 VPN. The mass percentage of alloy composition for this steel is given in Table 2.1. The discs were 100 mm in diameter and 10 mm thick and were ground to a finish better than 0.5 μm. A typical disc tested at the Exxon Research Centre, Abingdon, by talysurf in ten places showed a centre line average of 0.345 μm. Prior to each experiment the disc was cleaned in isopropyl alcohol followed by a petroleum vapour bath at 80°C for a period of 1 hour.

Table 2.1

Mass percentage composition of AISI 52100 steel

Element	Mass %
C	0.9 - 1.2
Si	0.1 - 0.35
Mn	0.3 - 0.75
S	0.06 max
P	0.06 max
Cr	1 - 1.6
Fe	Remainder

2.8.2 Pin Preparation

The pin specimens are of the same material as the discs with a 4 mm diameter wearing surface, and undergo the same grinding and cleaning processes. For the purposes of the lubricated wear experiments the wearing pin surface was further polished to better than 0.1 μm in situ, using 1 μm Silicon Carbide paper in the presence of lubricant. On completion of this the pin is once more removed and cleaned with a low additive solvent SBP2. This polishing process was essential for the lubricated test cases as it ensured that the whole of the apparent area of contact was presented to the disc at the start of an experiment to avoid hydrodynamic effects. The loading arm incorporates a small spirit level which allows minor adjustments to be made.

2.9 Wear Experiments

2.9.1 Unlubricated

Wear tests were conducted at loads of 4.9, 9.8, 19.6 and 49.1 N each at a range of speeds from 3×10^{-3} to 1.0 ms^{-1} or until the T_1 transition had been observed. Each experiment was run until an equilibrium wear mode had

been established. This usually occurred within ½ hour, often quicker, and then continued for periods sufficient to determine the equilibrium wear rates. The test durations were generally a few hours, however, 2 - 3 days was the norm for the lower speeds and loads. Wear debris was collected along with worn pin samples for analysis.

At the outset of an experiment the computer was initialised and instructed on how frequently to collect data based upon criteria from load and speed and wear severity considerations. All experiments were conducted at ambient temperature and once initiated the experiment would continue to conclusion with no further supervision required.

2.9.2 Lubricated

Wear tests were conducted under flooded lubrication conditions at ambient temperature with Esso Technical White Oil and Esso Technical White Oil plus 0.1% by weight of stearic acid. The acid was specially pure with minimum assay of 99% and sulphated ash content at less than 0.05%. The variation of the dynamic viscosity of the oil was measured at Exxon Research Centre, Abingdon, and for the purposes of this work was taken as 25 $m^2 s^{-1}$ kinematic equivalent.

The basic series of experiments was designed to compare the wearing system under boundary conditions with Technical White Oil with and without the organic acid additive. To this end, after an initial series of experiments to determine the boundary region, three loads were investigated: 49.1, 98.2 and 122.7 N, and six speeds corresponding to constant bearing numbers for each load. The duration of each test was at least 40 hours as it was necessary to measure an absolute wear value in excess of any statistical variations inherent in measuring low wear rates.

The experimental procedure here was the same as for the dry wear tests, except that the loading arm was lowered on to the disc and the wear transducer zeroed after starting the discs rotation. This was necessary to allow a fluid film to be developed at the start of a run. Failing this it was found that such serious damage was incurred in the first rotation of the disc that no surface conformation was thereafter possible, and catastrophic wear occurred in most cases. A constant disc-track radius was used in all unlubricated wear experiments to ensure constant conditions of fluid film support at the pin/disc interface.

It was not possible to collect sufficient debris in these tests for powder X-ray analysis although several unsuccessful methods were attempted. Wear debris collected from the unlubricated experiments was relatively abundant.

2.10 Microhardness Measurement

Taper sections of some selected worn pins were produced for different combinations of load and speed, and microhardness values taken using a Miniload Hardness Tester. The impressions were made by means of a diamond indenter under 25g load. The pin specimens were moulded into conducting bakelite and tapered to about 10° using 180 to 1200 grit silicon carbide paper and final polishing was achieved with 6 and 1 μm diamond paste. On average for each pin, six indentations were recorded at each depth from about 10 to 100 μm into the pin. Microhardness versus depth profiles were then compiled.

2.11 Powder X-ray Diffraction Analysis

The wear debris collected during the dry wear experiments was examined using powder X-ray diffraction. The wear debris was pulverised and placed in a 0.5 mm diameter capillary at the centre of a standard 114.6 mm diameter powder X-ray camera. The sample was rotated during an hour long irradiation by filtered Co Kα radiation of wavelength 1.7902 $\overset{0}{A}$. The X-ray tube was operated at 40 kv and 20 mA; potential and filament current

respectively. The interplanar spacings obtained from the developed X-ray film were compared with those noted in the X-ray powder file issued by the American Society for Testing Materaisl (ASTM) thereby obtaining compound identification. The relative intensities of debris samples investigated by powder X-ray diffraction were recorded using a microdensitometer which allowed some estimation of relative abundance to be made, although a complete proportional analysis was not attempted, and thus exact relative intensities are unknown.

2.12 Scanning Electron Microscopy

Scanning electron microscopy was used to study the topographical features of selected worn pin surfaces. The major advantage of this technique is the large depth of field. Utilising specimen tilt control, edge on pictures may be obtained of oxide layers, thus affording estimates of thickness. This technique has been used extensively with both unlubricated and lubricated worn pin specimens and has provided excellent generation and removal.

2.13 Auger Electron Spectroscopy

Auger electron spectroscopy (A.E.S.) has been used extensively on both lubricated and unlubricated worn pin specimens to determine the variation of oxygen concentrates with depth, and thus oxide thicknesses.

Briefly, the principle of the technique is that the sample is bombarded by an electron beam of a few microns diameter of 1 - 10 keV energy which penetrates the specimen to a depth of 1 - 2 μm. This excites atoms in this region which then eject photoelectrons and Auger electrons.

Auger electron energies are such that they can only escape from a surface within the first 5 - 10 $\mathring{A}$ (105) indicating the importance of the technique to surface analysts. Due to the large background, caused by back-scattered and photoelectrons, on which the Auger peaks lie the spectra are much easier to present and analyse if differentiated.

Several areas of a number of pin surfaces were examined, and differentiated Auger electron spectra were recorded between successive removal of atomic layers by argon ion bombardment. The ion beam was of 5 keV energy and 10 μA current, rastered over the whole sample, which provided a calculated removal rate of 30 $\mathring{A}\ min^{-1}$ corrected

for data obtained using a 225 Å thick silicon nitride standard. All spectra were recorded using a 5 keV incident electron beam from a 15 μm spot on the sample.

Relative atomic concentrations were taken from differentiated peak to peak heights using published sensitivity factors (106). A detailed explanation of the Auger electron process may be found elsewhere (107).

2.14 X-Ray Photoelectron Spectroscopy

X-ray Photoelectron Spectroscopy (X.P.S) has been used to examine selected worn pin surfaces of the lubricated system in order to elucidate any chemical changes occurring between the surface and the white oil and/or the organic acid.

X.P.S. differs from the Auger process in that the incident exciting beam is of X-rays, and that it is the photoelectrons which are detected and provide detailed information not only with respect to elemental identification but also of chemical state. Essentially X.P.S. is sensitive to the bonding structure of the surface and thus to the compounds present. It has been shown (108) that the thickness of the surface layer characterized is similar to that in A.E.S.

X.P.S is a large area analytical technique so quite large areas of several pins were examined specifically for the iron, oxygen and carbon photoelectron peaks. A magnesium K_α X-ray source was used with a gun voltage of 15 kV and a 15 mA gun current. The resulting spectra were then analysed and broken into their constituent energy curves, each of which was adjusted and recombined for subsequent comparison with the original spectra. This process of curve-fitting enables the relative abundance of chemical bonds and thus compounds to be estimated. More detailed information on this process and on X.P.S. may be found elsewhere (107).

2.15 Heat Flow Analysis

It is not possible to measure the temperatures generated at a rubbing contact directly, however, it is highly desirable to have some idea of their magnitudes. Thus a mathematical analysis of the heat flow into the pin has been performed in an effort to determine the general surface temperature, T_s. Two distinct analyses were performed, both of which will be presented here, the first ignores the attenuation to the heat flow in the pin due to its brass holder, the second incorporates this modification by considering the heat flow in two parts.

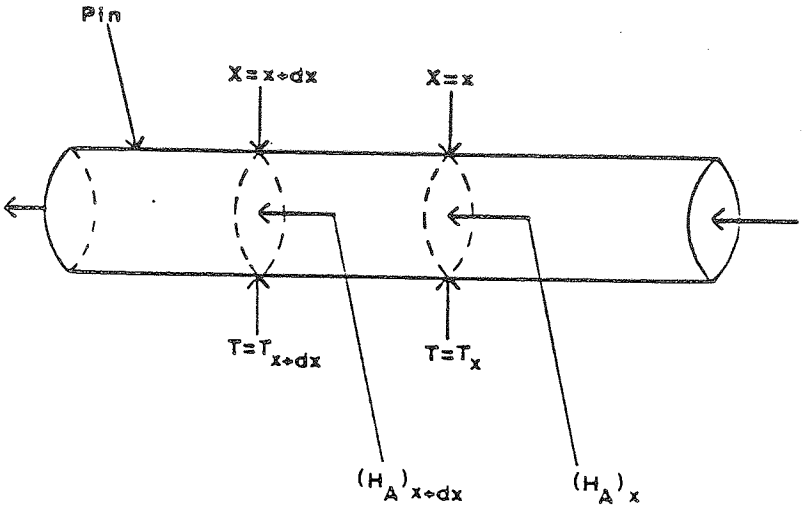

Figure 2.5

Temperature and heat flow in the pin.

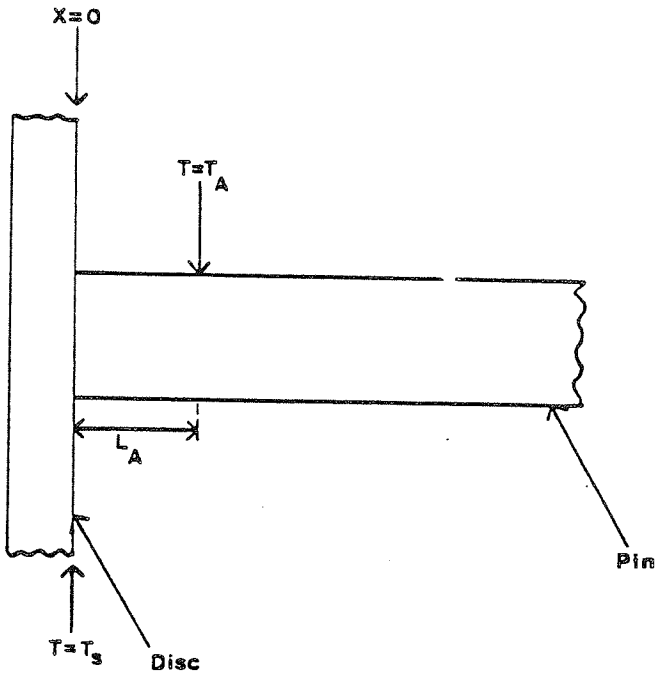

Figure 2.6

Heat flow diagram for the pin loaded against a disc, ignoring the pin brass holder

Consider firstly Figure 2.5, let the temperature of the pin at x be T_x. From elementary heat flow considerations the axial heat flow rate at x, $(H_A)_x$, is given by:

$$(H_A)_x = -k_s \pi R_t^2 \frac{dT_x}{dx} \qquad 2.1$$

where k_s is the thermal conductivity of steel and R_t is the pin radius

and the axial heat flow at $(x + \Delta x)$, that is $(H_A)_{x+\Delta x}$, is given by:

$$(H_A)_{x+\Delta x} = -k_s \pi R_t^2 \frac{dT_{x+\Delta x}}{dx} \qquad 2.2$$

expanding equation (2.2) by Taylor series gives:

$$(H_A)_{x+\Delta x} = -k_s \pi R_t^2 \frac{dT_x}{dx} + \frac{d^2 T_{x\Delta x}}{dx^2} \qquad 2.3$$

ignoring higher polynomials. Also ignoring the change of temperature between x and $x+\Delta x$, the radial heat flow through an element of unit what is given by:

$$H_R = 2\pi R_t h(T_x - T_E) \qquad 2.4$$

where h is the heat transfer coefficient between steel and air, and T_E is ambient air temperature.

Hence, for an element of length Δx, H_R is given by:

$$(H_R)_x = 2\pi R_t h(T_x - T_E)\Delta_x \qquad 2.5$$

At equilibrium the system is described by:

$$(H_A)_x = (H_A)_{x+\Delta x} + (H_R)_x \qquad 2.6$$

That is that the heat flow entering point x must equal the sum leaving x, radially and axially, thus:

$$-k_s \pi R_t^2 \frac{dT_x}{dx} = -k_s \pi R_t^2 \frac{dT_x}{dx} + \frac{d^2 T_x \Delta x}{dx^2} + 2\pi R_t h\ (T_x - T_E)\Delta x \qquad 2.7$$

which reduces to

$$k_s \pi R_t^2 d^2T_x \Delta x = 2\pi R_t h(T_x - T_E)\Delta x \qquad 2.8$$

That is

$$\frac{d^2T_x}{dx^2} = \frac{2}{k_s R_t} \cdot h \cdot (T_x - T_E) \qquad 2.9$$

which constitutes the general equation describing heat flow in the pin.

Letting

$$T_x - T_E = T$$

and

$$Z = \frac{k_s}{2hR_t}^{\frac{1}{2}}$$

we get

$$\frac{d^2T}{dx^2} = \frac{T}{Z^2R_t^2} \qquad 2.10$$

which has the general solution of the form:

$$T = B_1 \exp(\frac{x}{ZR_t}) + B_2 \exp(\frac{-x}{ZR_t}) + k \qquad 2.11$$

hence

$$T_K = B_1 \exp(\frac{x}{ZR_t}) + B_2 \exp(\frac{-x}{ZR_t}) + k \qquad 2.12$$

Now considering Figure 2.6, if we let $x \to \infty$, then $T_x \to T_E$ and thus $B_1 = 0$ and $k = 0$ such that

$$B_2 \exp(\frac{-x}{ZR_t}) \to 0$$

and

$$T_x \to T_E$$

now we have

$$T_x = B_2 \exp\left(\frac{-x}{ZR_t}\right) + T_E \qquad 2.13$$

when $X = L_A$, $T_x = T_A$, then equation (2.13) becomes

$$T_A = B_2 \exp\left(-\frac{L_A}{ZR_t}\right) + T_E$$

or

$$B_2 = \frac{(T_A - T_E)}{\exp\left(-\frac{L_A}{ZR_t}\right)} \qquad 2.14$$

when $x = 0$, $T_x = T_s$ and so

$$T_s = B_2 + T_E \qquad 2.15$$

substituting in B_2 gives

$$T_s = \frac{(T_A - T_E)}{\exp(-\frac{L_A}{ZR_t})} + T_E \qquad 2.16$$

Considering the parameters in equation (2.16), it is seen that the variables T_A and T_E are experimentally determinable temperatures, T_E being ambient, T_A being measured on the pin. The length of L_A is similarly measurable. The radius of the pin, R_t, is of course known, and the parameter Z is previously defined thus:

$$Z = (\frac{k_s}{2hR_t})^{\frac{1}{2}}$$

This analysis provides a good approximation to the general surface temperature provided that L_A is kept small. In this work L_A was typically 1-2 mm, and so equation (2.16) has been used with the appropriate L_A for each test to calculate general surface temperatures at the pin/disc interface.

CHAPTER THREE

EXPERIMENTAL RESULTS

3.1 Introduction

Friction and wear results, temperature and contact resistance together with results from the various methods of analysis are presented in this chapter. Both unlubricated and lubricated results are presented and will be displayed separately, although most techniques of analysis are common to both.

Sections 3.2 to 3.9 represent the results of unlubricated wear tests while sections 3.10 to 3.14 give those results from the lubricated experiments.

For the unlubricated portion of the results sections 3.2 and 3.3 deal with wear and friction, section 3.4 deals with temperature, while sections 3.5, 3.6 and 3.7 deals with scanning electron microscopy, microhardness and contact resistance respectively. Finally, sections 3.8 and 3.9 present powder X-ray spectra and Auger electron depth profiles.

Section 3.10 presents results from both friction and wear under lubricated conditions, while also for lubricated tests sections 3.11 and 3.12 present contact resistance and scanning electron microscopy results and sections 3.13 and 3.14 present Auger electron depth profiles and X-ray photoelectron spectra.

3.2 Unlubricated Wear

The results presented in this section are from the like on like pin on horizontal disc configuration of AISI 52100 low alloy steel. At the beginning of each sliding period wear rate, friction and surface temperatures were high before gradually reducing to an equilibrium mode. Figure 3.1 shows the typical variation of wear rate and general surface temperature for 9.8 N and 0.2 ms^{-1} at the start of a test. In this case there is a rapid increase in wear rate and temperature to about 1.5 x 10^{-11} m^3 m^{-1} and 33°C respectively over a period of 40 minutes when a gradual decrease occurs and they attain their equilibrium values of about 2 x 10^{-13} m^3 m^{-1} and 29°C, with a corresponding decrease in friction coefficient. These two orders of magnitude decrease in wear rate is typical of severe to mild wear transitions and is observed in almost every case. The metallic wear debris produced in this

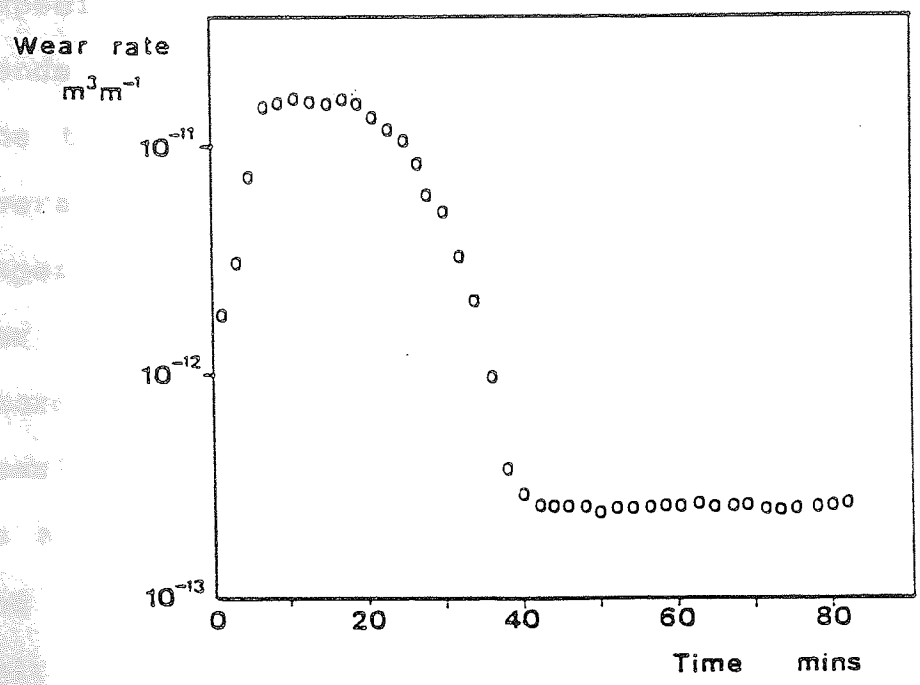

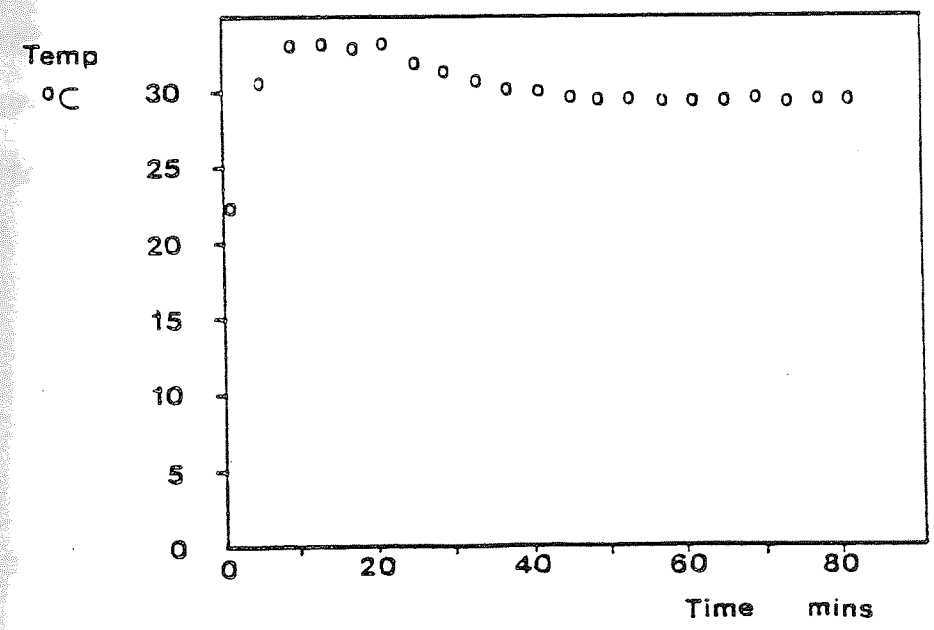

Figure 3.1

Variation of wear rate and general surface temperature with time, for 9.8 N at 0.2 ms^{-1} showing the establishment of equilibrium wear.

severe wear running-in period is observed to be minimal, especially for the lower speeds where the wear-in time also tends to lower values. After the onset of equilibrium wear the test was run on for several hours and the wear rates averaged over that period. Figure 3.2 shows the experimental variation of equilibrium wear rate with speed for loads of 4.9, 9.8, 19.6 and 49.1 N. In each case increase in speed in the mild oxidational wear region results in a decrease in wear rate until the T_1 transition is approached when there is a rapid increase in wear rate and severe metallic wear ensues. In these cases the initial high wear rates are maintained and general surface temperatures and friction coefficients are seen to be high. Figure 2.3 further shows that, as would be expected, wear rate increases with load and that the T_1 transition moves to lower speeds with increase in load. In connection with the model developed in a later section, a further load of 14.7 N was investigated. Figure 3.3 shows the variation of wear rate with speed at this load.

3.3 Unlubricated Friction

Coincident with the high wear rates during wear-in and during equilibrium severe wear, the coefficient of friction between the rubbing pair is high. Figure 3.4 shows a typical curve of coefficient of friction, μ, with time for

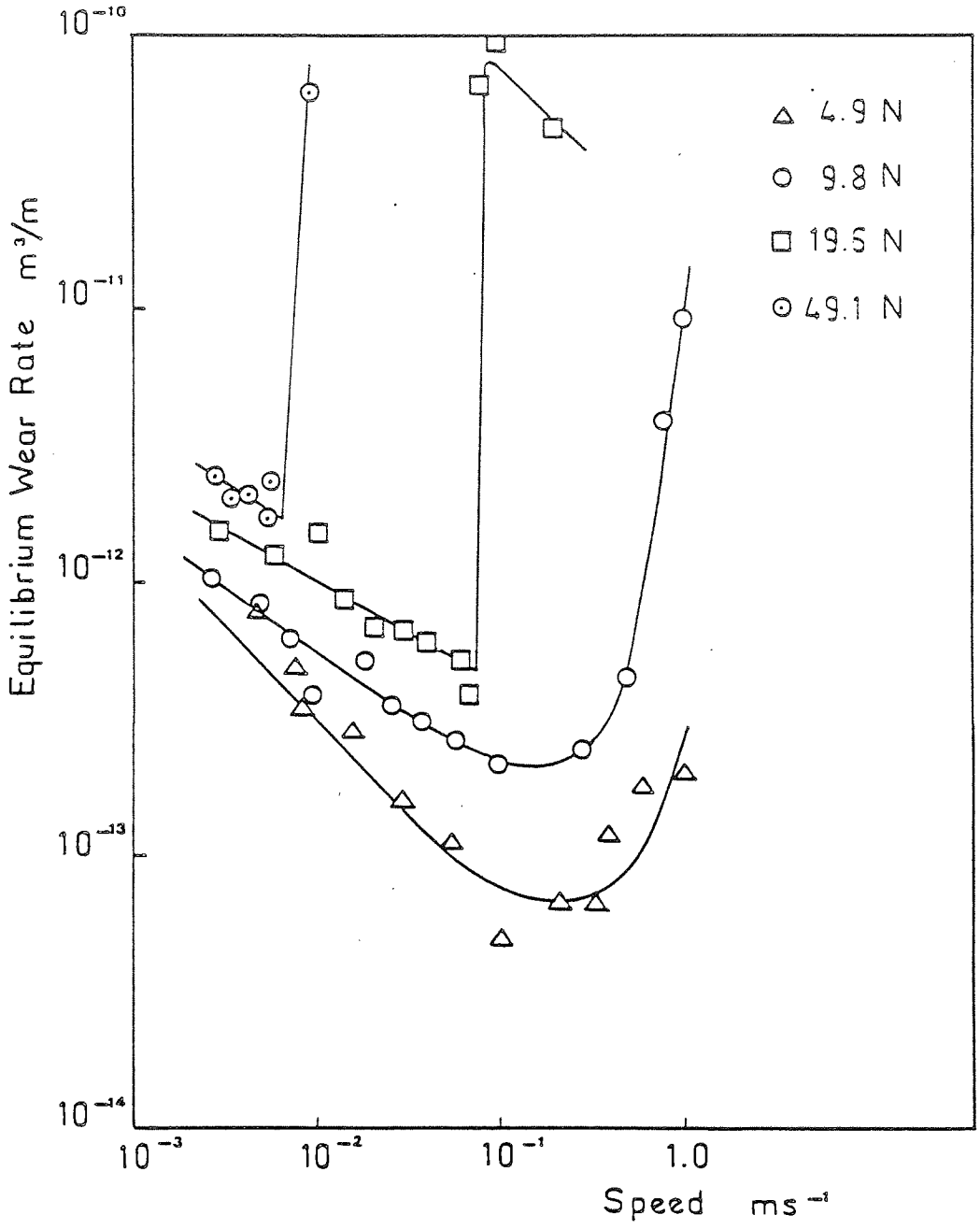

Figure 3.2

Wear rate versus speed for loads of 4.9, 9.8, 19.6 and 49.1 N.

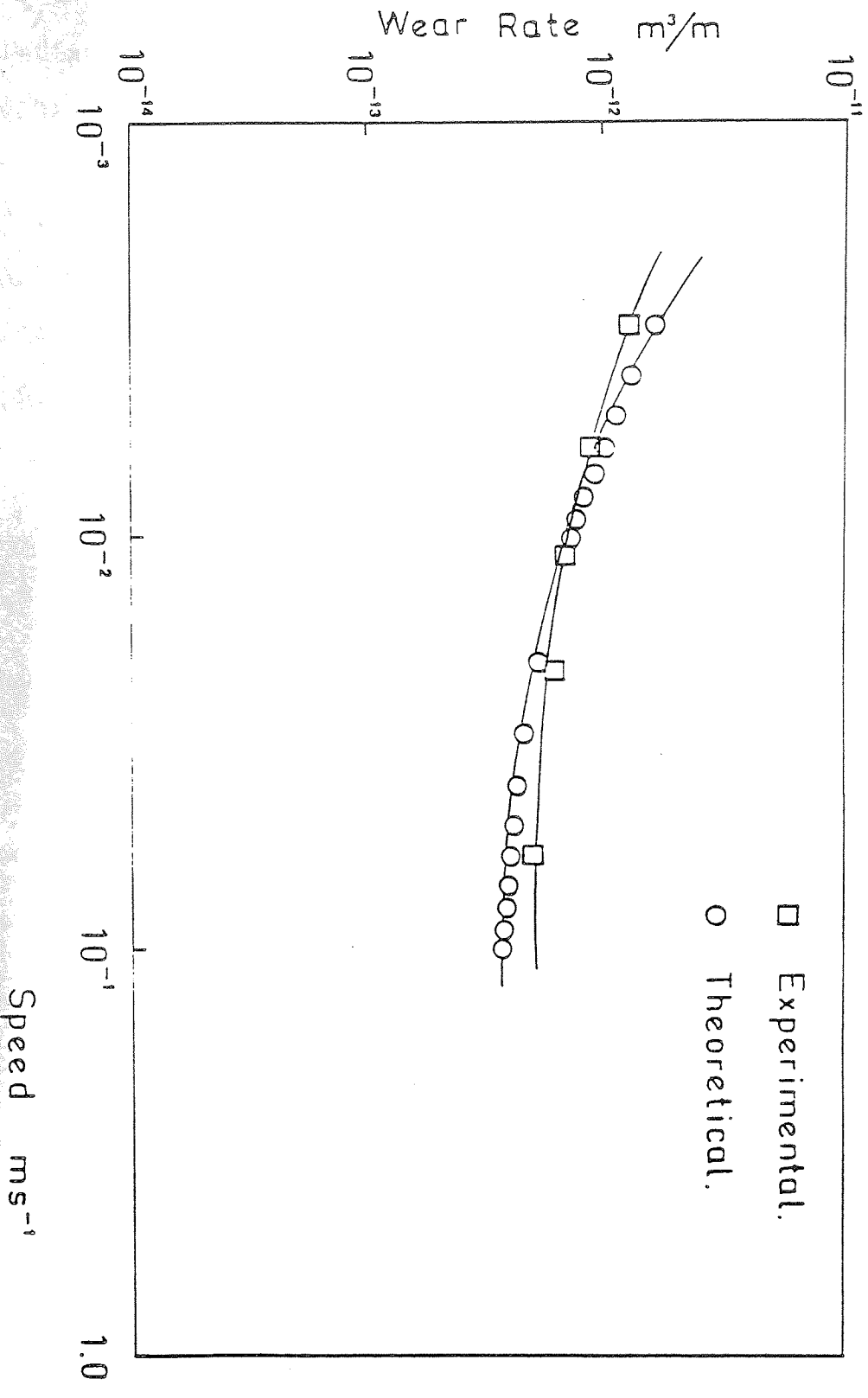

Figure 3.3

Wear rate versus speed curve for a 14.7 N load, showing also the theoretical Welsh curve for that load.

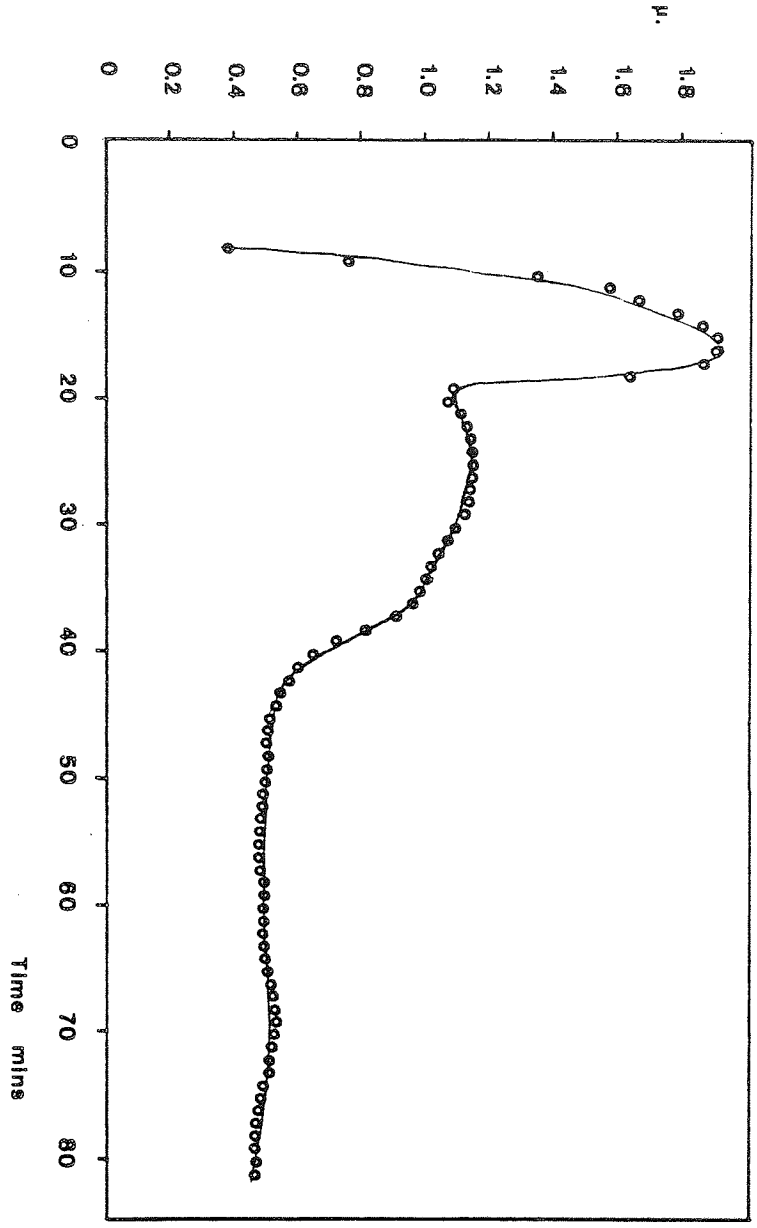

Figure 3.4

Typical variation of friction coefficient with time at the start of a test, showing attainment of equilibrium coefficient of friction.

9.8 N and 0.2 ms^{-1} at the start of a run. The trace is similar to those reported by Wilson et al[73] where the initial high friction peak of about 1.9 is explained as due to the breakdown of the air formed oxide layer at the start of rubbing. There then follows a period of high friction, with a corresponding coefficient of about 1.0, during severe wear-in as the surfaces conform; the completion of this process leads to equilibrium mild wear and another drop in friction coefficient to its equilbrium value around 0.4 or 0.5

Figure 3.5 shows the variation of equilibrium friction coefficient with speed for loads of 4.9, 9.8, 14.7, 19.6 and 49.1 N. The equilibrium values are fairly constant with load but show some increase at higher speeds. This is due to an increased proportion of metallic contact where transition effects lead to an increased proportion of metallic debris.

In this region the friction coefficient increases abruptly to about 0.7 to 0.9. This is shown most clearly in the 19.6 and 49.1 N loads where the Welsh T_1 transition is more abrupt than in the lower load curves. For speeds corresponding to the region above the T_1 transition and before the T_2 transition, there is no decrease in friction value after the initial severe wear-in period and severe adhesive metallic wear continues with characteristically high friction coefficients.

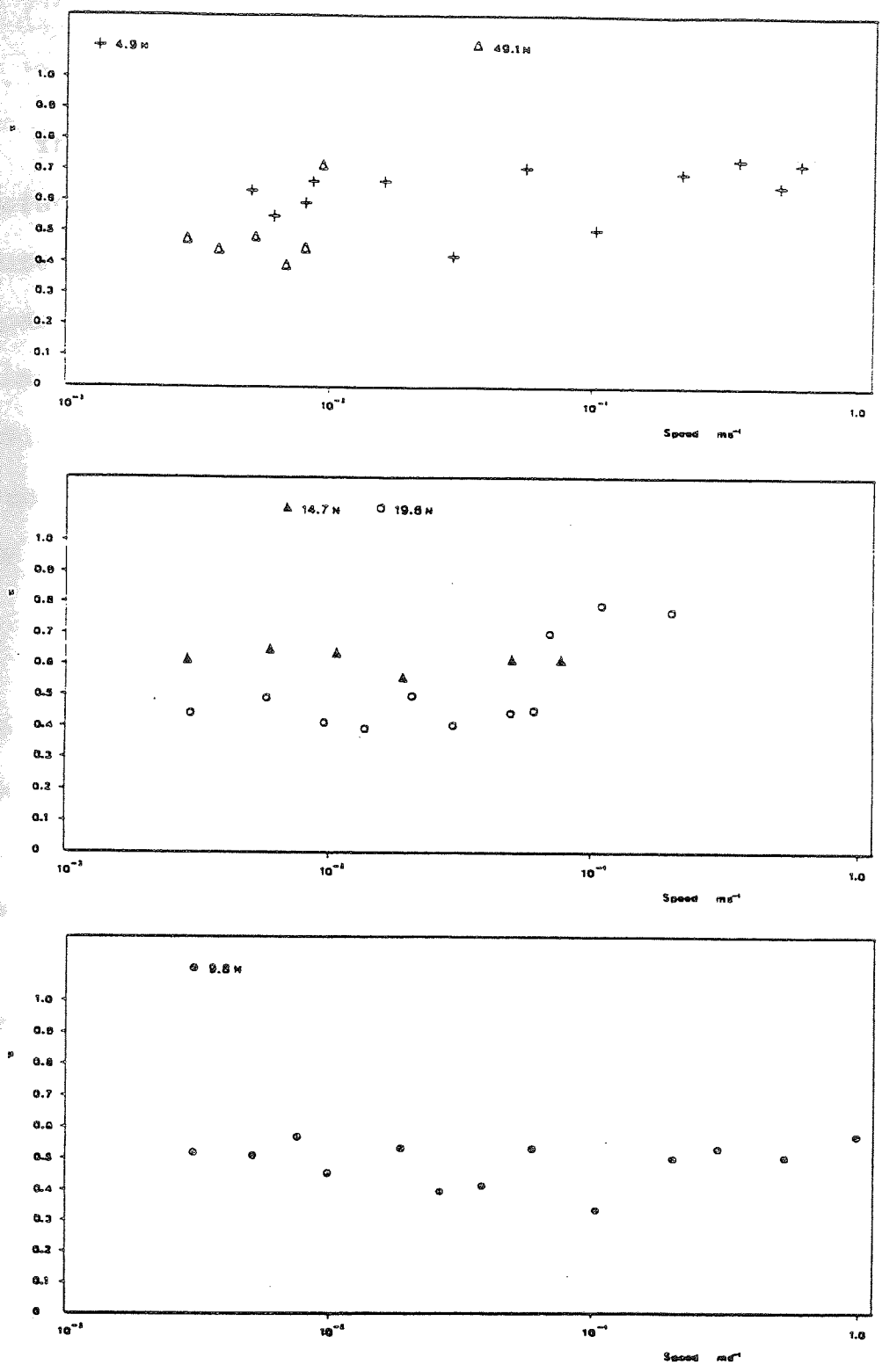

Figure 3.5

Variation of the equilibrium coefficient of friction with sliding speed for loads of 4.9, 9.8, 14.7, 19.6 and 49.1 N.

3.4 Temperature During Unlubricated Sliding

The temperatures presented in this section were obtained after equilibrium wear had been established. Figure 3.1 shows a sharp rise in general surface temperature at the start of a run which is maintained during wear-in until mild wear ensues, where there is a gradual reduction to an equilibrium level. If severe wear is maintained then, as with friction and wear, a higher more unstable general surface temperature is observed.

Equilibrium general surface temperatures, calculated using the theory presented in the previous chapter, are shown in relation to sliding speed for loads of 4.9, 9.8 and 19.6 N in Figure 3.6. It may be seen that in every case below the speeds where transition effects occur that the temperatures are very low when compared with those obtained for similar wear rates above the T_2 transition (109). This is to be expected where the lower speeds lead to less frictional heating. This is seen more clearly in Figure 3.7 where the appropriate ambient temperature has been subtracted from the general surface temperatures shown in Figure 3.6, to give the excess temperature at the pin surface. It may be seen that the curves display little difference at speeds below 10^{-1} ms^{-1} indicating negligible frictional heating in the region. At speeds corresponding to the T_1 transition, however, the curves indicate that

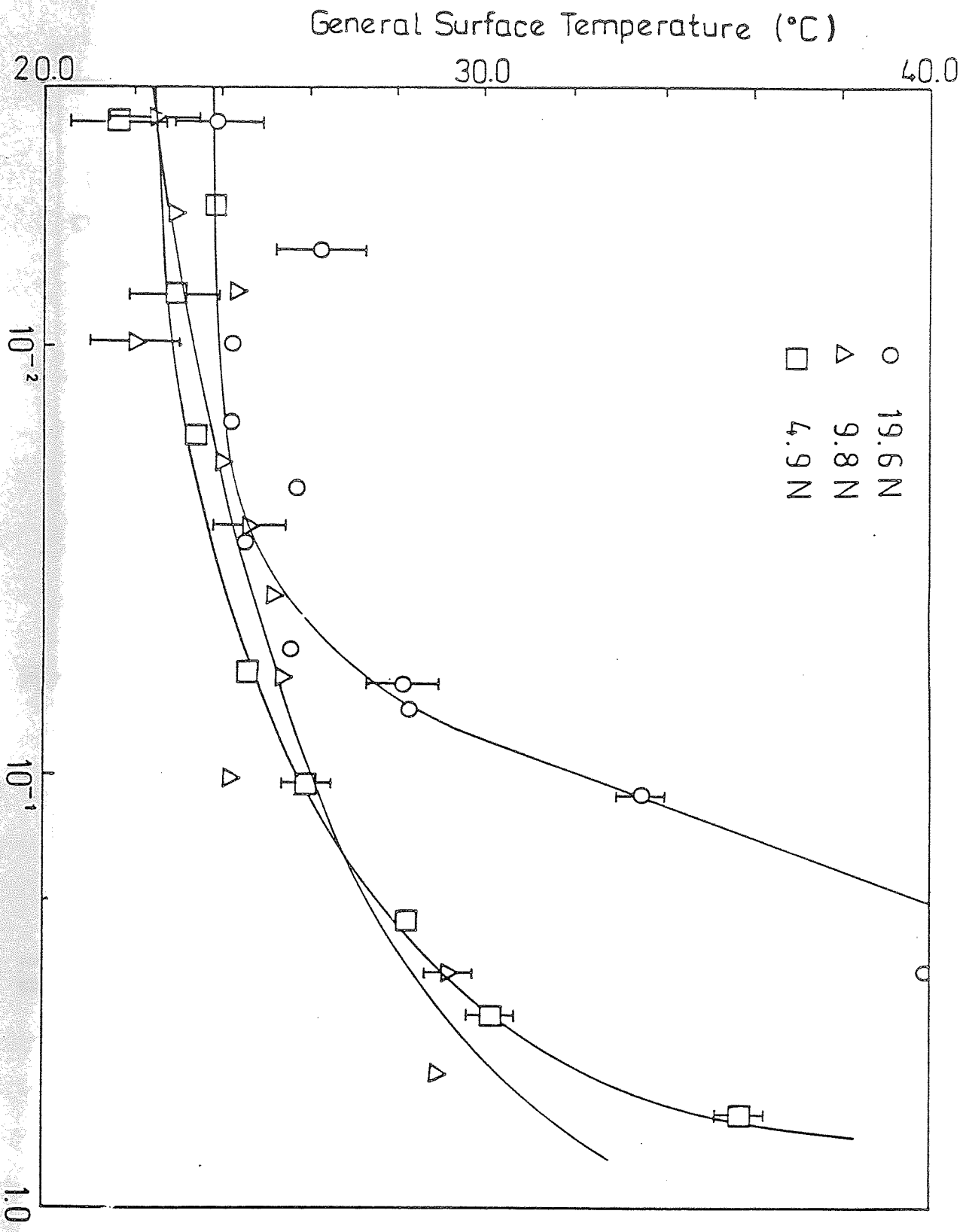

Figure 3.6

Variation of general surface temperature with speed for loads of 4.9, 9.8 and 19.6 N.

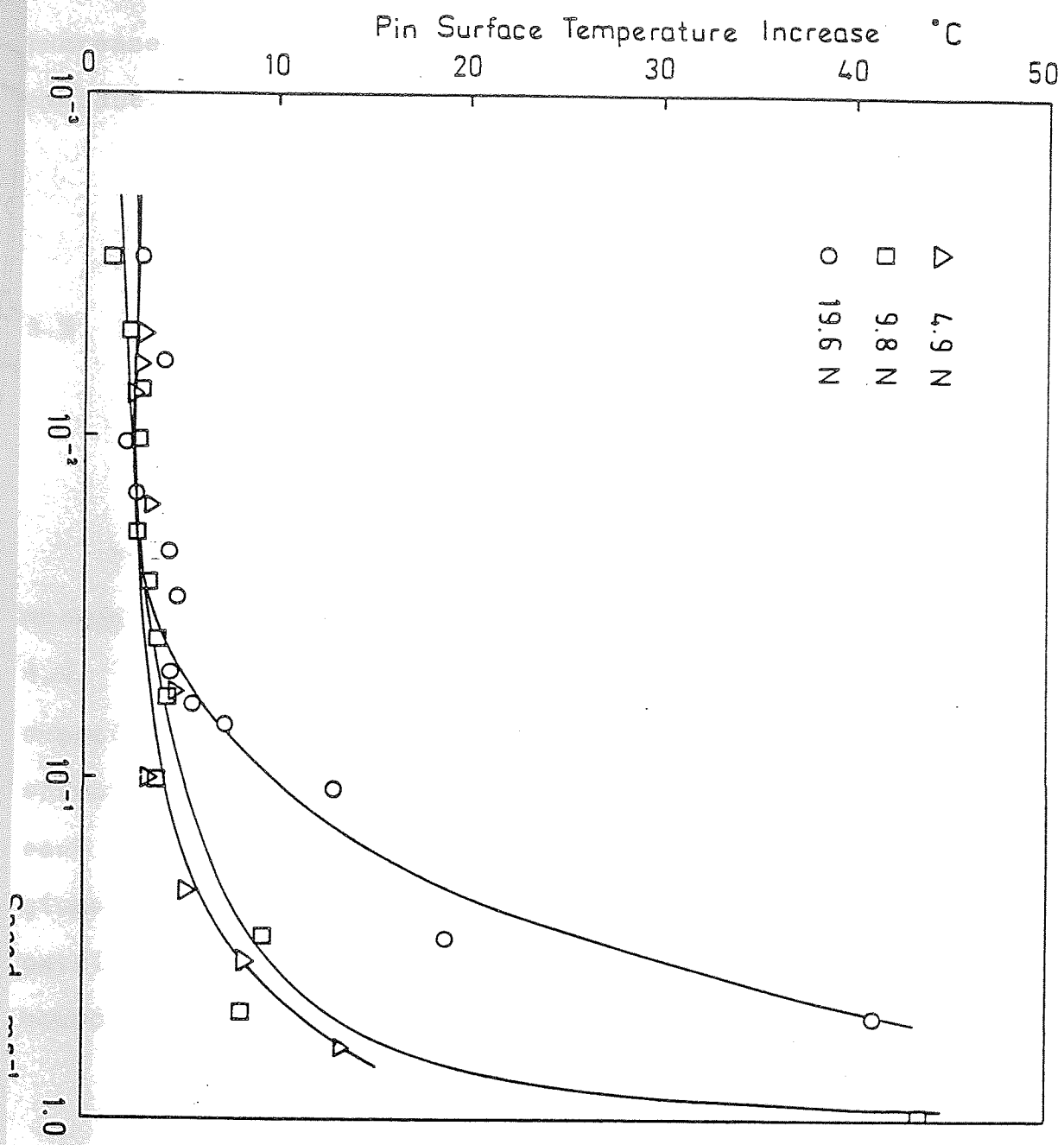

Figure 3.7

Variation of frictionally generated general surface temperature with speed for loads of 4.9, 9.8 and 19.6 N.

large increases in temperature occur, coincident with increased coefficients of friction and greater metallic contact.

3.5 Scanning Electron Microscopy using Samples from Unlubricated Sliding

This section presents typical scanning electron micrographs of selected worn pin surfaces for the loads 4.9, 9.8 and 19.6 N each for a high and low speed experiment for comparison, although a complete range of speeds has actually been examined by this technique. In each case, where possible, a low magnification view is given, followed by two micrographs which illustrate some particular surface feature, especially oxide/metal boundaries and plateaux edges.

Figure 3.8 shows micrographs of a worn pin surface from an experiment run at 4.9 N load and for $0.005 ms^{-1}$. Figure 3.8a shows that the oxide layer has been formed by transfer and growth of material over existing surface features. Figures 3.8b and c show the smooth, uniform nature of the oxide at another position and a high magnification view of an oxide edge respectively.

Figure 3.8

Scanning electron micrographs of worn pin surfaces run at a load 4.9 N and at 0.005 ms^{-1}

a.

b.

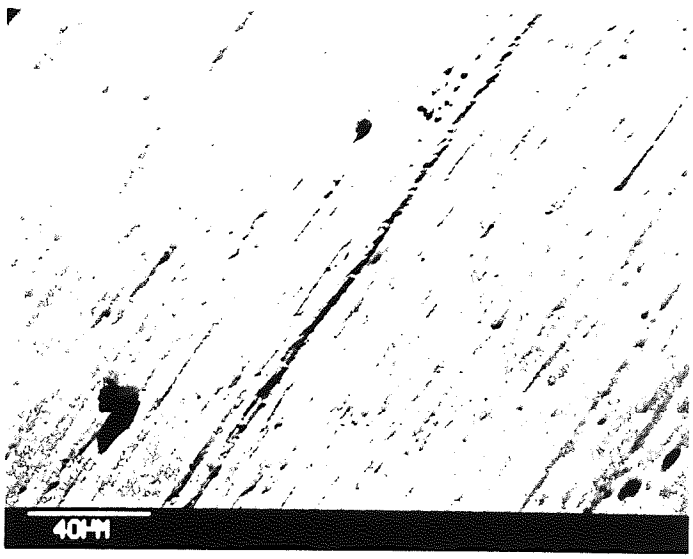

c.

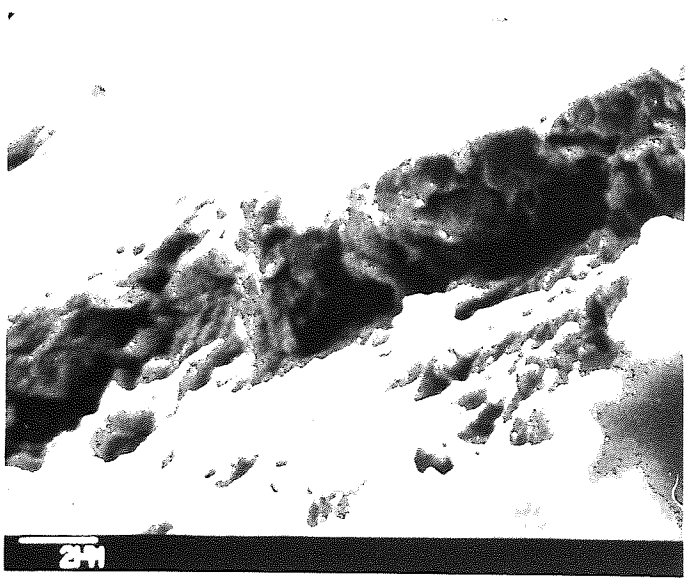

Figure 3.9 is of a pin run at 4.9 N and 0.1 ms^{-1}, this figure also shows that the oxide has formed over existing surface features. Comparing Figures 3.8c and 3.9c shows some difference in the oxide thicknesses for these two speeds.

Figure 3.10 shows a large oxide plateaux, at 9.8 N and 0.003 ms^{-1}, about to break away from the surface. Figures 3.10b and c clearly show the agglomerate nature of this plateaux, layers of oxide may be distinguished and some fine structure to the oxide is apparent. For the same load but 0.216 ms^{-1}, Figure 3.11c displays similar fine structure to Figure 3.10c, but is much thicker. Figure 3.11 displays a much more uniform surface with extensive oxide coverage, which is typical of all surfaces examined.

Figures 3.12 and 3.13 show pin surfaces for 19.6 N and 0.003 ms^{-1} and 0.05 ms^{-1} respectively. Once again extensive oxide coverage is seen. In particular, Figure 3.12c shows the granular nature of the oxide, and as is postulated in a later section, the sintered nature of the oxide. Figure 3.13c shows an oxide plateaux breaking away from the surface. This micrograph displays many features seen on surfaces examined; the oxide appears thicker than that shown in Figure 3.12c and if inspected closely shows the same sintered structure, appearing more compacted than that in Figure 3.12c. Also apparent is the non-uniform surface of the metal substrate indicating that the oxide has been

Figure 3.9

Scanning electron micrographs of worn pin surfaces run at a load of 4.9 N and at 0.1 ms^{-1}

a.

b.

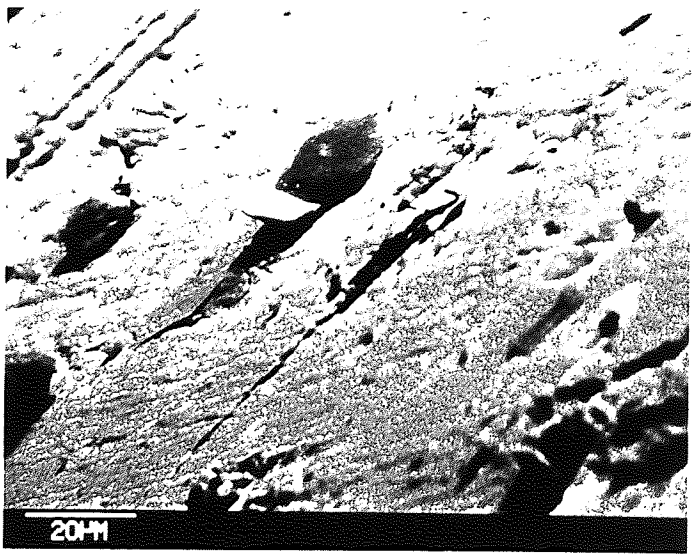

c.

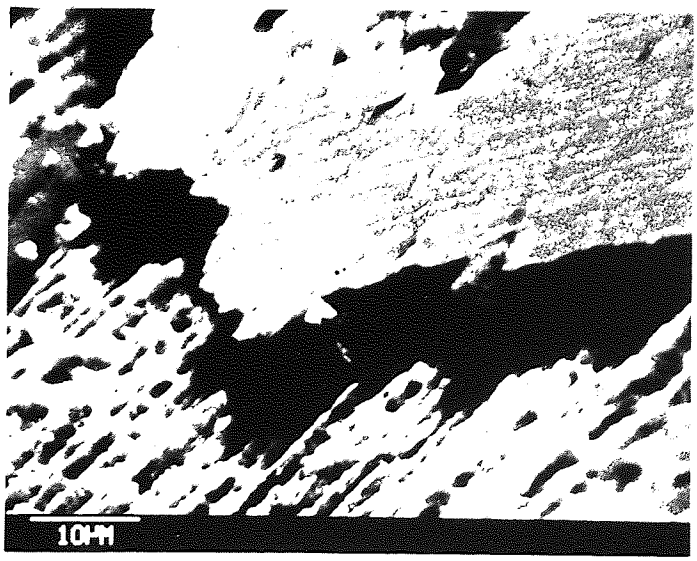

Figure 3.10

Scanning electron micrographs of worn pin surface run at a load of 9.8 N and at 0.003 ms^{-1}

a.

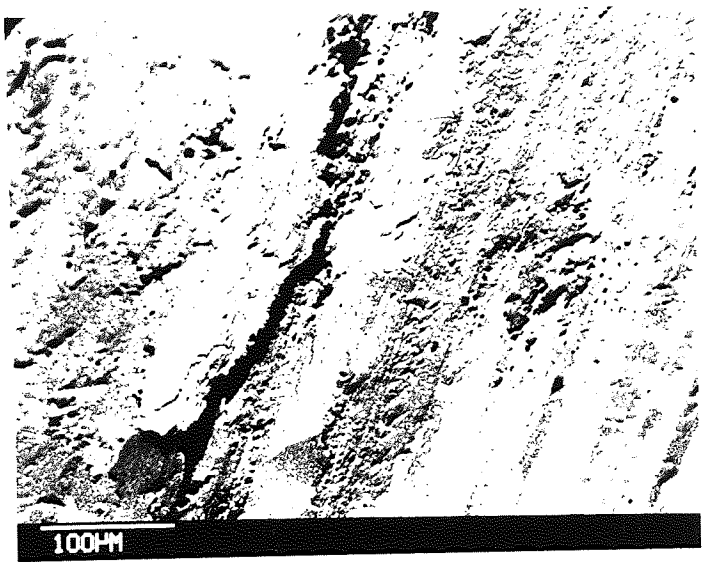

b.

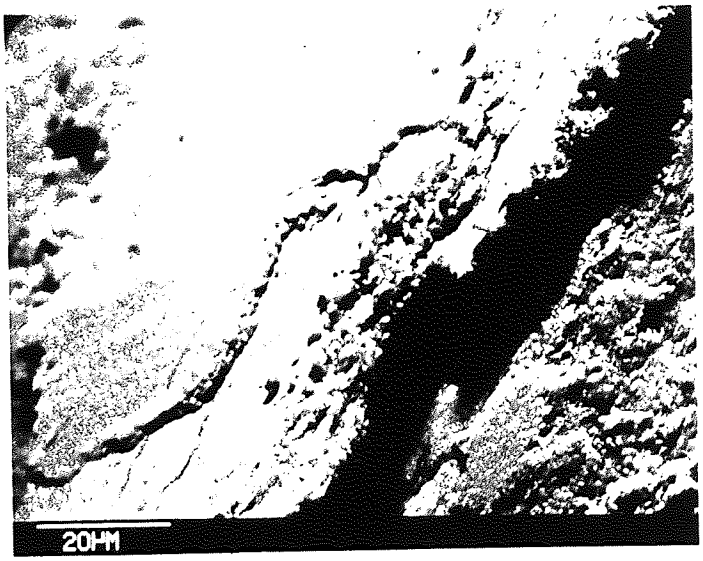

c.

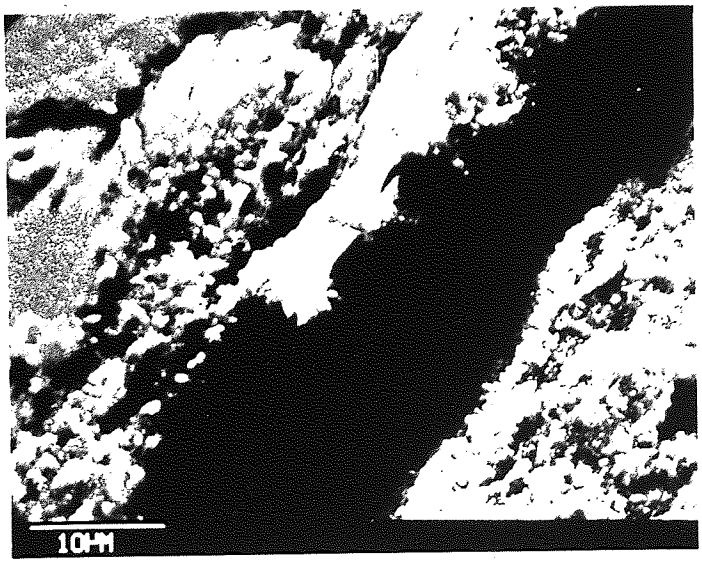

Figure 3.11

Scanning electron micrographs of a worn pin surface run at a load of 9.8 N and at 0.216 ms^{-1}

a.

b.

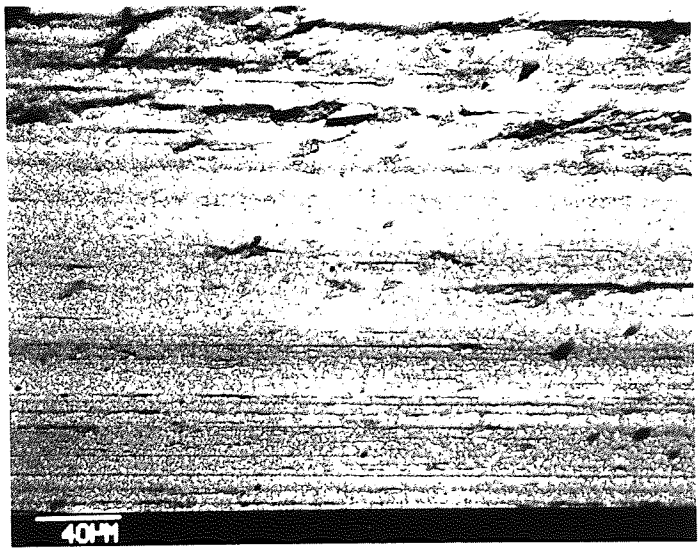

c.

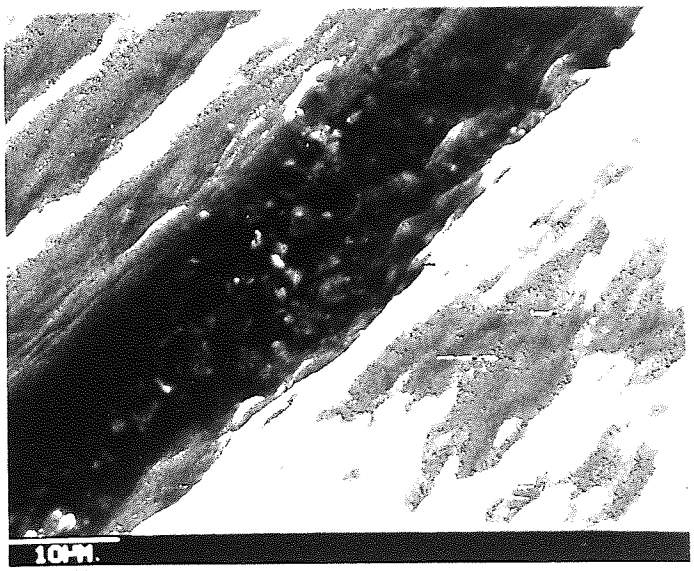

Figure 3.12

Scanning electron micrographs of a worn pin surface run at a load of 19.6 N and at 0.003 ms^{-1}

a.

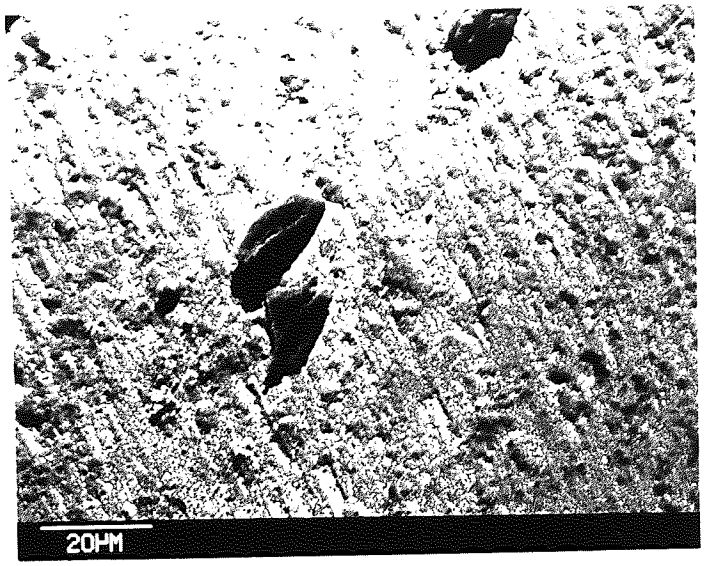

b.

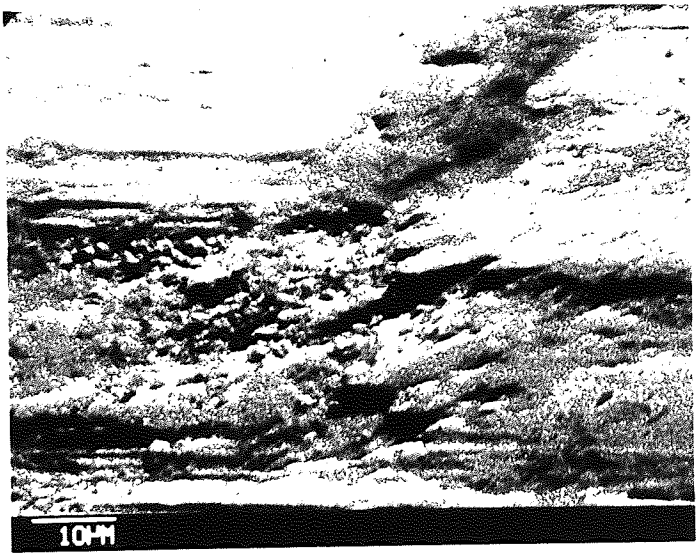

c.

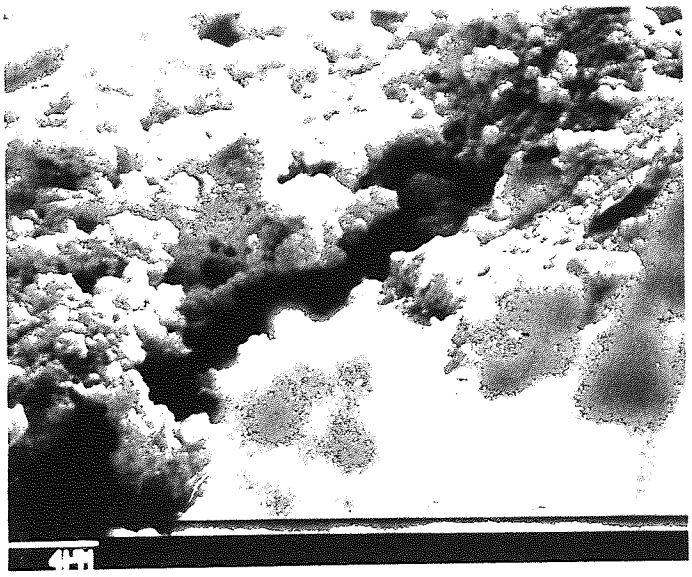

Figure 3.13

Scanning electron micrographs of a worn pin surface run at a load of 19.6 N and at 0.05 ms^{-1}

a.

b.

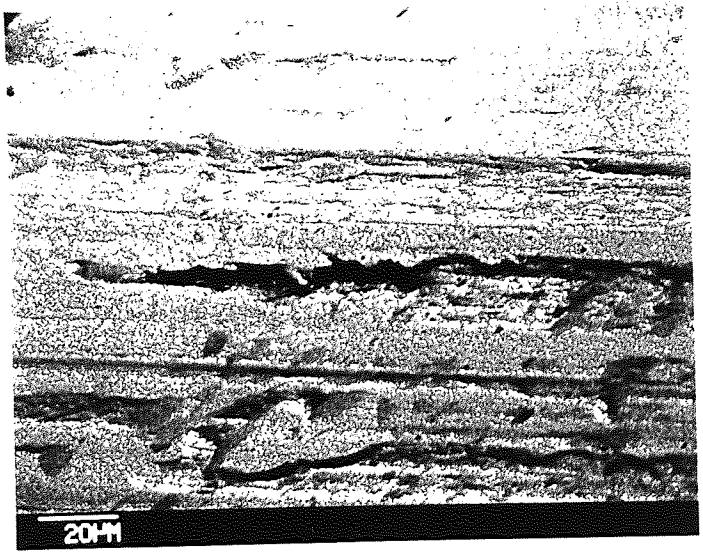

c.

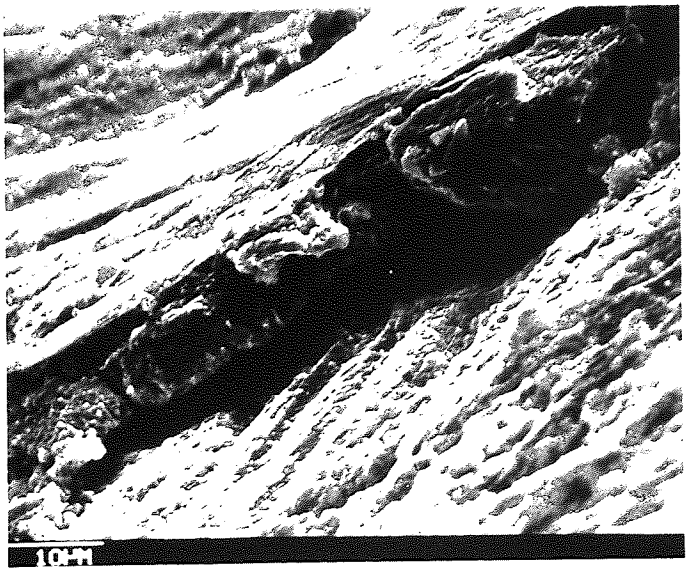

enerated, transferred and deposited here from another area f the pin.

3.6 Microhardness Determined for Samples from Unlubricated Sliding

Microhardness versus depth curves from some selected worn pin specimens are shown in Figure 3.14. The figure shows two conditions of speed of 5×10^{-3} ms^{-1} and 0.1 ms^{-1} (0.05 ms^{-1} for 19.6 N) each for loads of 4.9, 9.8 and 19.6 N. It can be seen in all cases that immediately below the surface are work hardened layers. As shown in the figure, the depth of the layer increases with speed and hardness values are generally higher for higher loads.

For the 19.6 N load it was necessary to use a lower speed specimen to remain below the T_1 tranisition. The indentations do not go any closer to the surface than 8μm due to the problem of cracking and thus irregularity in the diamond indentation.

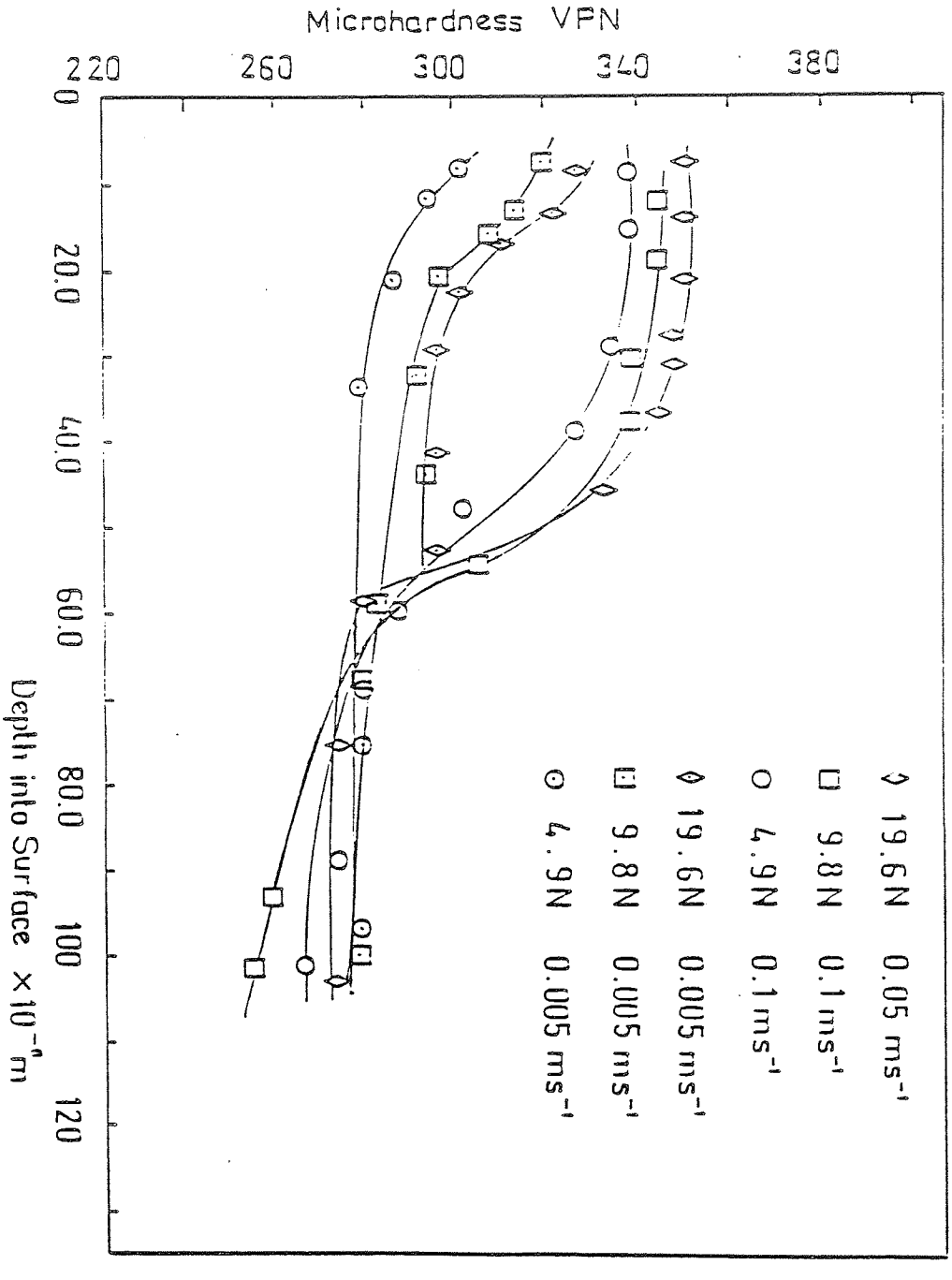

Figure 3.14

Variation of microhardness values with depth into the surface for differing load and speed variations.

3.7 Contact Resistance Measurements for Unlubricated Sliding

The contact resistance between pin and disc was monitored periodically during many of the wear experiments. It was found, however, that the chart recorder interfered in some way with the A/D converter and so continuous measurement was obtained in some cases by repeating an experiment. Otherwise contact resistance could be observed by the use of an oscilloscope. The characteristics of the contact resistance traces are typical of those observed by other workers (103). At the outset of an experiment the contact resistance is seen to be low, indicating metal-metal contact, fluctuating rapidly with no consistent trends apparent. This is typical of severe wear, and in the region above the T_1 transition where this is maintained the contact resistance trace quickly drops to the short circuit 1Ω region and remains there.

However, in the region below the T_1 transition where mild oxidational wear ensues quite rapidly a trace typical of that shown in figure 3.15 is seen. The contact resistance, instead of dropping to zero, climbs yet higher and commences a more uniform fluctuation as a protective, and electrically insulating, oxide layer builds up. Two regions from this schematic are shown in figure 3.16 and represent parts of the trace taken at 9.8 N and 0.1 ms^{-1}.

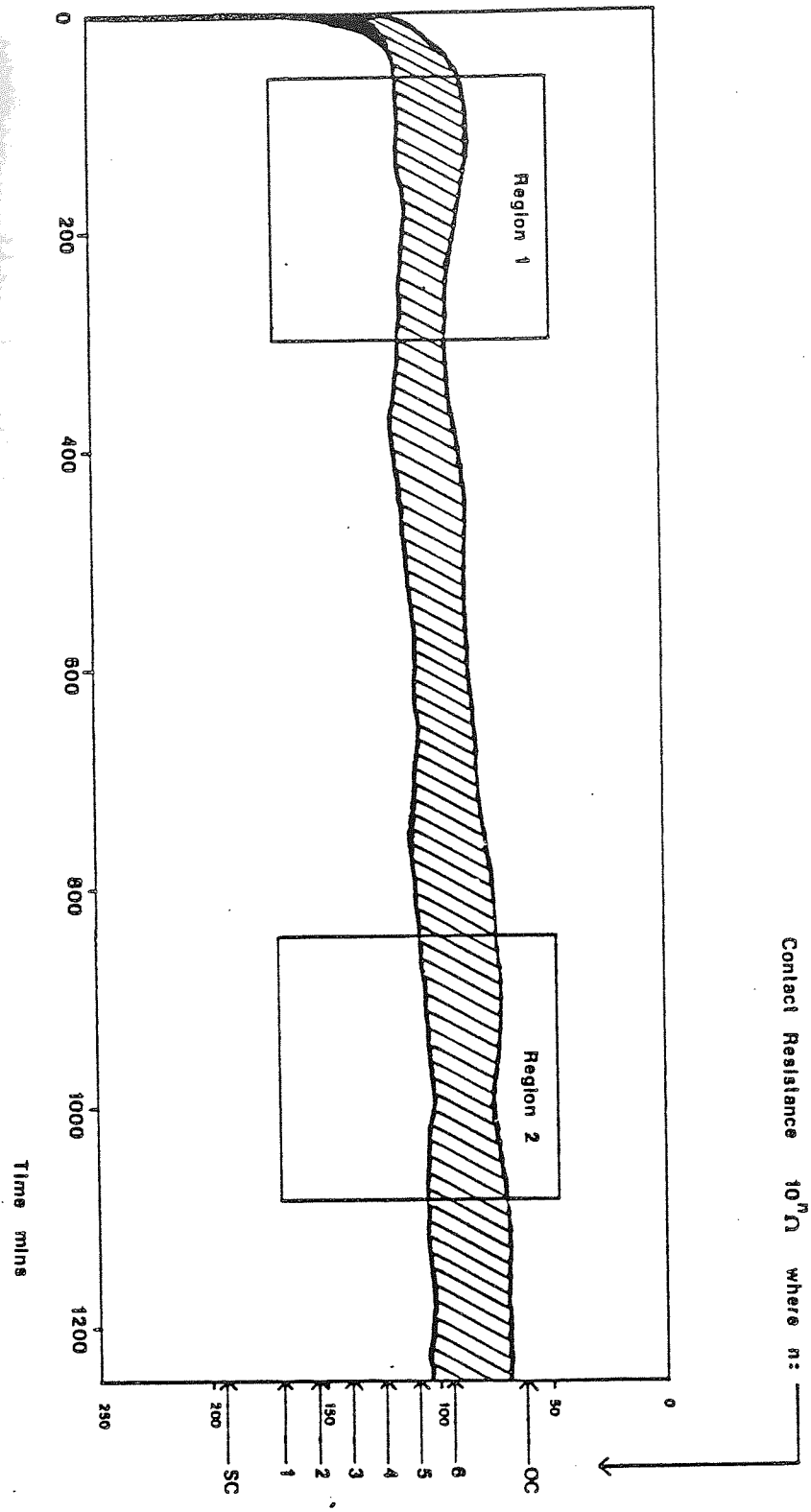

Figure 3.15

Representation of the contact resistance trace, from a load of 9.8 N and 0.1 ms^{-1}, with time. In the diagram OC is open circuit and SC is short circuit.

Region 1.

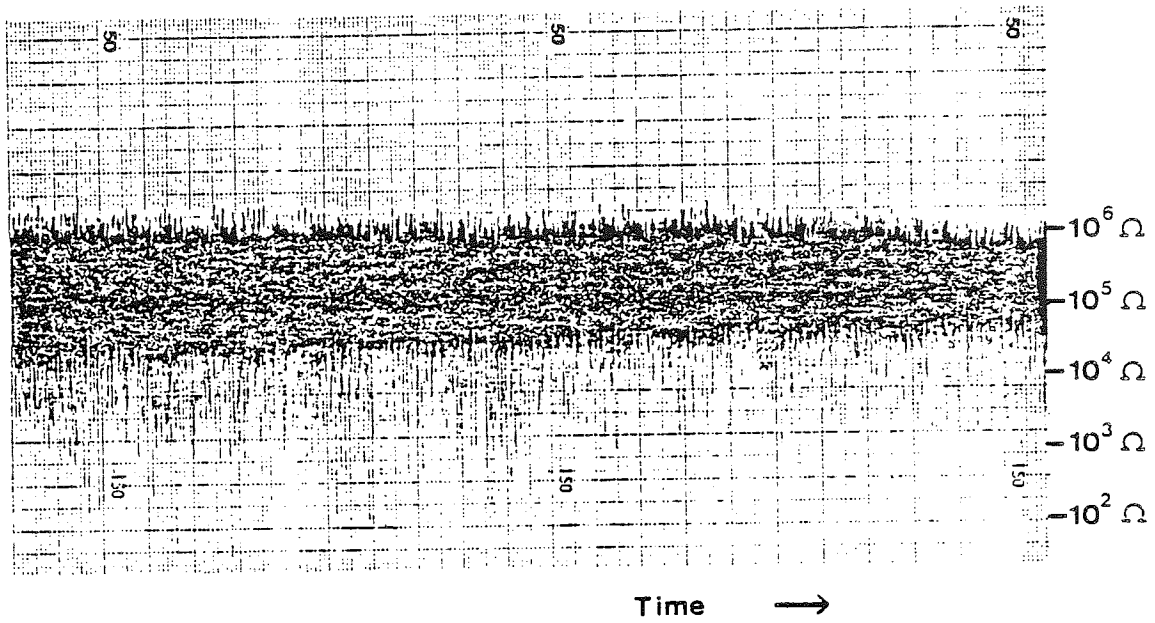

Region 2.

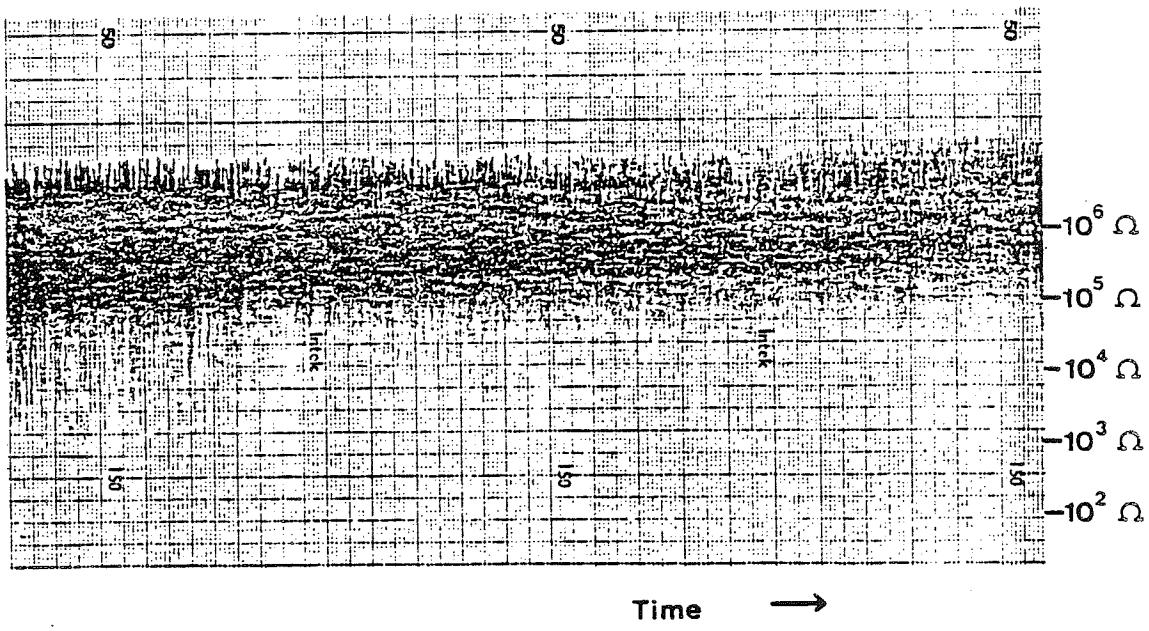

Figure 3.16

Contact resistance traces of two regions of the curve shown in Figure 3.15 showing the actual transient variation.

The original scale of these traces was 1 mm min^{-1} but is now more, due to photocopier reduction; the actual scale may be seen more clearly with reference to figure 3.15, comparing the two regions the contact resistance can be seen to have increased from about $10^5\Omega$ to $10^6\Omega$ in the space of 10^3 minutes. The sharp fluctuations in the traces are due to metallic asperity contact which causes a rapid transient drop in resistance. Notice how there is little comparative fluctuation at the high resistance side of the traces. Each trace is about 5 x $10^5\Omega$ in width showing a great variation in contact resistance during the rotation of the disc. From figure 3.15 it may be seen that there are also long term fluctuations in contact resistance which may be due to the periodic removal of large oxide plateaux, which disturbs for a time the contact resistance equilibrium. The contact resistance device has a non-linear characteristic below $10^0\Omega$, and above $10^6\Omega$ and thus the trace in figure 3.15 varies in fact only a little above $10^6\Omega$.

3.8 Powder X-Ray Diffraction of Debris Collected from Unlubricated Sliding

This section presents microdensitometer traces resulting from powder diffraction X-ray photographs for four loads of 4.9, 9.8, 19.6 and 49.1 N. Care should be

taken when comparing traces between loads and also between speeds at a given load; this is due to variations in the densitometer sensitivity, sample purity and developer concentration, any or all of which may change between films.

Figures 3.17 to 3.20 show microdensitometer traces for constant load but with increasing speed. Figure 3.17 is from 4.9 N load and shows (a) 0.006 ms^{-1}, (b) 0.008 ms^{-1}, (c) 0.016 ms^{-1}, (d) 0.1 ms^{-1} and (e) 0.6 ms^{-1}. Figure 3.18 is from 9.8 N load and shows (a) 0.005 ms^{-1}, (b) 0.0075ms^{-1},(c) 0.02 ms^{-1}, (d) 0.06 ms^{-1} and (e) 0.8 ms^{-1}. Figure 3.19 is from 19.6 N load and shows (a) 0.005 ms^{-1}, (b) 0.01 ms^{-1}, (c) 0.03 ms^{-1} and (d) 0.1 ms^{-1}. Figure 3.20 is from 49.1 N load and shows (a) 0.003 ms^{-1}, (b) 0.004 ms^{-1}, (c) 0.005 ms^{-1}, (d) 0.007 ms^{-1} and (e) 0.01 ms^{-1}. In each case, seen most clearly in Figures 3.17 and 3.18, the α-Fe content of the debris is seen to increase while the α-Fe_2O_3 decreases accordingly. This is to be expected as increased speed reduces oxidation time between successive asperity encounters giving rise to an increased proportion of encounters producing metallic debris. This effect is predicted by the oxidational wear model developed in a later section where increased speed reduces the effectiveness of the oxidation component of the wear which leads ultimately to the T_1 transition and purely metallic debris seen in Figures 3.18 (e), 3.19 (d) and 3.20 (e).

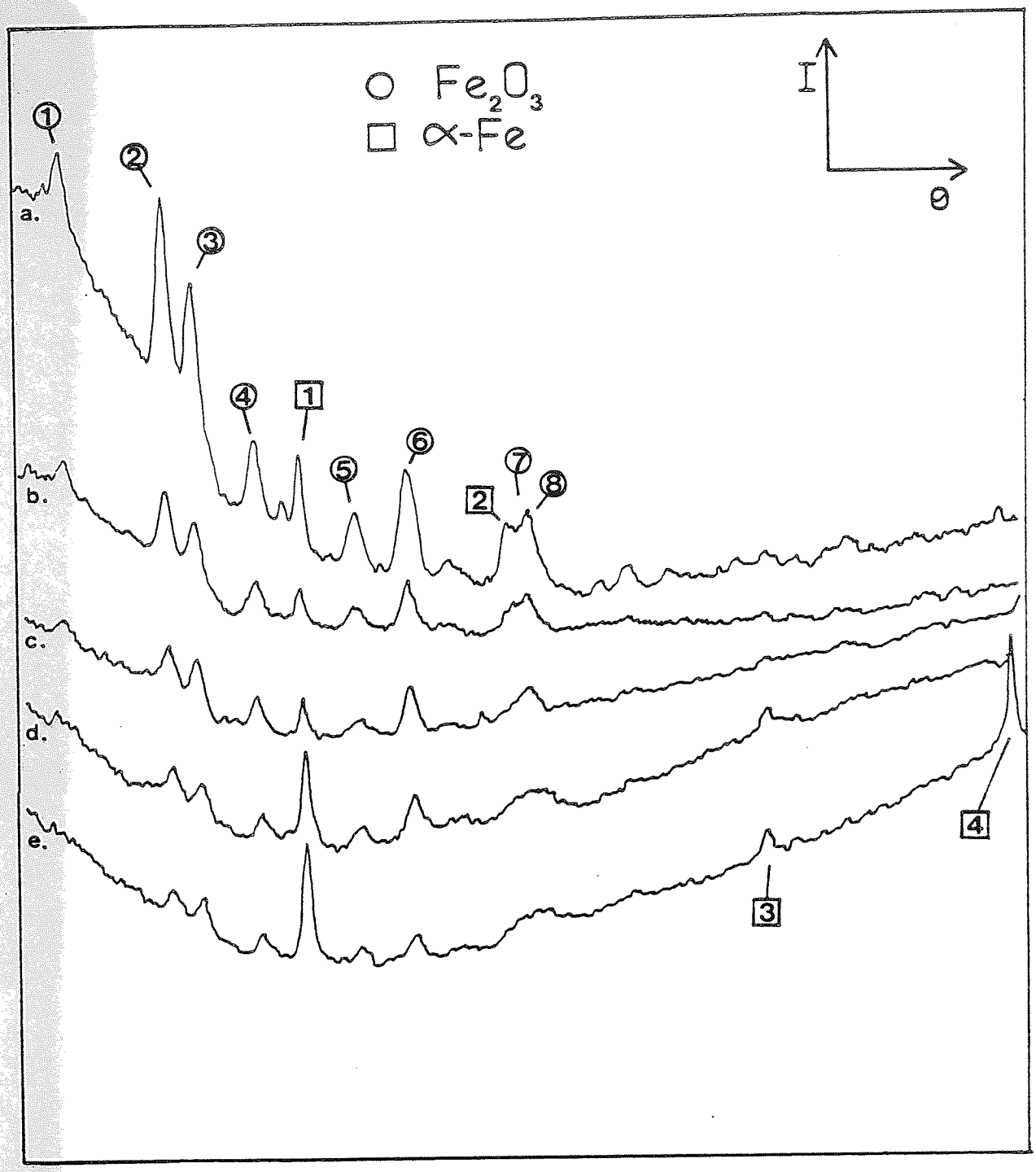

Figure 3.17

Microdensitometer traces for a load of 4.9 N and speeds of (a) 0.005, (b) 0.008, (c) 0.016, (d) 0.1, and (e) 0.6 ms^{-1}.

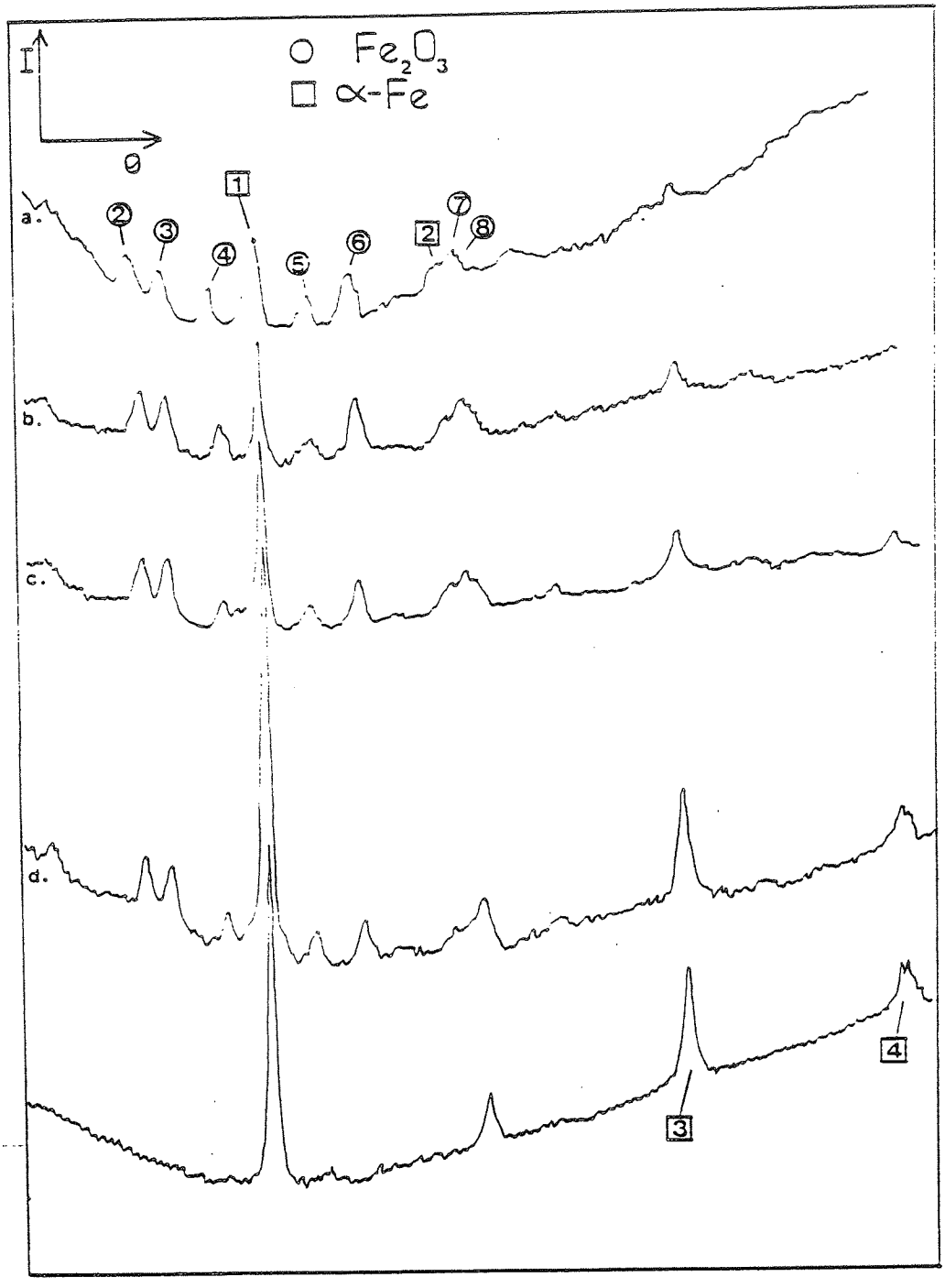

Figure 3.18

Microdensitometer traces for a load of 9.8 N and speeds of (a) 0.005, (b) 0.0075, (c) 0.02, (d) 0.06 and (e) 0.8 ms^{-1}

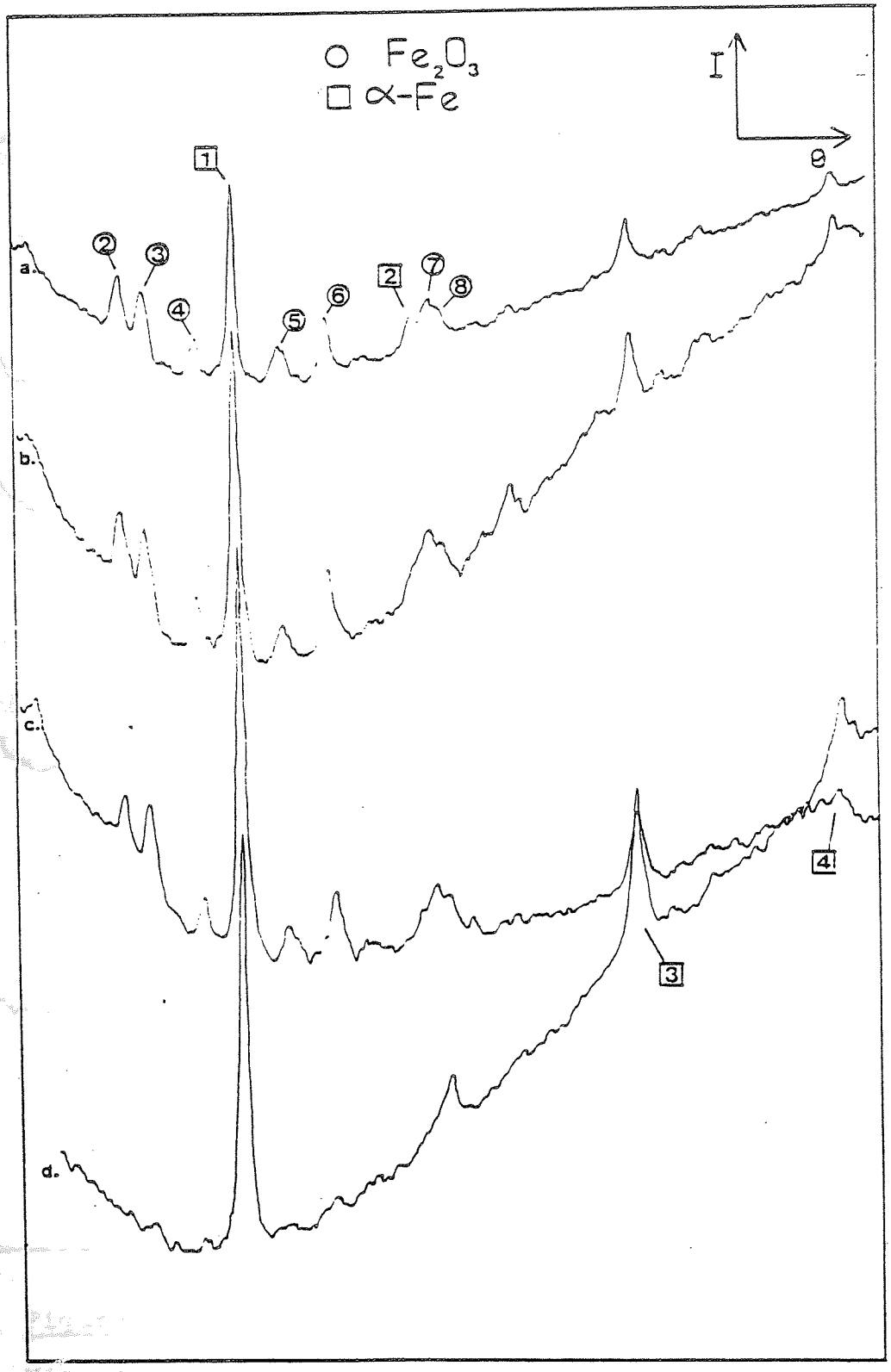

Figure 3.19

Microdensitimeter traces for a load of 19.6N and speeds of (a) 0.005, (b) 0.01, (c) 0.03 and (d) 0.1 ms^{-1}

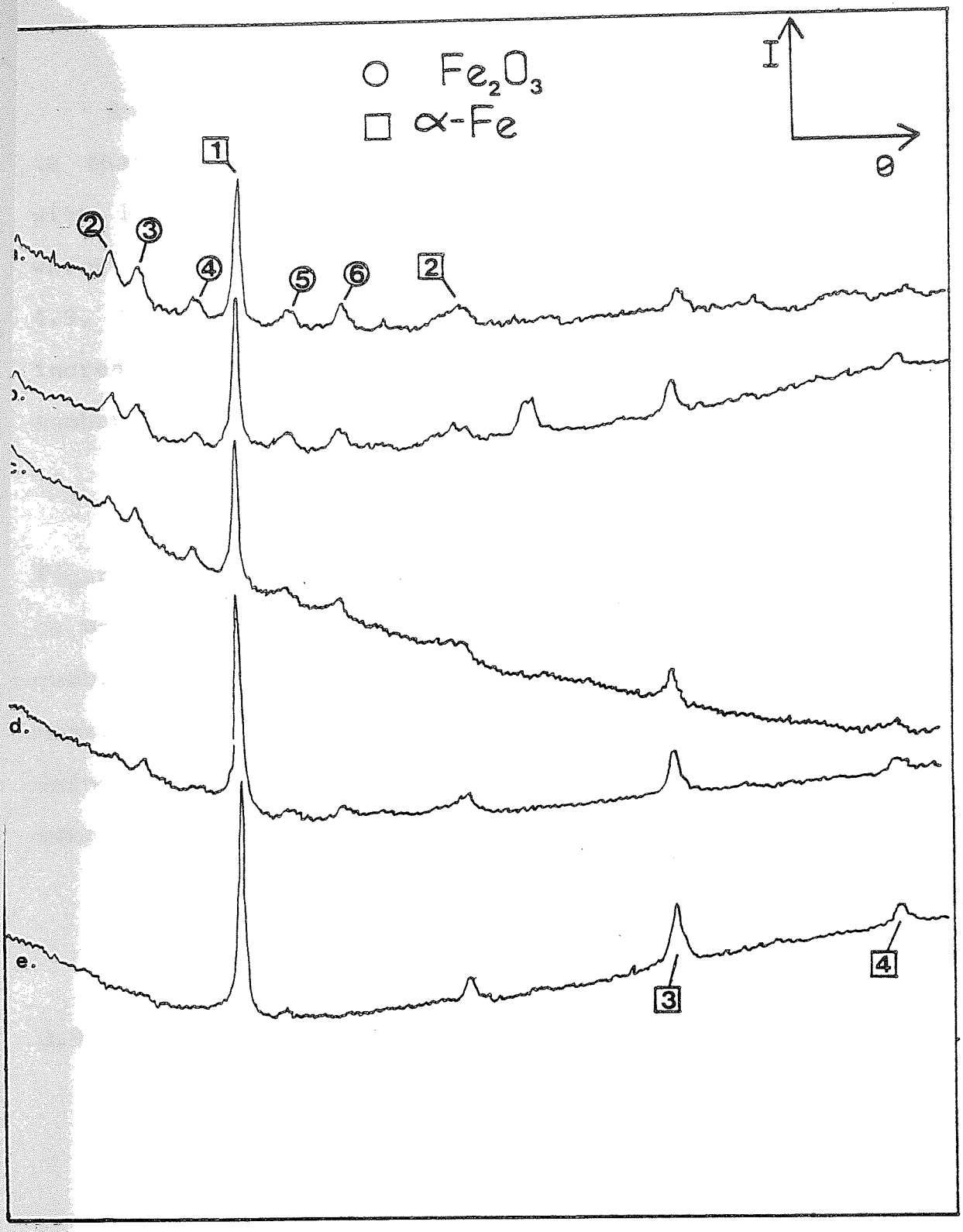

Figure 3.20

Microdensitometer traces for a load of 49.1 N of (a) 0.003, (b) 0.004, (c) 0.005, (d) 0.007 and (e) 0.01 ms^{-1}.

Another feature which is apparent from these figures is that for a given speed the metallic debris increases with load. This is shown more clearly in Figure 3.2.1 which shows traces for a speed of 0.005 ms^{-1} and for loads 4.9, 9.8 and 19.6 N. The α-Fe peak is clearly seen to increase with load, which is due to an increase in the number and frequency of metallic contacts.

In every case the microdensitometer traces seen in Figures 3.17 to 3.21 show the rhombohedral oxide α-Fe_2O_3 or α-Fe_2O_3 mixed with α-Fe. Under no speed or load combinations below the T_1 transition was any other oxide observed. This is an important point to note in favour of using the general surface temperatures as the oxidational temperature while modelling the wear mechanism.

3.9 Auger Electron Spectroscopy using Samples from Unlubricated Sliding.

The Auger electron depth profiles presented here provide important information on the oxide thickness and on the mechanism of formation of the oxide.

Figure 3.22 shows the depth profiles for a speed of 0.005 ms^{-1} and (a) 4.9, (b) 9.8 and (c) 19.6 N loads.

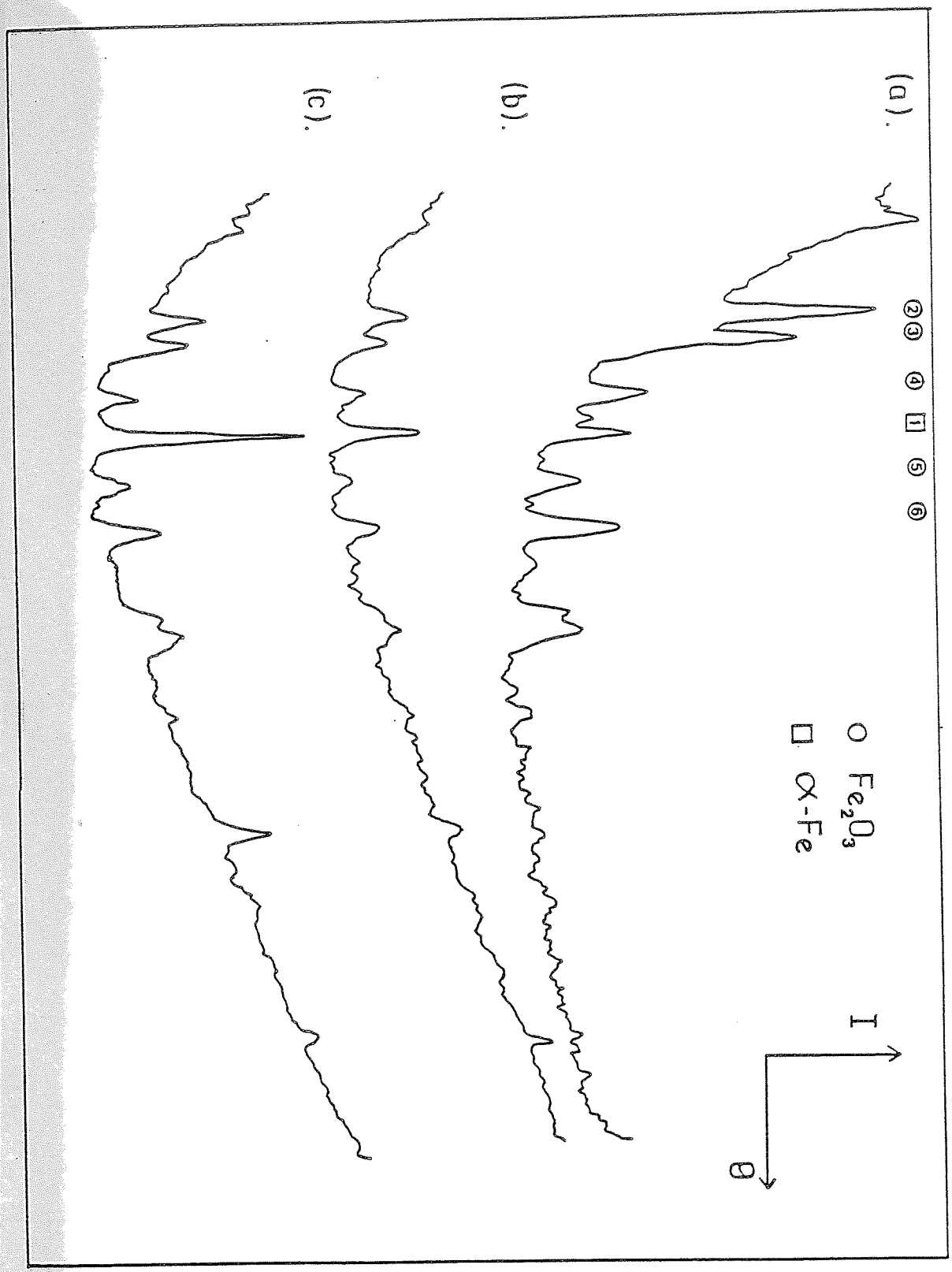

Figure 3.21

Microdensitometer traces for a speed of 0.005 ms^{-1} and loads of (a) 4.9, (b) 9.8 and (c) 19.6N.

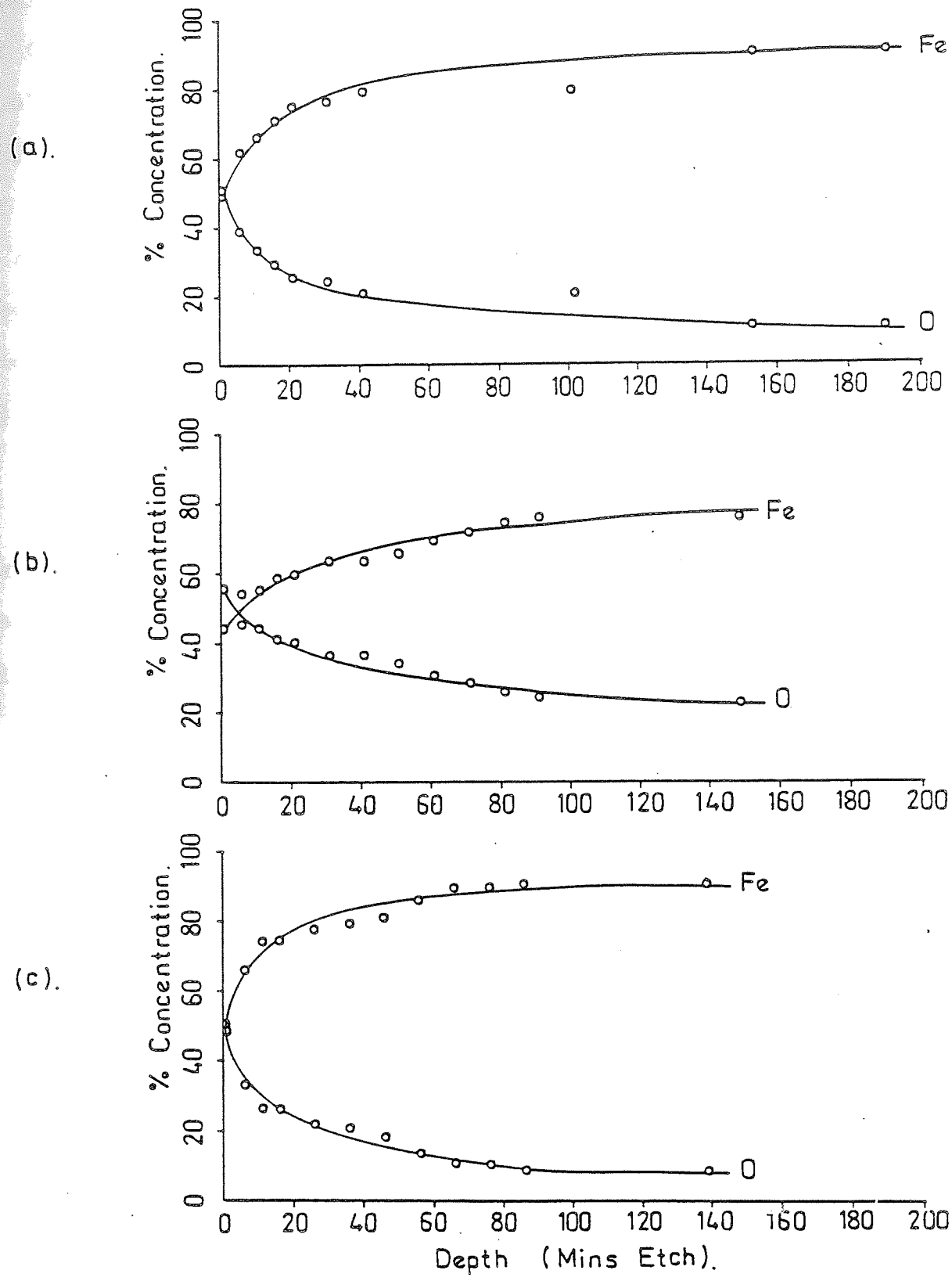

Figure 3.22

Auger electron depth profiles for a speed of 0.005 ms^{-1} and loads of (a) 4.9, (b) 9.8 and (c) 19.6 N.

Similarly Figure 3.23 shows the profiles for a speed of 0.1 ms^{-1} and (a) 4.9, (b) 9.8 N loads, and (c) for 0.05 ms^{-1} at 19.6 N load. The profiles show two features which are important in the understanding of the mechanism of formation of the oxide film. Firstly the profiles show a gradation of oxide (oxygen) through the oxide layer and secondly, they show a marked increase in thickness with increase in speed, the latter result supports the evidence of the scanning electron micrographs (section 3.5).

In each case there is an 8% background of adventitious oxygen. With a calculated removel rate of 30 $\mathring{A}\ min^{-1}$ etch the results here give good agreement with those of scanning electron microscopy. In cases of figures 3.23 (a) and (b) the curve has been terminated at 20%, or more, oxygen for clarity. The experiments continued for around 1500 - 2000 minutes corresponding to oxide thicknesses of 4.5 to 6.0 µm. The curves in figures 3.22 (a) and (c) are complete and correspond to oxide thicknesses around 0.5 to 1.0 µm. The etch rate is not very consistent, but the difference in oxide thickness with speed is nevertheless quite apparent.

The reduction of oxide (oxygen) with depth into the oxide layer is typical of agglomerate oxide profiles, and will be discussed in a later section.

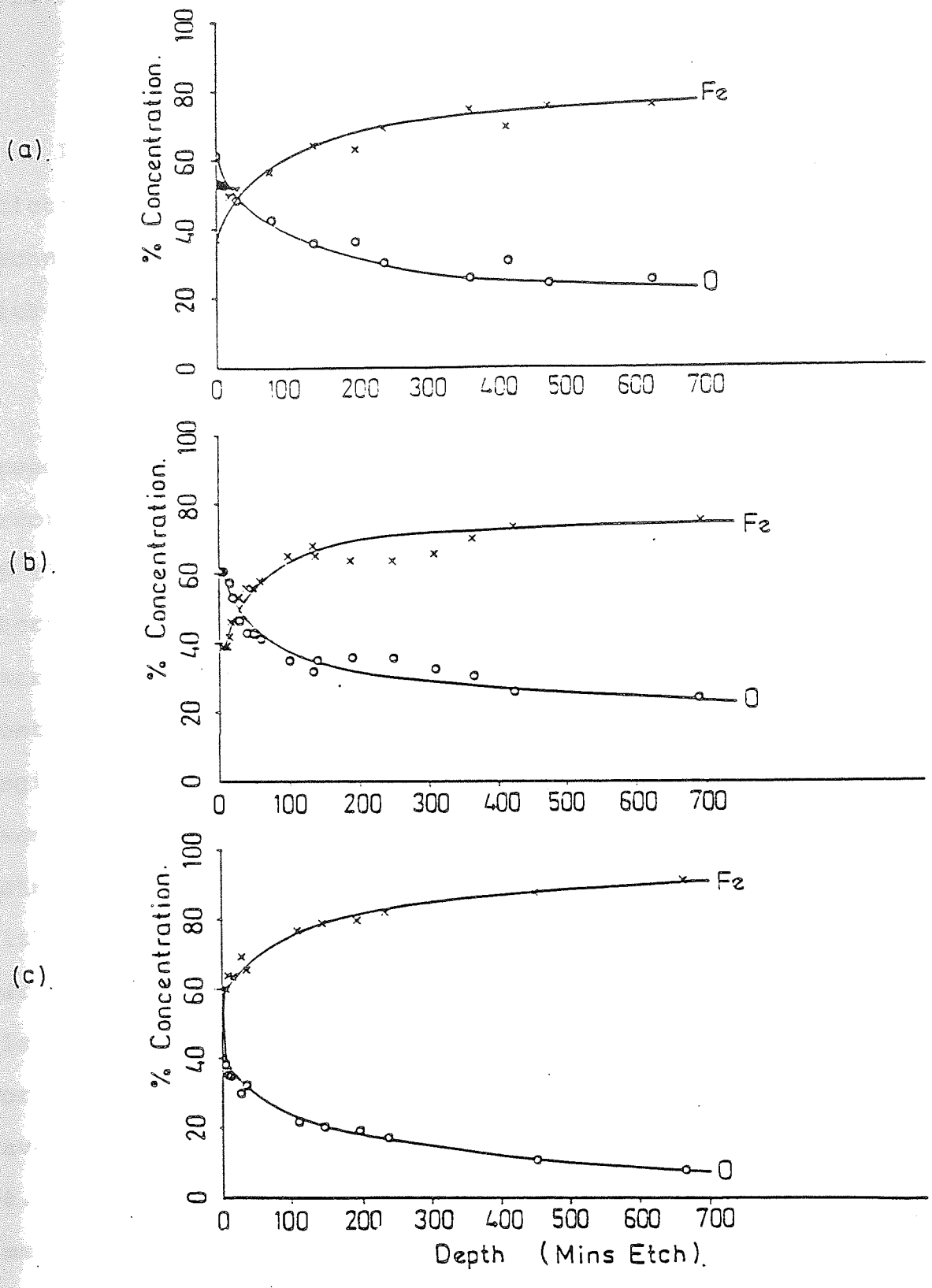

Figure 3.23

Auger electron depth profiles for a speed of 0.1 ms^{-1} and loads of (a) 4.9 and (b) 9.8 N and (c) of 0.05 ms^{-1} and 19.6 N load.

3.10 Lubricated Friction and Wear

In this section the variation of wear rate and friction will be presented for experiments conducted in Technical White Oil and for those in Technical White Oil with a 0.1% stearic acid additive.

Figure 3.24 shows the variation of wear rate with speed for loads of 49.1, 98.2 and 122.7 N. Experimental error in the wear rate is estimated at $\pm 10^{-15}$ m^3/m in each of the figures presented here. The wear rates are seen to decrease with increasing speed as would be expected due to increased hydrodynamic lift reducing asperity - asperity contact and thus wear rate. Below 0.2 ms^{-1} the wear rates begin to increase for each load as the fluid film support decreases allowing more asperity - asperity contact. Wear rates are higher for higher load. Comparing these results with the curves in Figure 3.25, which show the same variation but with 0.1% stearic acid additive, there is a clear increase in wear rate with load seen especially well for the 122.7 N load. The organic acid additive appears to have had a profound effect on the wear rates for 49.1 and 98.2 N loads, decreasing them markedly to almost immeasurable levels whilst otherwise not changing the 122.7 N load curve very much. Due to the difficulty in measuring wear rate at these levels the experimental scatter in the points is large and the lines are meant only to give a general indication of the trend.

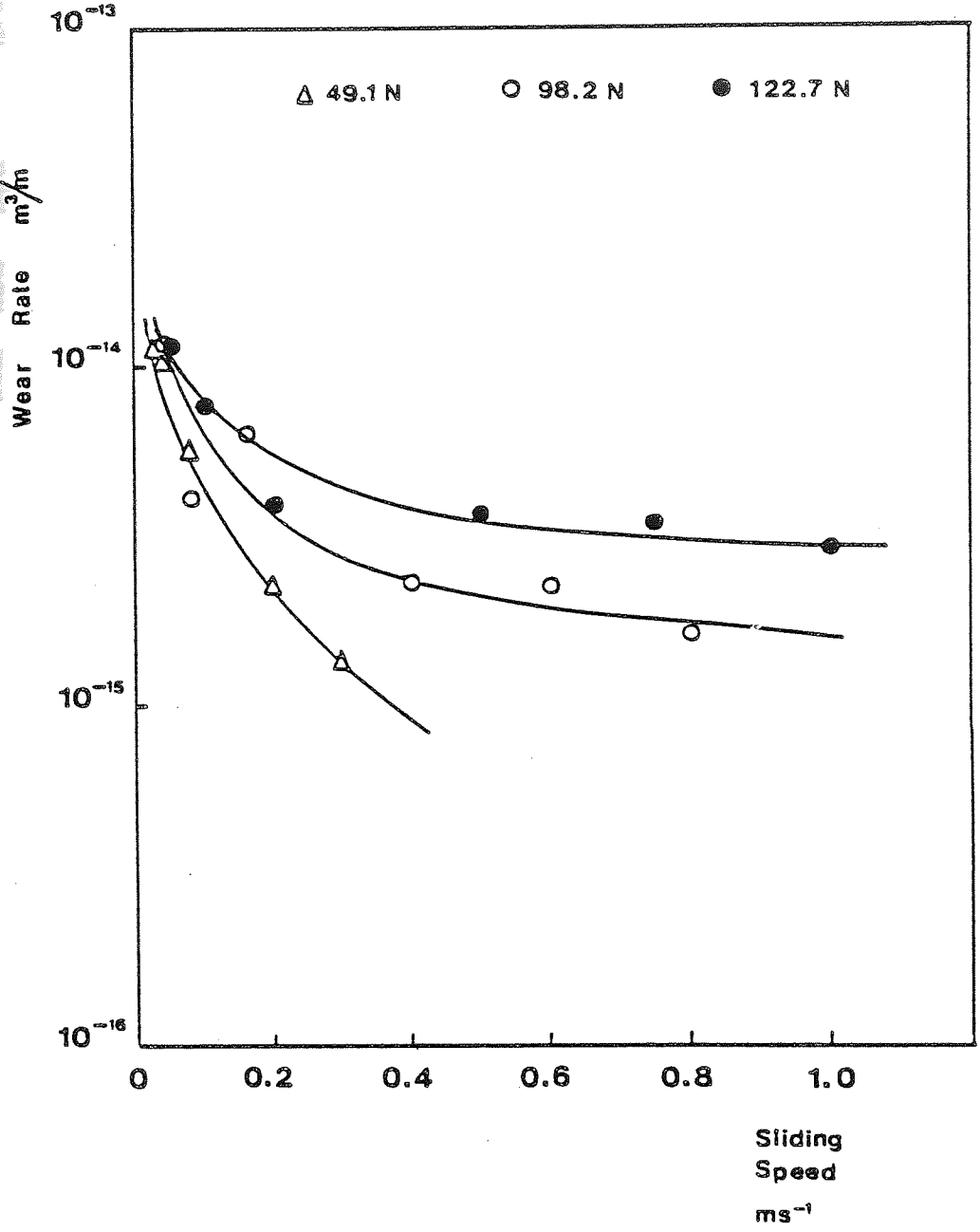

Figure 3.24

Variation of wear rate with speed for loads of 49.1, 98.2 and 122.7 N from tests conducted in Technical White Oil.

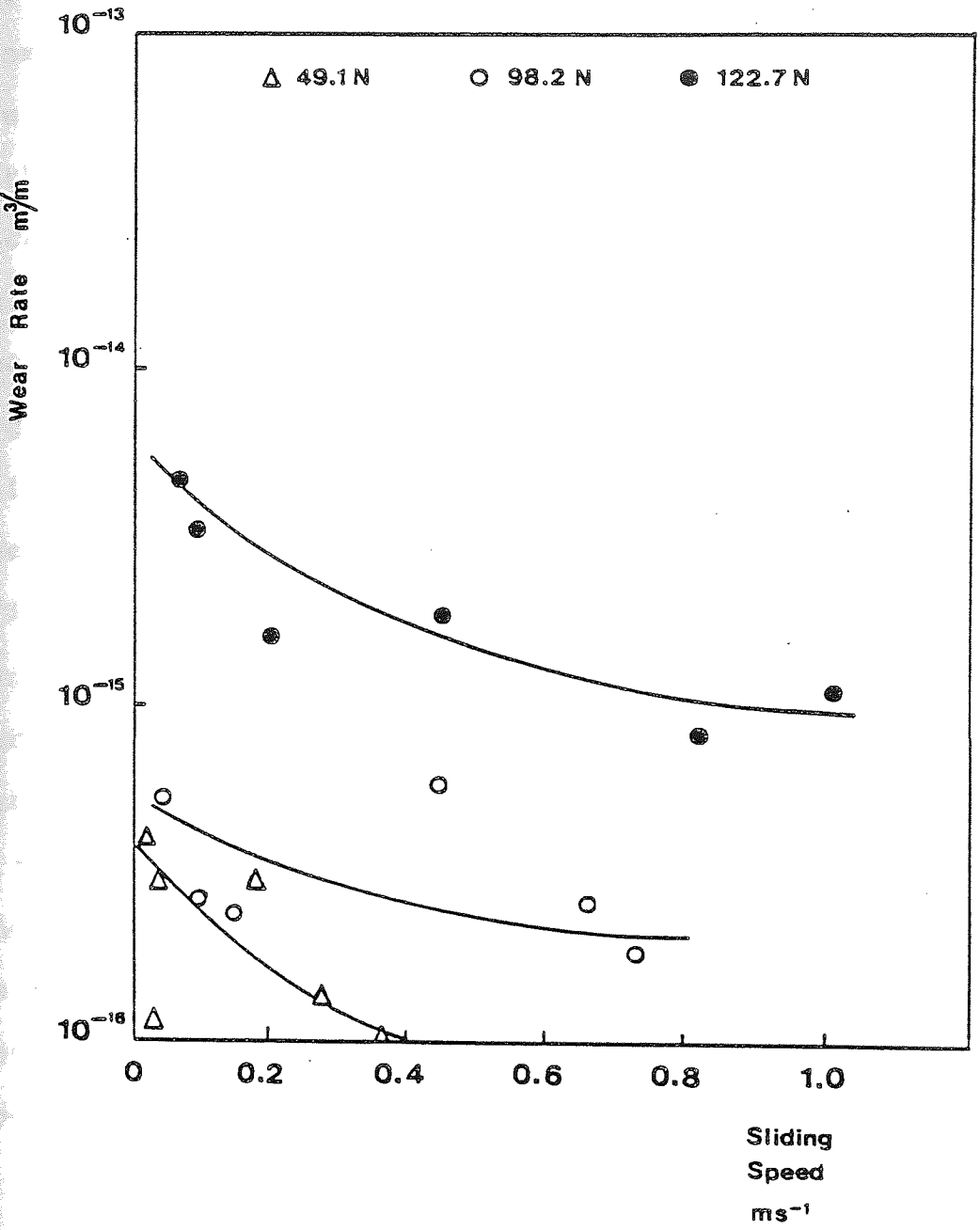

Figure 3.25

Variation of wear rate with speed for loads of 49.1, 98.2 and 122.7 N from tests conducted in Technical White Oil with 0.1% stearic acid additive.

Figure 3.26 shows the variation of wear rate with friction coefficient for loads of 49.1, 98.2 and 122.7 N from tests conducted in Technical White Oil. The points lie on a straight line with an 85% correlation coefficient with log of wear rate plotted against friction coefficient. Because figure 3.26 is a log-linear relationship, there is in actuality a rapid increase in wear rate with only a small increase in friction coefficient due to the logarithmic ordinate, which itself is due to a reduction in sliding speed leaving more asperity contact. This is again due to the asperity - asperity contact leading to increased friction coefficient as a reduction in speed reduces hydrodynamic lift and fluid film thickness between the surfaces. Because of this a clear relationship between wear rate and friction coefficient is expected, further to this, a relationship between wear rate and fluid film thickness should be apparent. An expression for fluid film thickness for fixed geometry pads, developed by Cameron[110], has been used to approximate that obtained with a pin on disc geometry. From this experssion:

$$h \propto \sqrt{\frac{W}{U}} \qquad (3.1)$$

The wear rate would be expected to vary inversely with fluid film thickness and directly with load, hence:

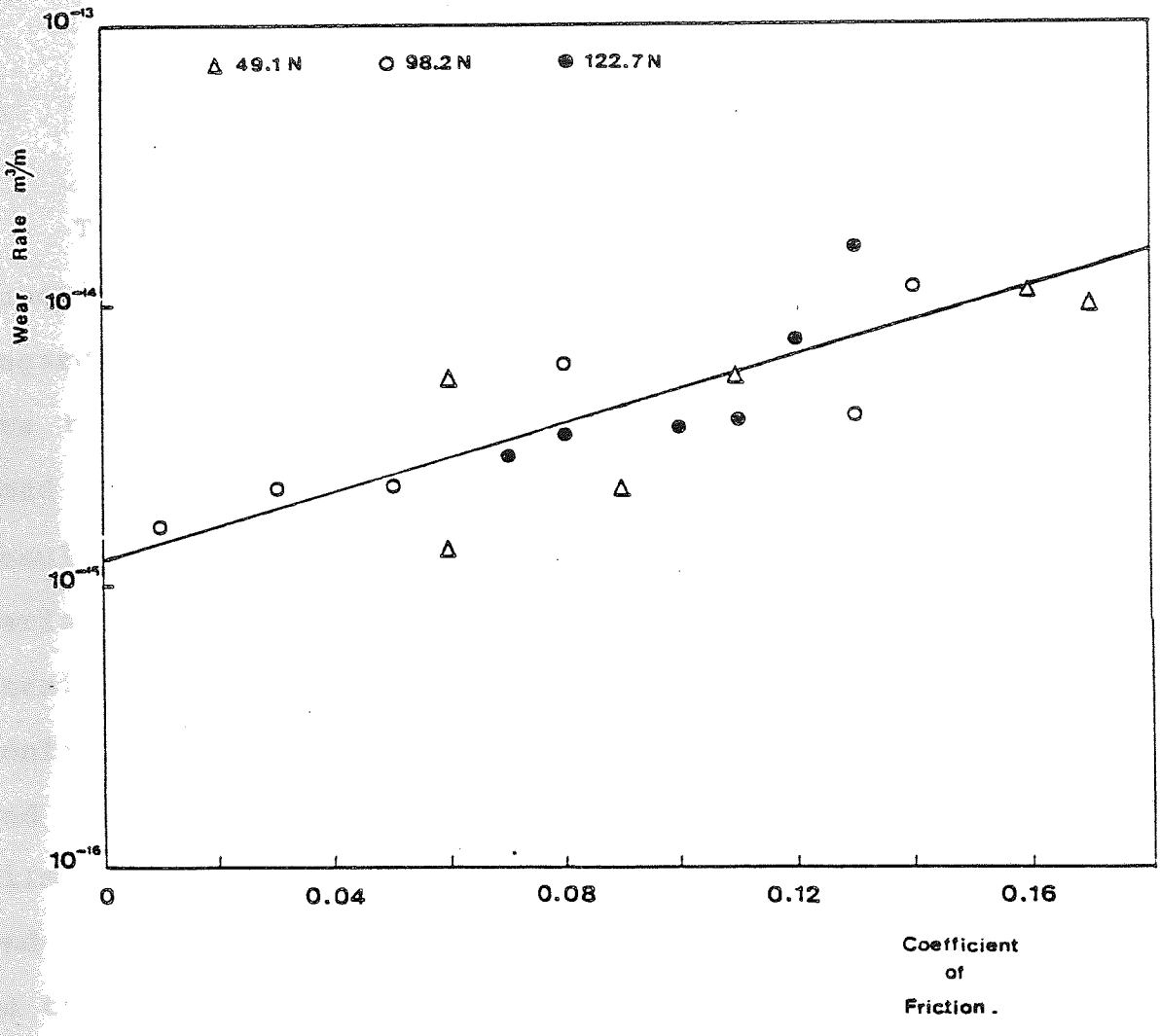

Figure 3.26

Variation of wear rate with friction coefficient for loads of 49.1, 98.2 and 122.7 N from tests conducted in Technical White Oil.

$$\omega \propto \frac{1}{h} W$$

or

$$\omega \propto W^{3/2} U^{-1/2} \qquad (3.2)$$

The values of experimental wear rate should vary as a function of $W^{3/2} U^{-1/2}$ if the previous assumptions regarding coefficent of friction and fluid film thickness are true. Table 3.1 gives the wear rate, sliding speed, load and function $W^{3/2} U^{-1/2}$ for the lubricated wear results presented in Figure 3.26. Figure 3.27 shows the variation of wear rate with $W^{3/2} U^{-1/2}$ to indeed be a straight line with a correlation coefficient of 75%, confirming that the asperity contact, friction coefficient and wear rate are, as expected, dependent upon the fluid film thickness. The relationships shown in figures 3.26 and 3.27 are not apparent when the stearic acid is present as the variability of the experimental wear rates makes the determination of these values difficult, although the wear rates should still depend upon the amount of asperity contact and fluid film thickness. The great reduction of wear rates on addition of the stearic acid then shows that asperities are being successfully protected by a metallic soap.

Table 3.1

Experimental wear rate, load, sliding speed and function $W^{3/2} U^{-1/2}$ for lubricated tests in Technical White Oil.

ω $m^3\ m^{-1}$	W N	U ms^{-1}	$\frac{W^{3/2}}{U^{1/2}}$
1.17×10^{-14}	98.2	0.04	4865
4.02×10^{-15}	"	0.08	3440
6.32×10^{-15}	"	0.16	2432
2.30×10^{-15}	"	0.4	1539
2.27×10^{-15}	"	0.6	1256
1.65×10^{-15}	"	0.8	1088
1.6×10^{-14}	122.7	0.05	6078
7.53×10^{-15}	"	0.1	4298
3.91×10^{-15}	"	0.2	3039
3.77×10^{-15}	"	0.5	1922
3.49×10^{-15}	"	0.75	1569
2.94×10^{-15}	"	1.0	1359
1.13×10^{-14}	49.1	0.03	1986
1.02×10^{-14}	"	0.04	1720
5.71×10^{-15}	"	0.08	1216
2.25×10^{-15}	"	0.2	769
1.35×10^{-15}	"	0.3	628

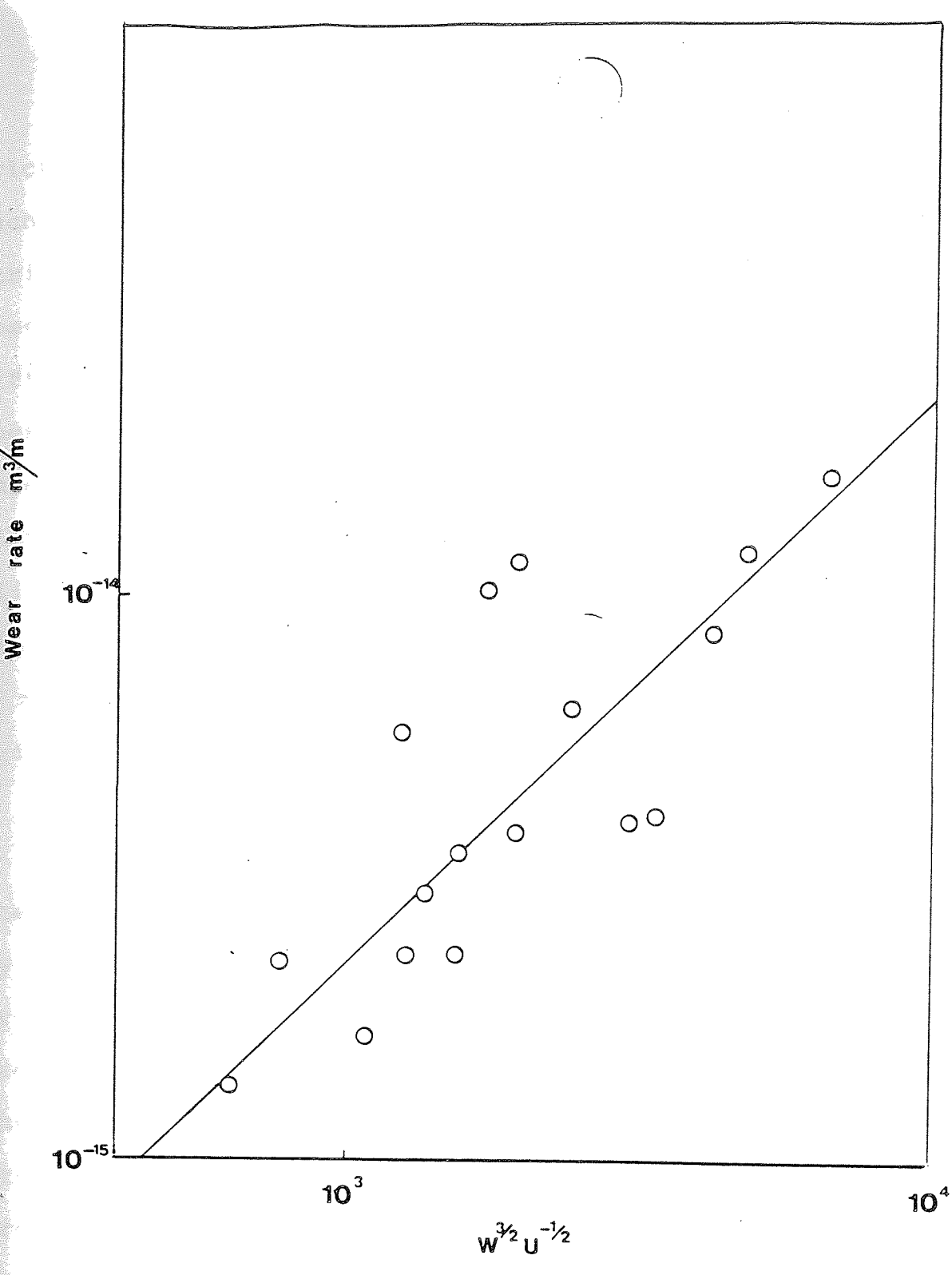

Figure 3.27

Variation of experimental wear rate for loads of 49.1, 98.2 and 122.7 N against a parameter, $W^{3}/_{2}\ U^{-1}/_{2}$, related to the fluid film thickness.

Figure 3.28 shows the variation of the coefficient of friction with speed for loads of 49.1, 98.2 and 122.7 N, in Technical White Oil alone. This figure shows a typical Stribeck variation for the friction coefficient; as the speed is reduced from about 1.0 ms^{-1}, where hydrodynamic lift contributes the major wear reduction factor by physically separating the wearing surfaces and eliminating asperity contact, the friction coefficient is seen to rise with reduced speed as asperity interaction increases. When sliding speed decreases below 0.1 ms^{-1} there is little fluid film support and the surfaces will ultimately wear in a manner similar to dry wear, with correspondingly high friction coefficients.

Figure 3.29, however, shows the same variation but in the presence of the boundary lubricant stearic acid at 0.1% by weight. In this case the coefficient of friction is greatly reduced, even at the lower speeds. This is probably due to the surface protection afforded by a chemisorbed layer of iron stearate, with further layers of stearic acid cohesively bound to this layer. Without this protection wear would occur via a direct asperity - asperity contact; however the asperities are covered with this protective soap layer with a low shear stress which leads to reduced friction coefficients and thus wear rates.

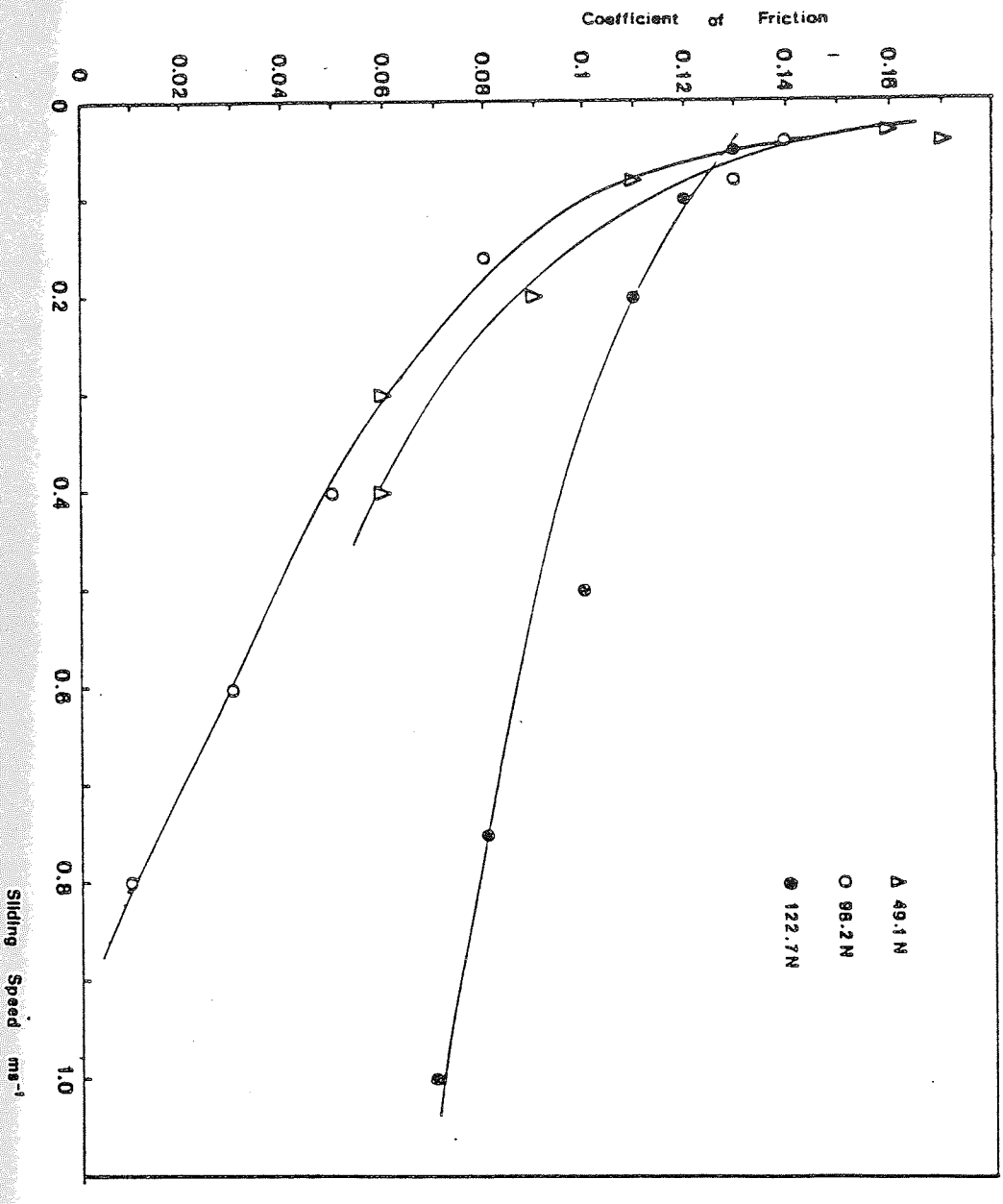

Figure 3.28

Variation of friction coefficient with speed for loads of 49.1, 98.2 and 122.7 N from experiments conducted in Technical White Oil.

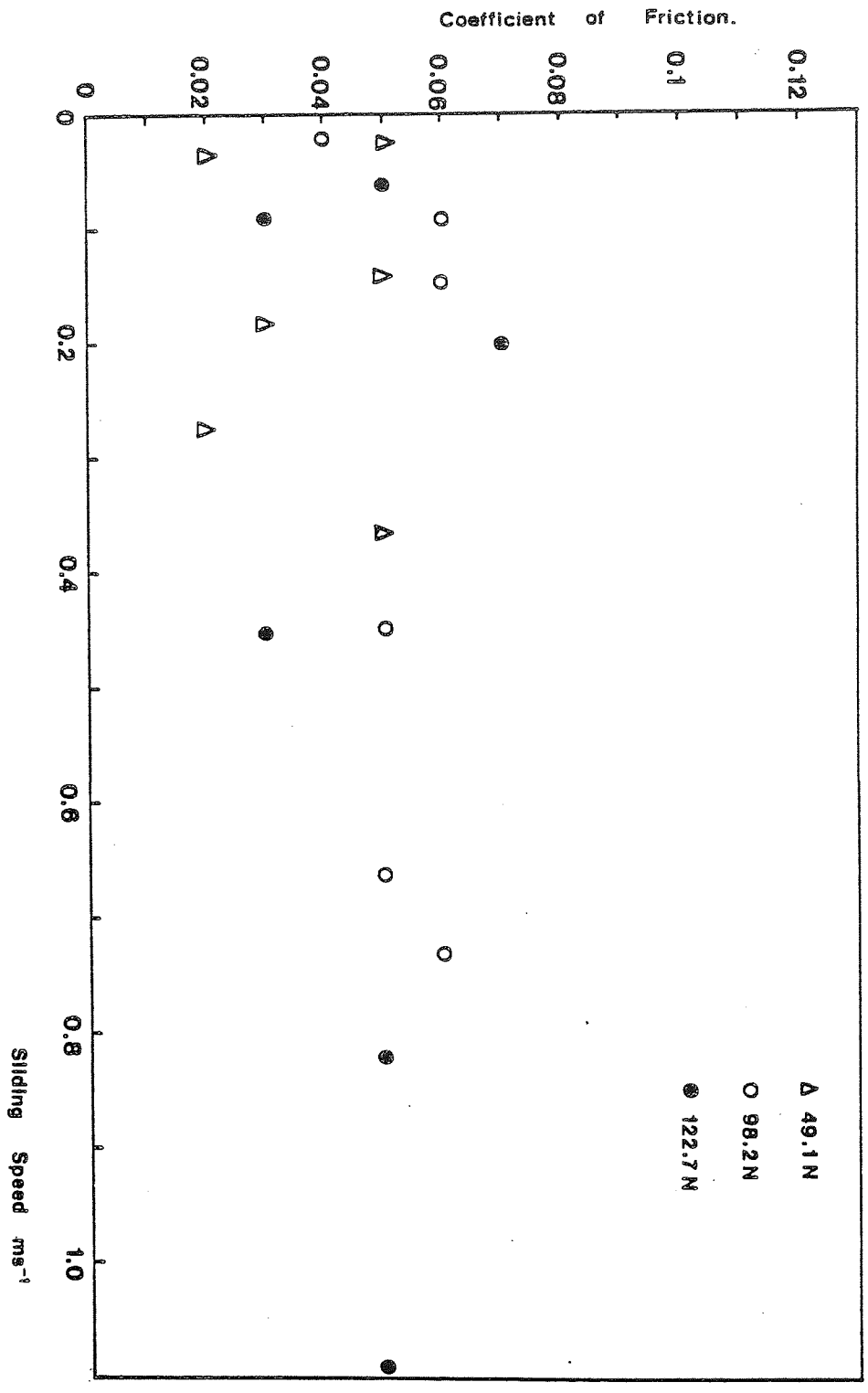

Figure 3.29

Variation of friction coefficient with speed for loads of 49.1, 98.2 and 122.7 N from experiments conducted in Technical White Oil with a 0.1% stearic acid additive.

The addition of stearic acid to the Technical White Oil was also found to increase the load bearing capacity of the oil. Seizure occurred at a load of 147.3 N in Technical White Oil, but in the presence of stearic acid this was increased to 246.5 N using 28.6 N increments, which is up to a 40% increase in load bearing capacity. This effect is thought to occur due to initial surface protection afforded by the acid, which allows time for a protective surface soap layer to form. This is a low load effect as higher loads cause higher surface temperatures, thus more readily leading to surfactant desorption.

3.11 Contact Resistance Measurements for Lubricated Sliding

The contact resistance traces presented here are from an experiment conducted under 98.2 N load and at a speed of 0.08 ms^{-1} corresponding to a bearing number of 1×10^{-9} with the stearic acid additive present. In all cases there was no discernable difference in lubricated contact resistance traces over load and speed ranges and with or without the additive.

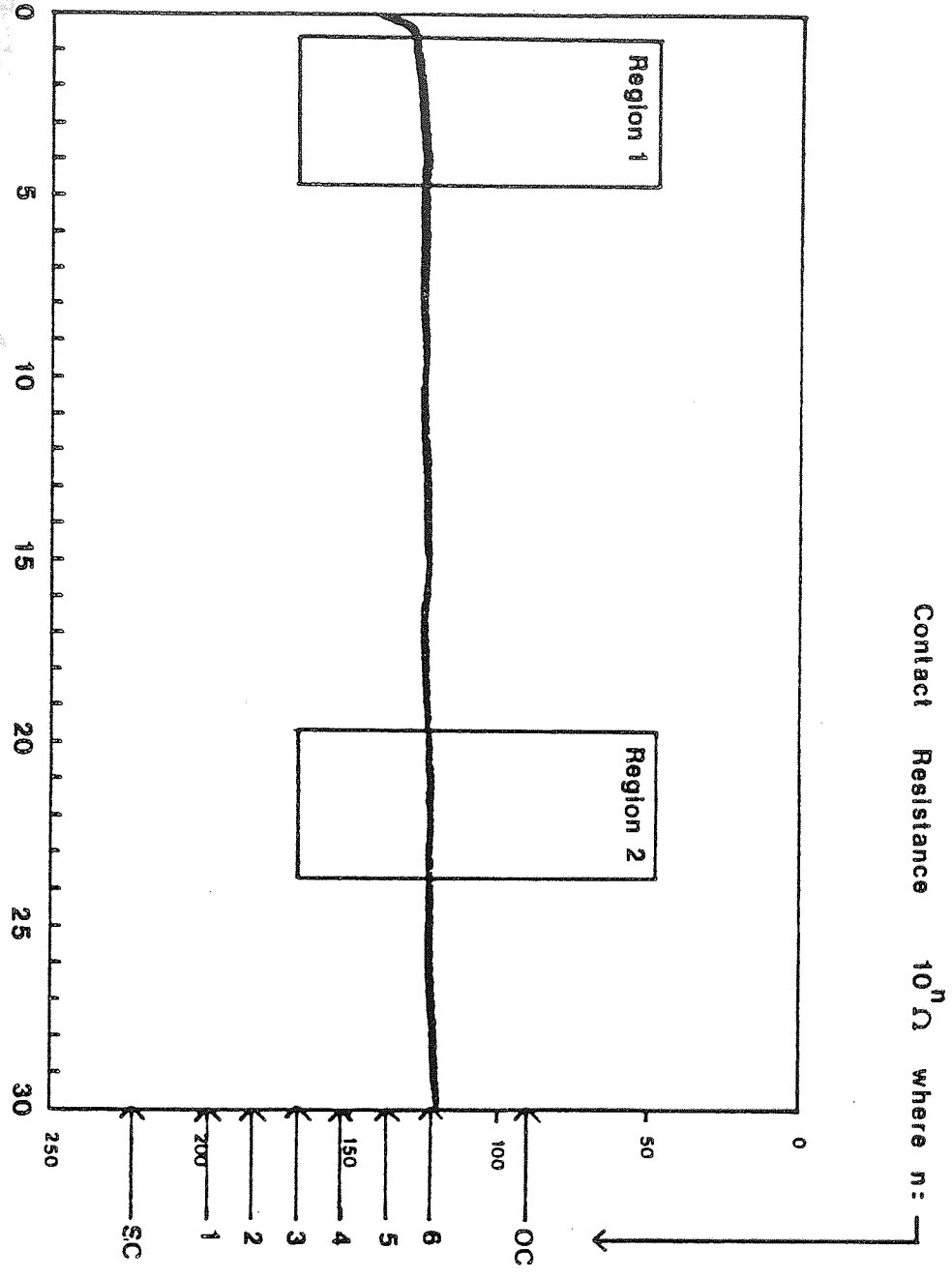

Figure 3.30

Representation of the contact resistance trace, from a load of 98.2 N and speed of 0.08 ms^{-1}, with time. The experiment was conducted in Technical White Oil with a 0.1% stearic acid additive.

Region 1.

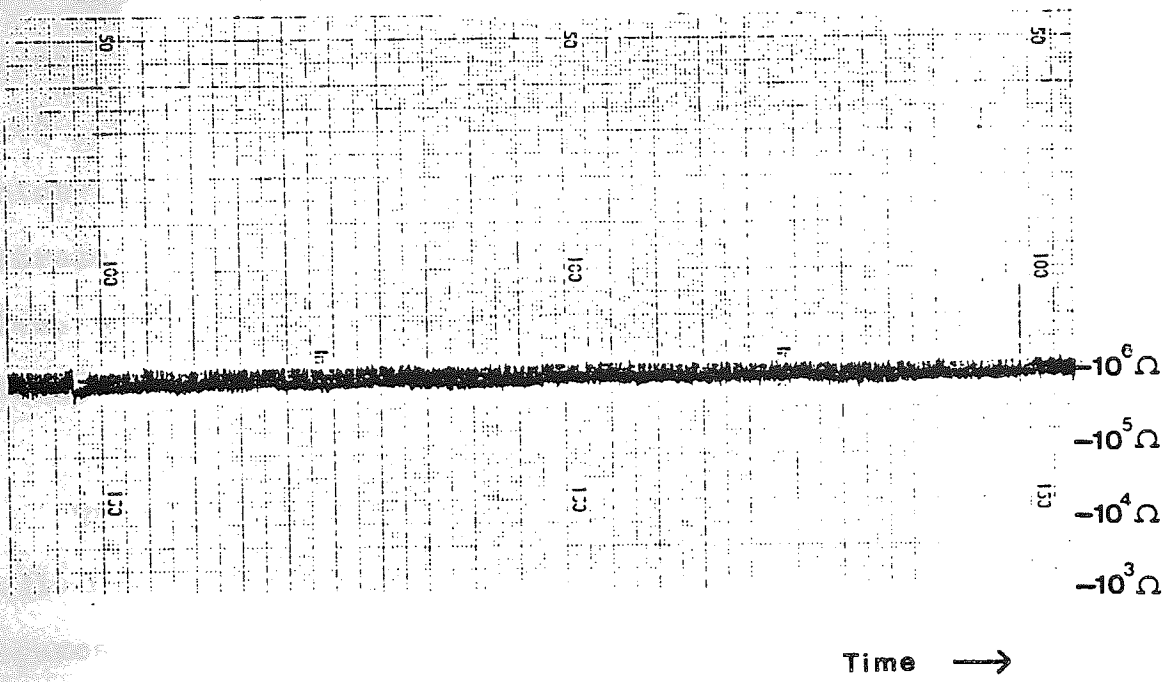

Region 2.

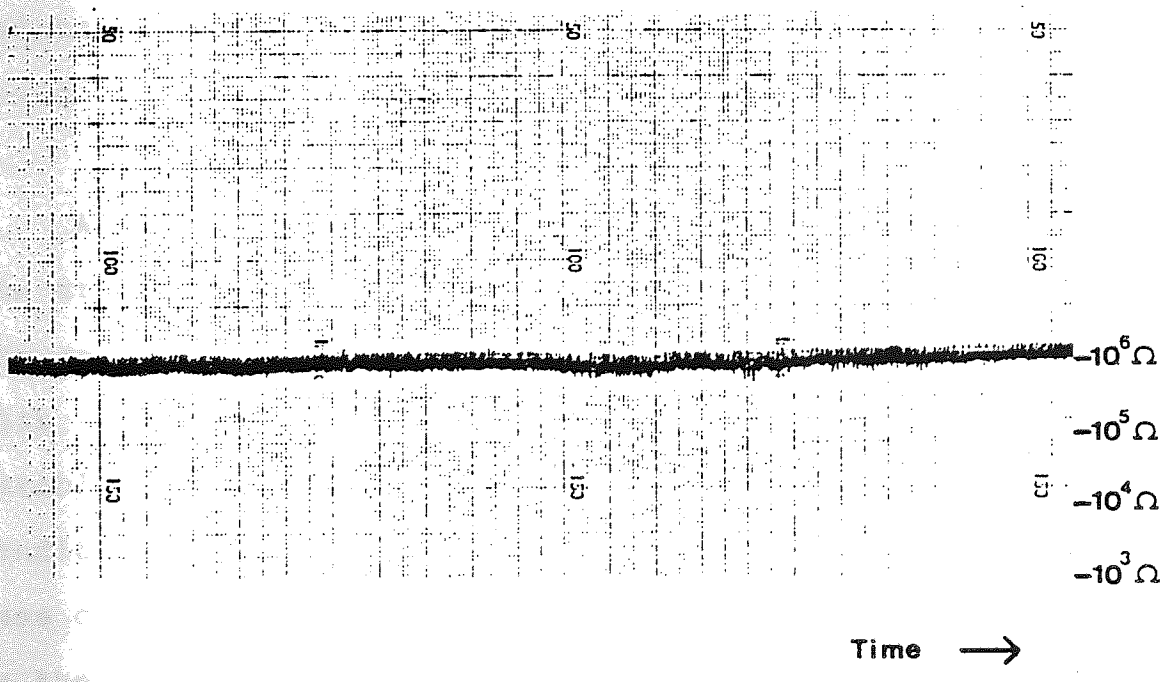

Figure 3.31

Contact resistance traces of the two regions of the curve shown in figure 3.30 showing the actual transient variation.

Important differences are noticeable, however, if the traces in figures 3.30 and 3.31 are compared with those of 3.15 and 3.16 which show similar traces but for unlubricated wear. Figure 3.30 shows a schematic representation of the variation of contact resistance with time, and figure 3.31 shows the actual transient variation resulting from the test shown in figure 3.30.

The first important feature seen in figures 3.30 and 3.31 is the range of variation of the traces, in these figures the contact resistance varies perhaps $10^5\Omega$ from spike to spike. The absence of the spikes which correspond to zero resistance is noticeable showing that the oil is maintaining some separation of the surfaces in places which would otherwise be subject to metal - metal contact.

A second feature of these traces is the consistency of the trace. There is very little variation in the value of the contact resistance from about 1 - 30 hrs running time. This shows that once equilibrium conditions have been established that the lubricant maintains that equilibrium condition indefinitely with very little variation. In the case of the unlubricated traces, relatively large variation in the overall contact resistance is apparent.

The consistency of these traces is thought to be due to the uniform oxide layer which was observed in all experiments, combined to the fluid film support of the oil

film present, maintaining a constant separation and thus resistance between the rubbing surfaces.

3.12 Scanning Electron Microscopy Using Samples from Lubricated Sliding

The scanning electron micrographs presented in this section are from experiments conducted under flooded conditions in Esso Technical White Oil and in the White Oil with a 0.1% stearic acid additive. In every case the worn pin surfaces were completely covered with a uniform oxide layer which displayed no outstanding surface features, even at extreme magnification, as seen in figures 3.32 (a) and (b). This figure shows two high magnification views of a pin worn as 98.2 N and 0.08 ms^{-1} in the presence of stearic acid. These photomicrographs are typical of all pins studied in this way and give no real indication of oxide thickness or composition.

One of the major advantages of this analytical technique is its ability to facilitate direct measurement of oxide thicknesses by studying plateaux edges. To this end, and in view of the extremely smooth nature of the surfaces, the worn pins were crushed in a vice prior to mounting in the scanning electron microscope. Photomicrographs taken after this treatment are now atypical of

Figure 3.32

Scanning electron micrographs of a pin worn at 98.2 N and at a speed of 0.08 ms^{-1} in Technical White Oil. The surface is unaltered.

a.

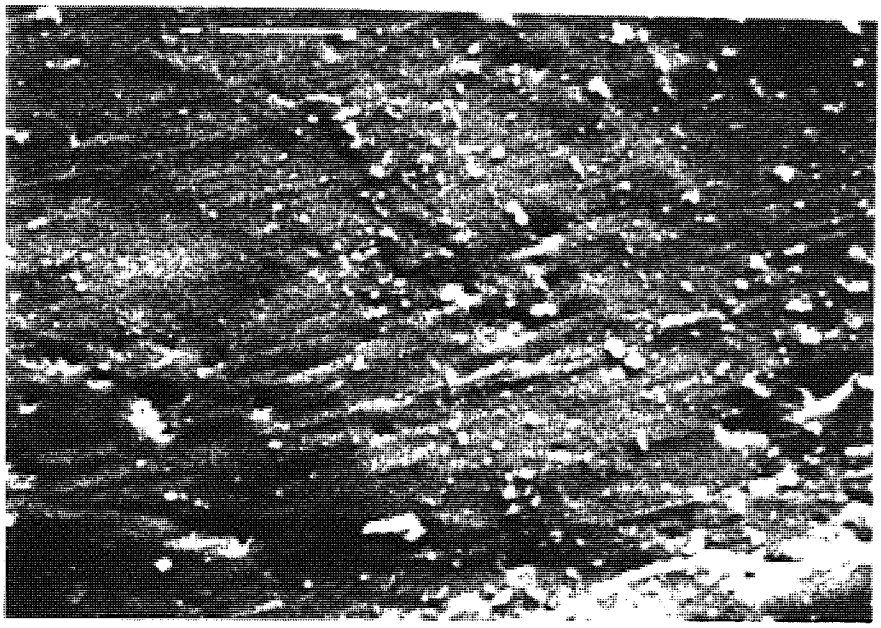

b

real worn pin surfaces, but they provide excellent views of the plateaux edges and their homogeneity.

Figure 3.33 shows high magnification photomicrographs of a pin worn at 98.2 N and at a speed of 0.8 ms^{-1} in Technical White Oil. A 0.1 μm bar is shown in the upper left hand corner of all photomicrographs presented here. Figure 3.34 shows similar photomicrographs for the same load, but for a speed of 0.15 ms^{-1} and in the presence of 0.1% stearic acid.

3.13 Auger Electron Spectroscopy using Samples from Lubricated Sliding

Auger electron depth profiles have been produced for a wide range of load and speed combinations in Technical White Oil both with and without the stearic acid additive.

Figures 3.35 to 3.40 show depth profiles from worn pin surfaces run at a load of 122.7 N and for speeds of 0.06, 0.09, 0.2, 0.45, 0.82 and 1.09 ms^{-1} respectively in Technical White Oil. Allowing for some variation due to error in the etch rate the depth profiles show virtually identical characteristics and correspond to very similar depths of about 0.15 μm.

Figure 3.33

Scanning electron micrographs of crushed pin surfaces worn at a load of 98.2 N and at a speed of 0.8ms^{-1} in Technical White Oil.

a.

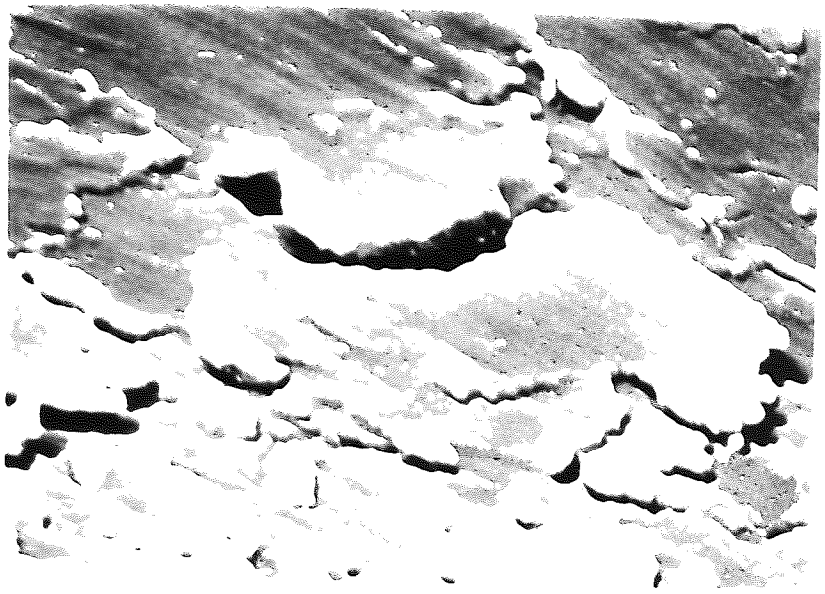

b.

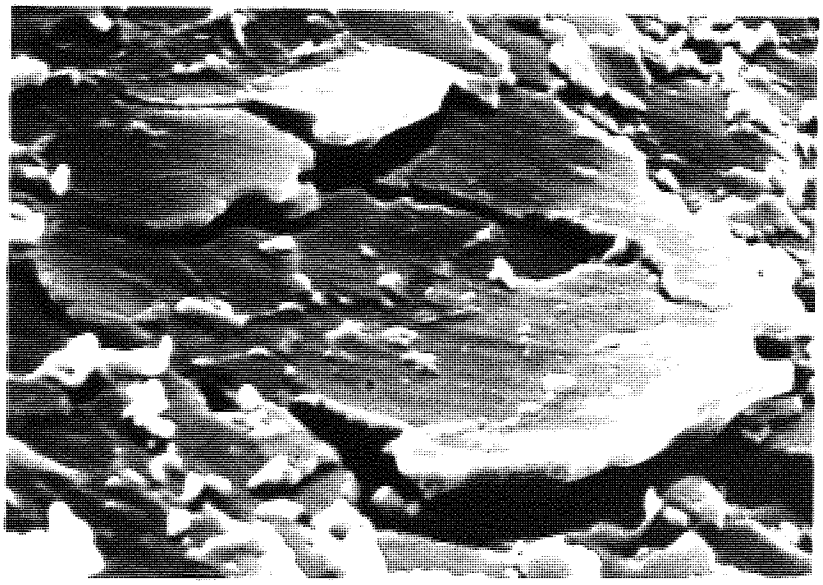

c.

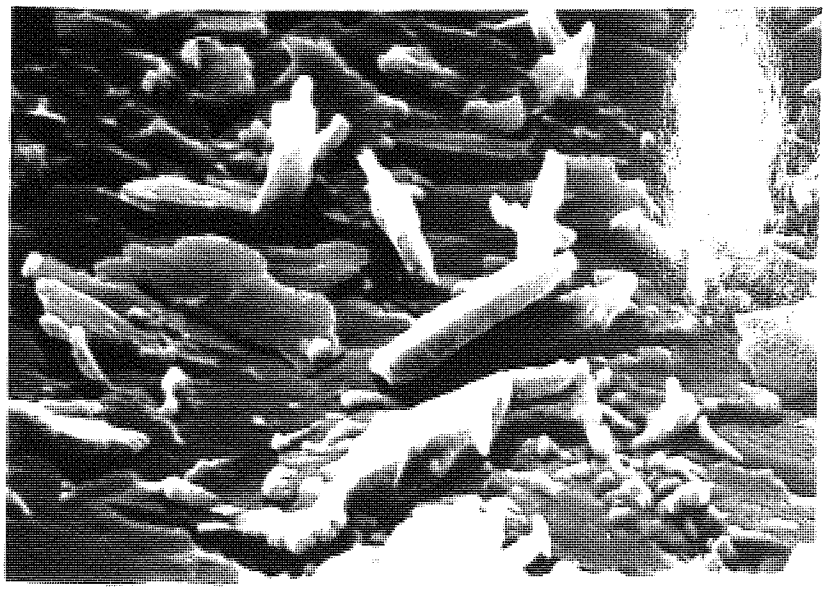

Figure 3.34

Scanning electron micrographs of crushed pin surfaces worn at a load of 98.2 N and at a speed of 0.15 ms^{-1} in Technical White Oil with 0.1% stearic acid additive.

a.

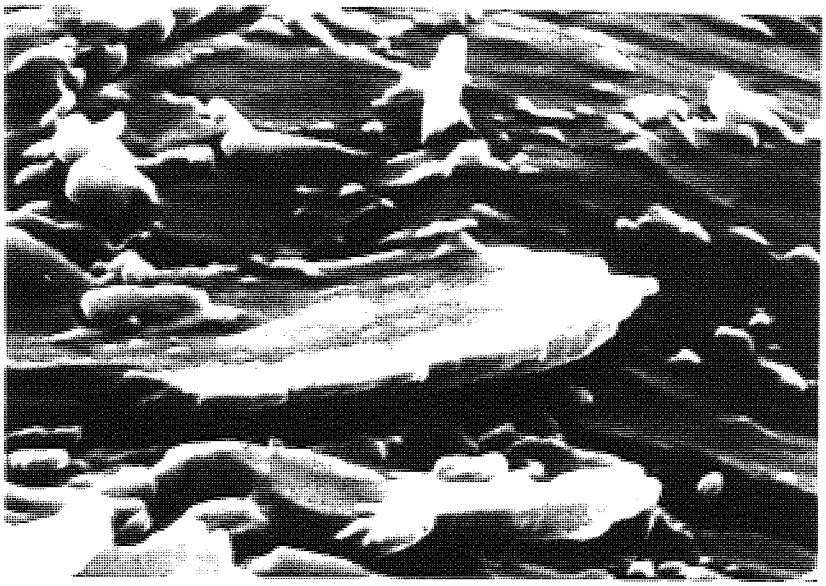

b.

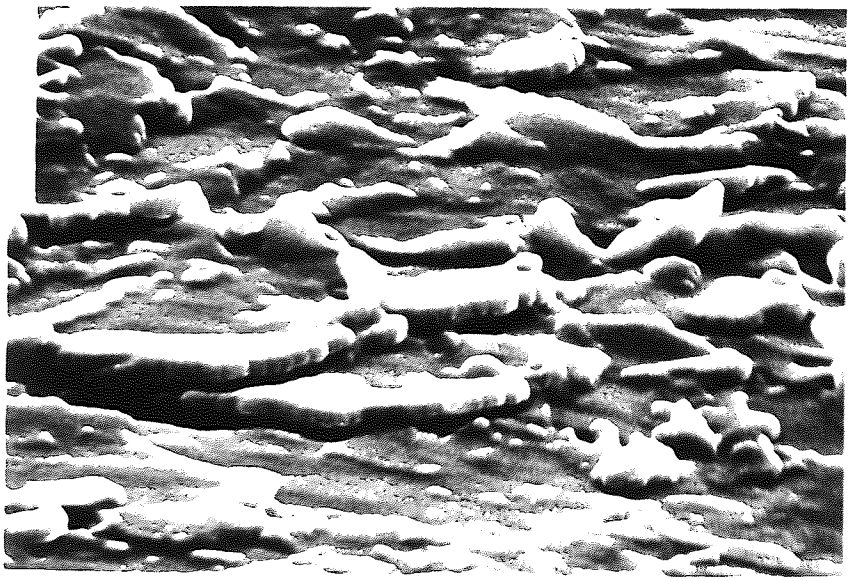

c.

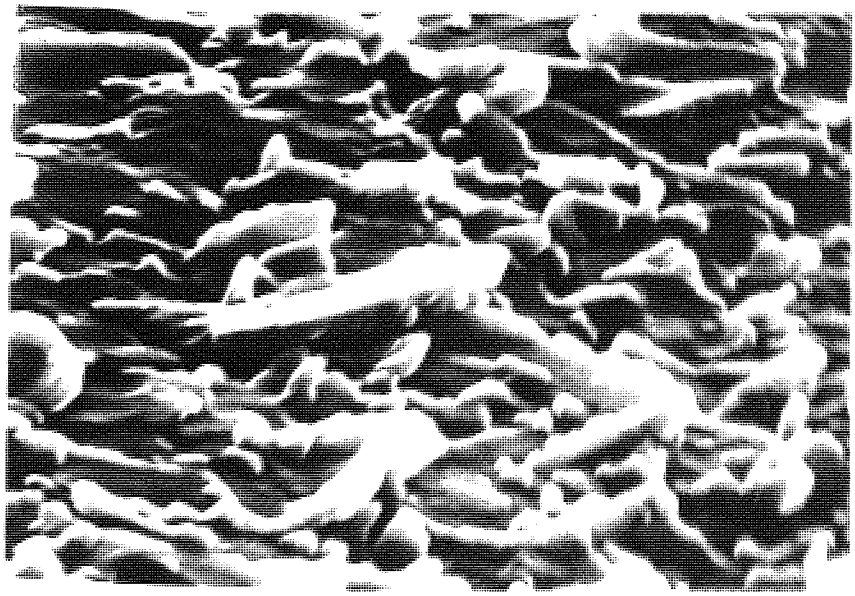

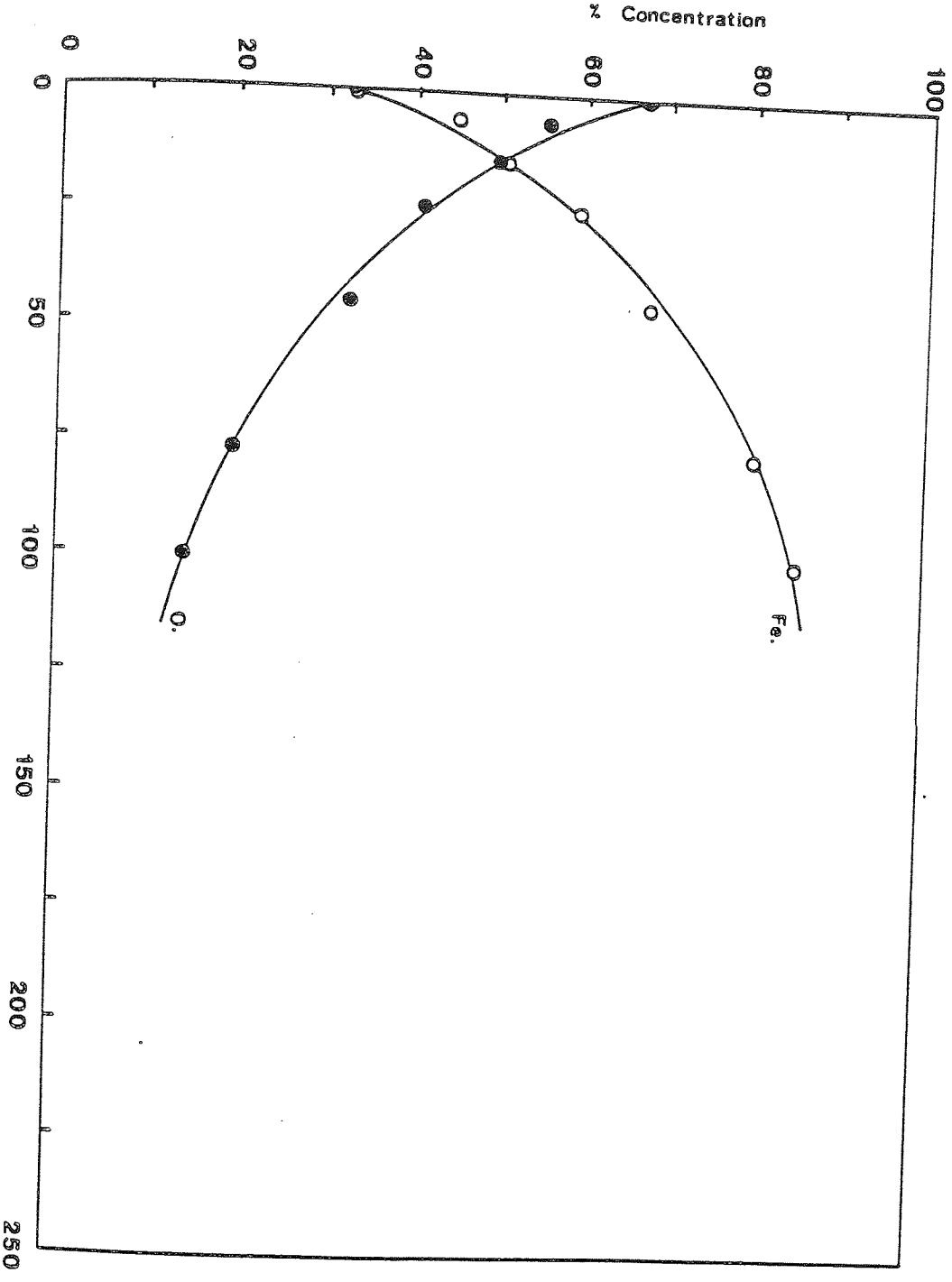

Figure 3.35

Auger electron depth profile for a pin run at 122.7 N load and 0.06 ms^{-1} in Technical White Oil

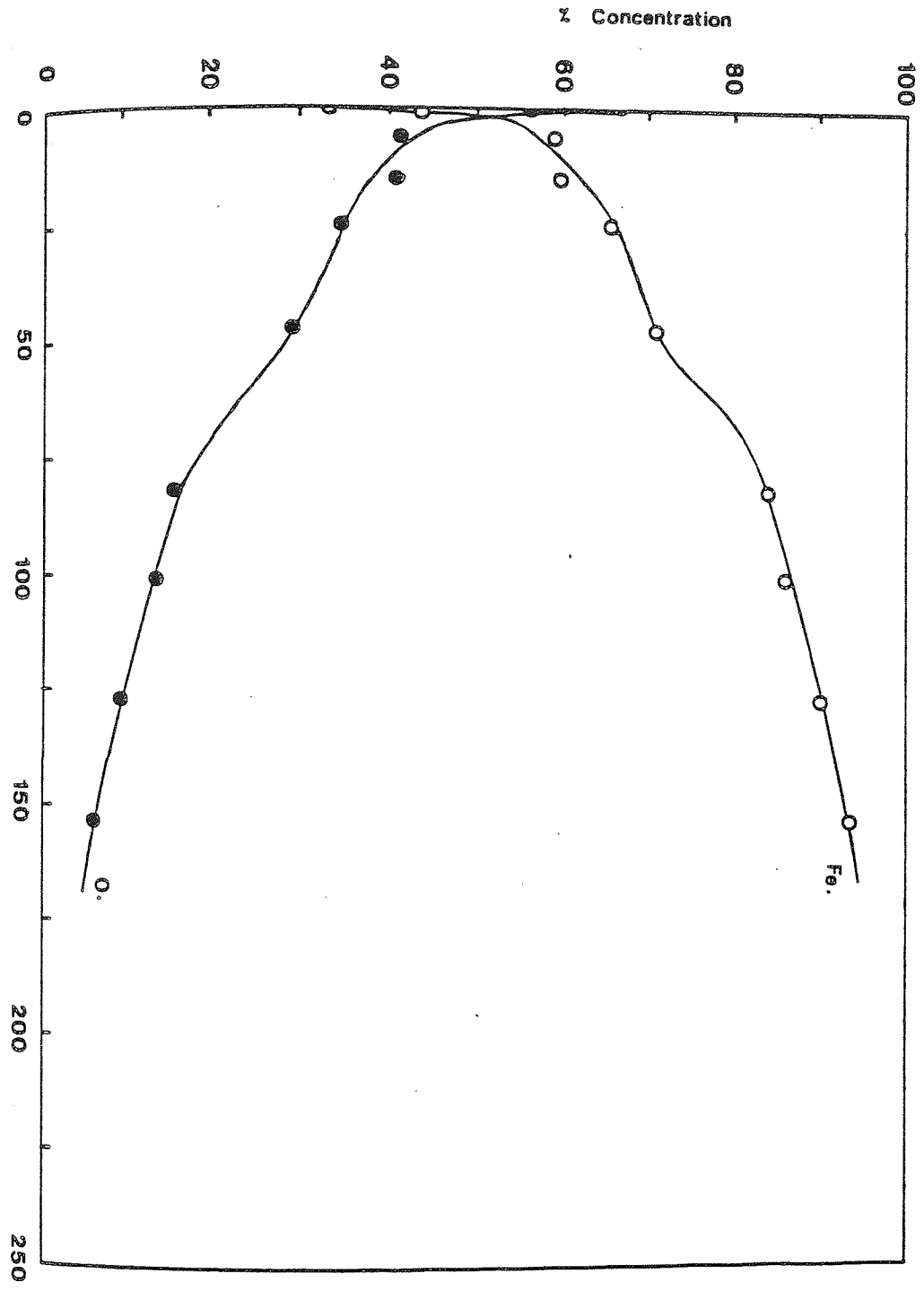

Figure 3.36

Auger electron depth profile of a pin run at 122.7 N load at 0.09 ms^{-1} in Technical White Oil

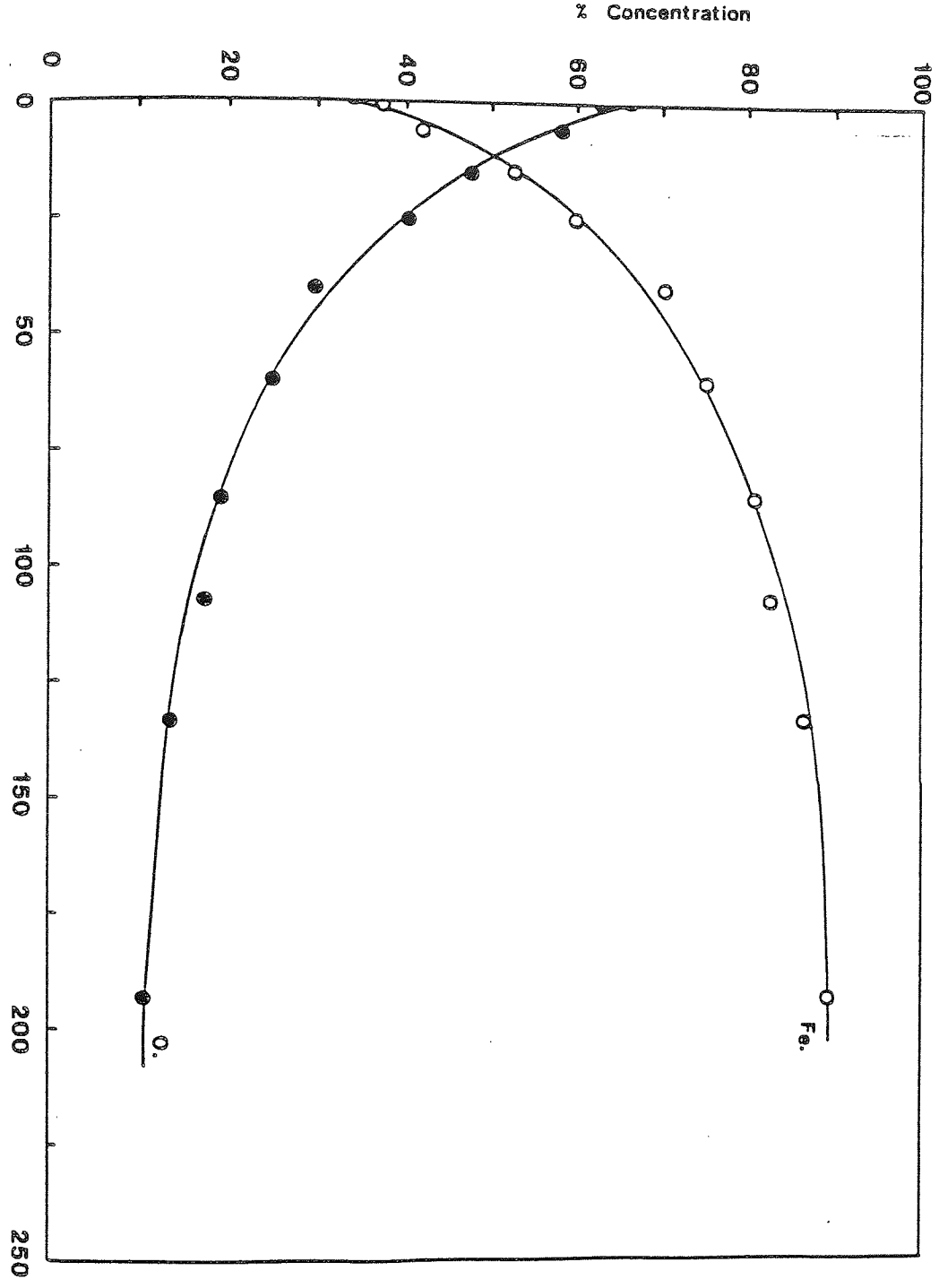

Figure 3.37

Auger electron depth profile of a pin worn at 122.7 N load at 0.2 ms^{-1} in Technical White Oil

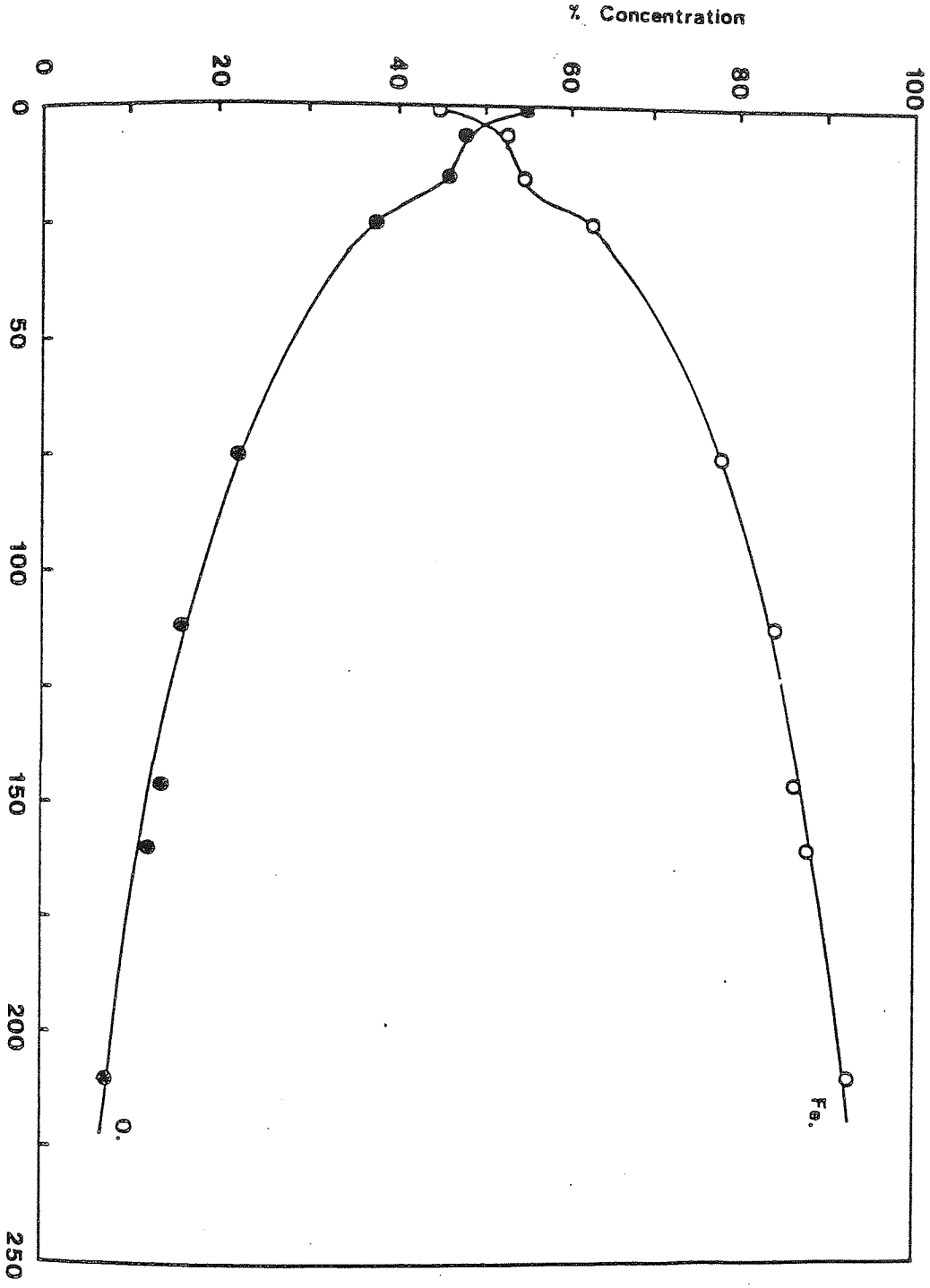

Figure 3.38

Auger electron depth profile of a pin worn at 122.7 N at a speed of 0.45 ms^{-1} in Technical White Oil

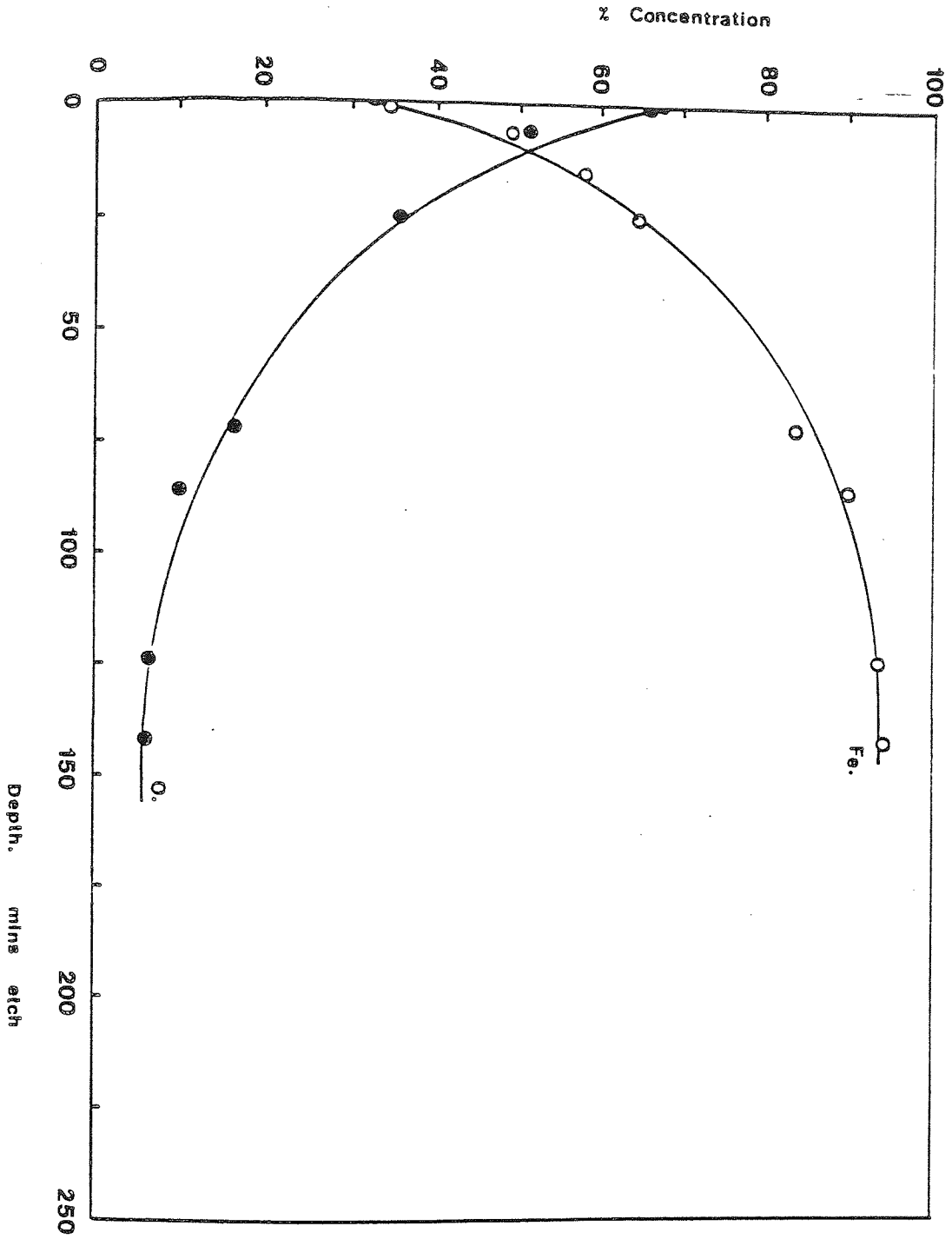

Figure 3.39

Auger electron depth profile of a pin worn at 122.7 N load at 0.82 ms^{-1} in Technical White Oil

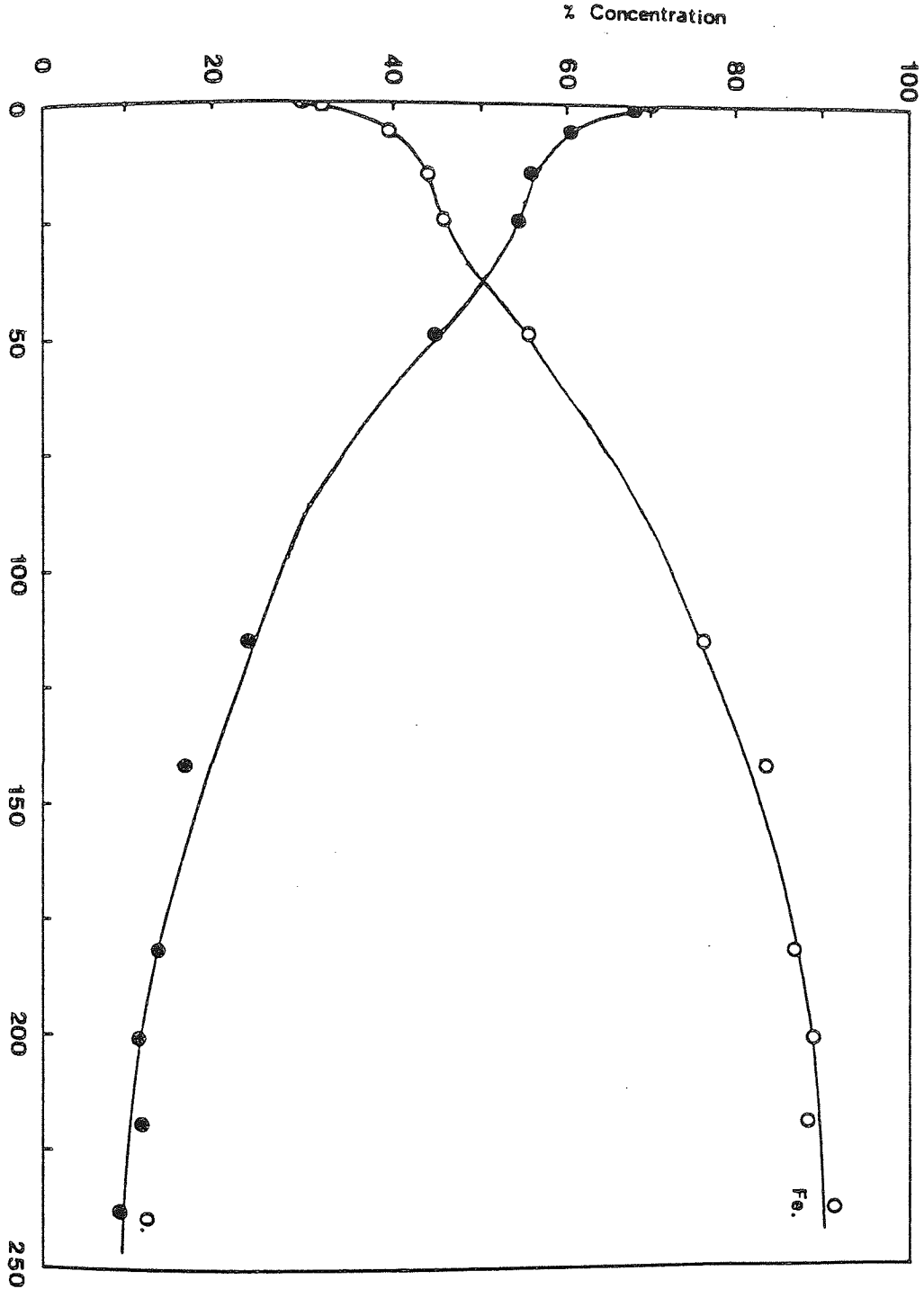

Figure 3.40

Auger electron depth profile of a pin worn at 122.7 N load at a speed of 1.09 ms^{-1} in Technical White Oil

In some cases, figures 3.36, 3.38 and 3.40 there appears to be a homogeneous type variation in oxygen concentration in the outer portion of the oxide layer.

Initial inspection of these figures shows a characteristic similar to those for unlubricated worn pin surfaces as seen in figures 3.22 and 3.23.

This effect is, however, misleading due to the very thin nature of these oxides. Scanning electron micrographs, figures 3.32 to 3.34, show that the oxide is homogeneous and is approximately 0.1 - 0.2 μm in depth. This oxide is thin enough to allow non-uniformities on the surfaces to alter considerably the resultant Auger signals, as one area may have a slightly thicker oxide layer, and therefore take longer to expose the metal substrate, as in figure 3.41a. This, in effect, will give rise to the tailing portion of the ideal characteristic seen in figure 3.41b, which when expanded to appropriate scale will appear as those of figures 3.35 - 3.40. This effect is only apparent with very thin layers and rough surfaces and may be misleading when not considered in view of other analytical evidence such as the scanning electron micrographs.

The Auger electron depth profile shown in figure 3.42 is for a 98.2 N load and a speed of 0.08 ms^{-1}. It is typical of those studied at 98.2 N and is again very similar to those in the series of 122.7N curves. Along

a.

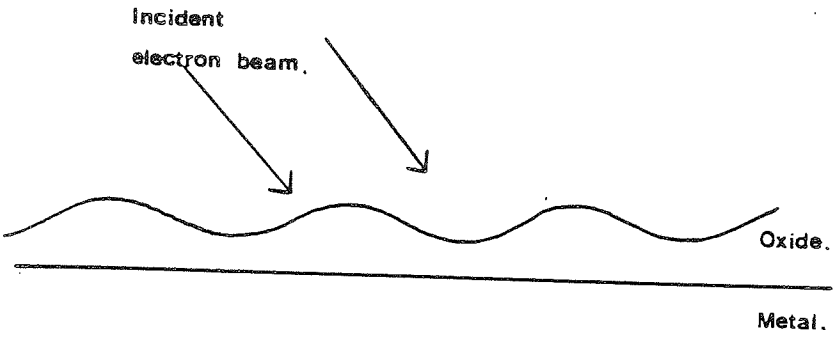

b.

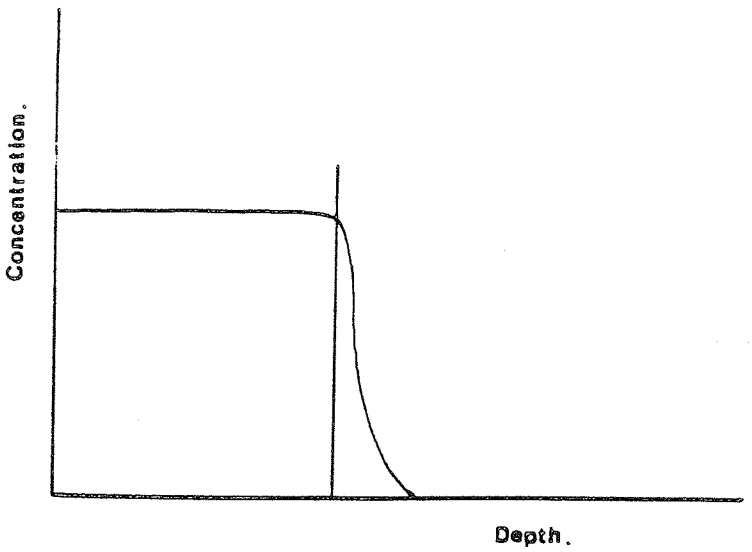

Figure 3.41

Idealised representations of
(a) a very thin oxide layer
under electron bombardment and
(b) an oxygen Auger depth profile
of a homogeneous oxide showing the
rapid fall off in concentration at
the oxide/metal boundary.

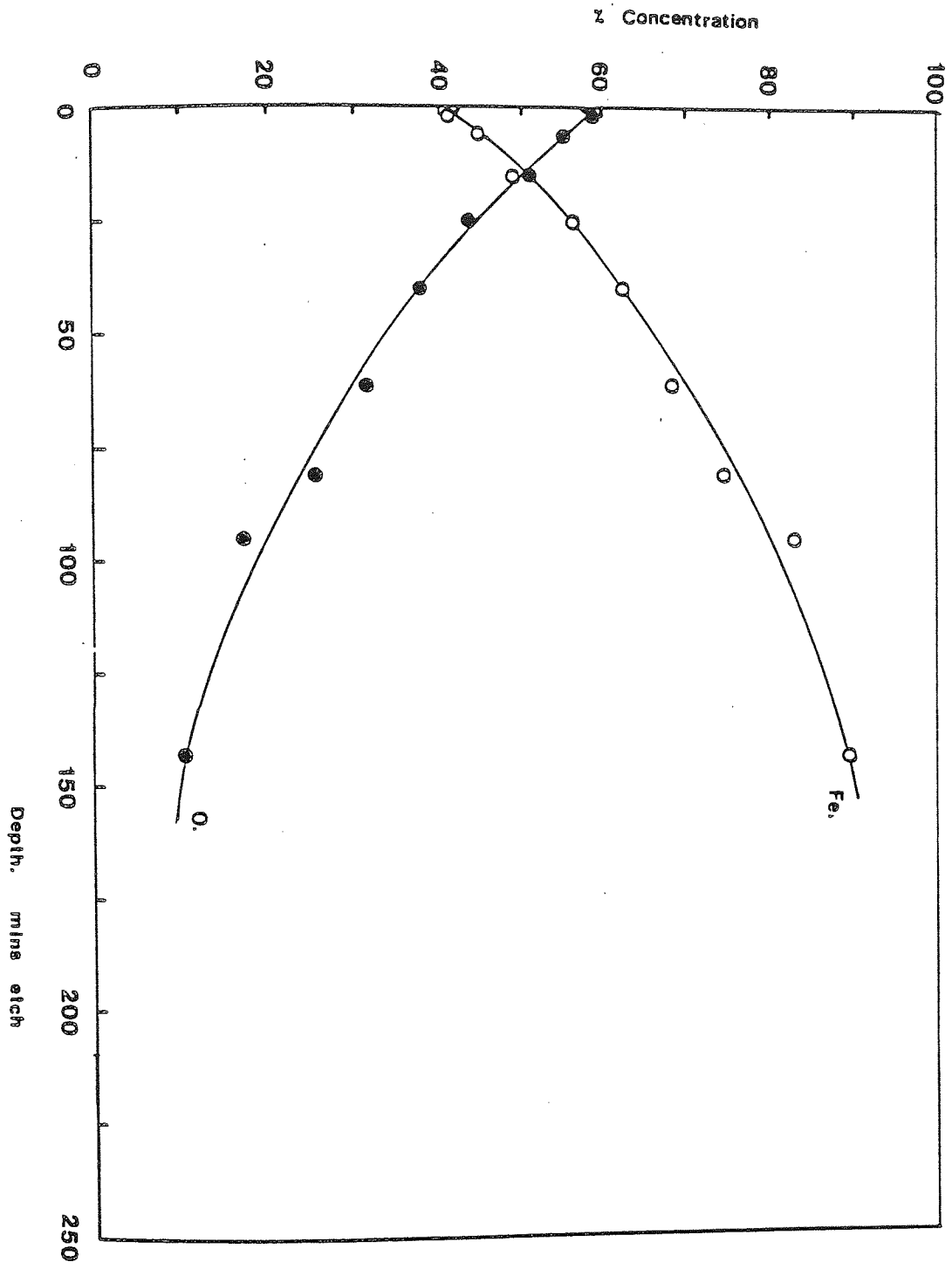

Figure 3.42

Auger electron depth profile of a pin worn at 98.2 N load at a speed of 0.08 ms^{-1} in Technical White Oil

with those variations in Figures 3.43 to 3.46, which show Auger depth profiles from experiments conducted with 0.1% stearic acid additive, for loads of 122.7, 98.2 and 49.1 N and speeds of 0.06, 0.82, 0.66 and 0.02 ms^{-1} respectively, little difference may be seen in the curves with load or speed or indeed presence of the organic acid except in figures 3.44 and 3.45 where the thin homogeneous variation is apparent. This is in support of the scanning electron micrograph evidence, which despite exhaustive investigation provided no systematic variation in either surface topography or oxide thickness.

3.14. X-Ray Photoelectron Spectroscopy of Samples from Lubricated Sliding

The X-ray photoelectron spectra presented here show an outer envelope which is the experimentally collected spectrum, along with the computer-generated curve fitted peaks which collectively comprise the outer envelope. The curves are shown as variations of binding energy (BE) with number of counts (C). The horizontal line is broken by the peak height, while the binding energy is placed on the line in eV. Each figure shows two spectra, the upper represent the carbon 1s peaks and the lower the oxygen 1s peaks. The 1s core electron level notation relates the energy transition giving rise to that particular peak.

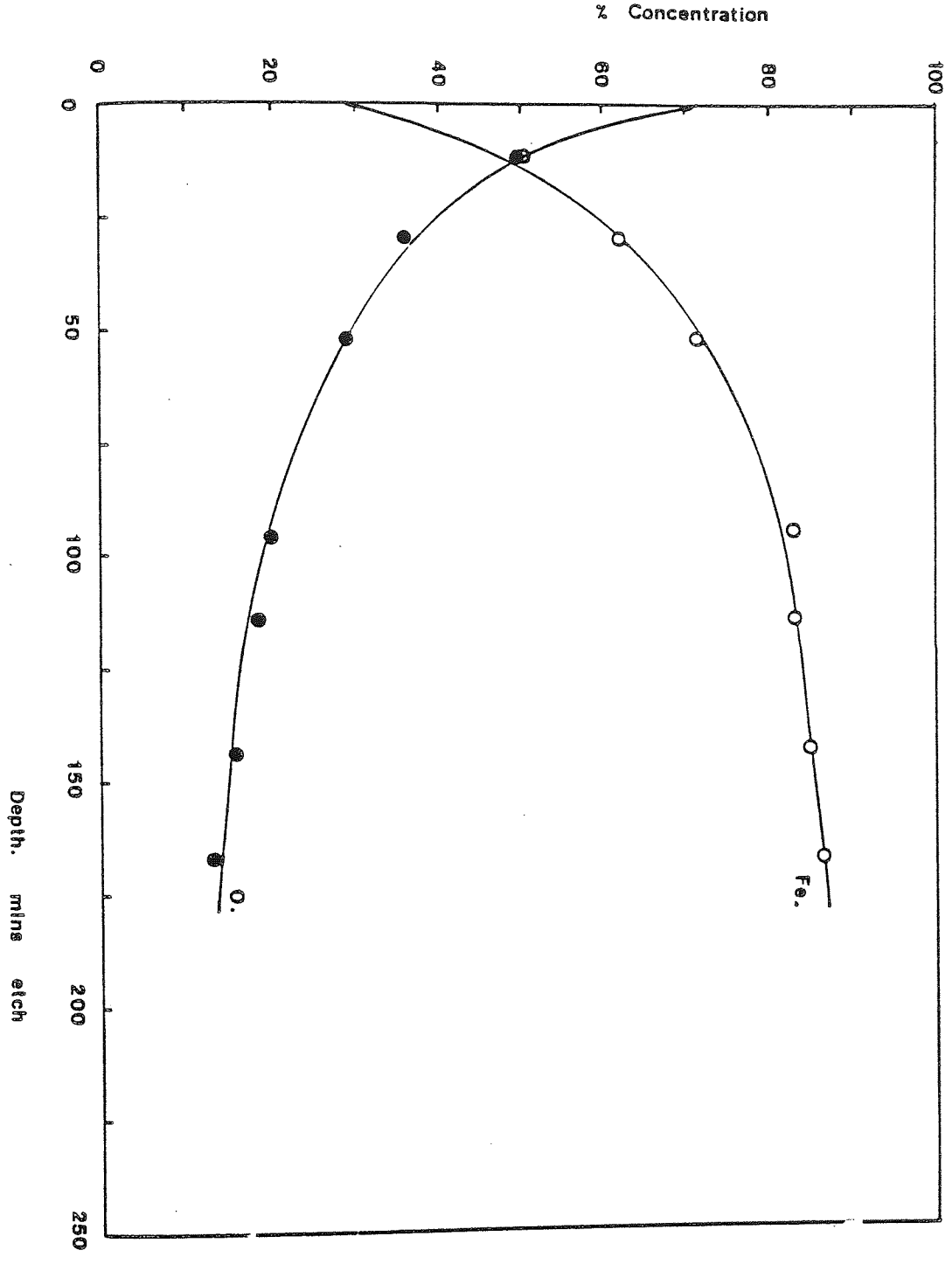

Figure 3.43.

Auger electron depth profile of a pin worn at 122.7 N load at a speed of 0.06 ms^{-1} in Technical White Oil with 0.1% stearic acid

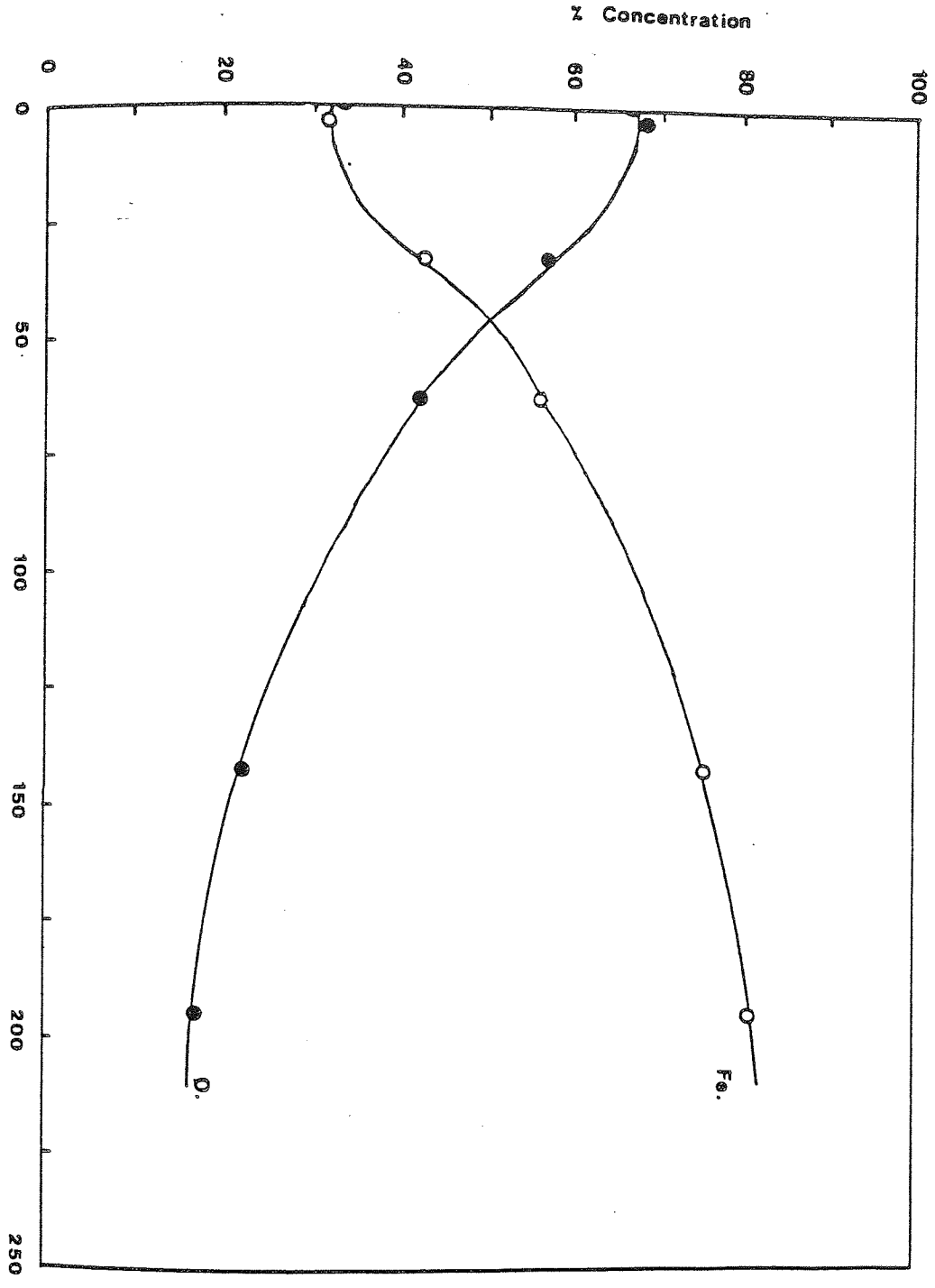

Figure 3.44

Auger electron depth profile of a pin worn at 122.7 N load at a speed of 0.82 ms^{-1} in Technical White Oil with 0.1% stearic acid

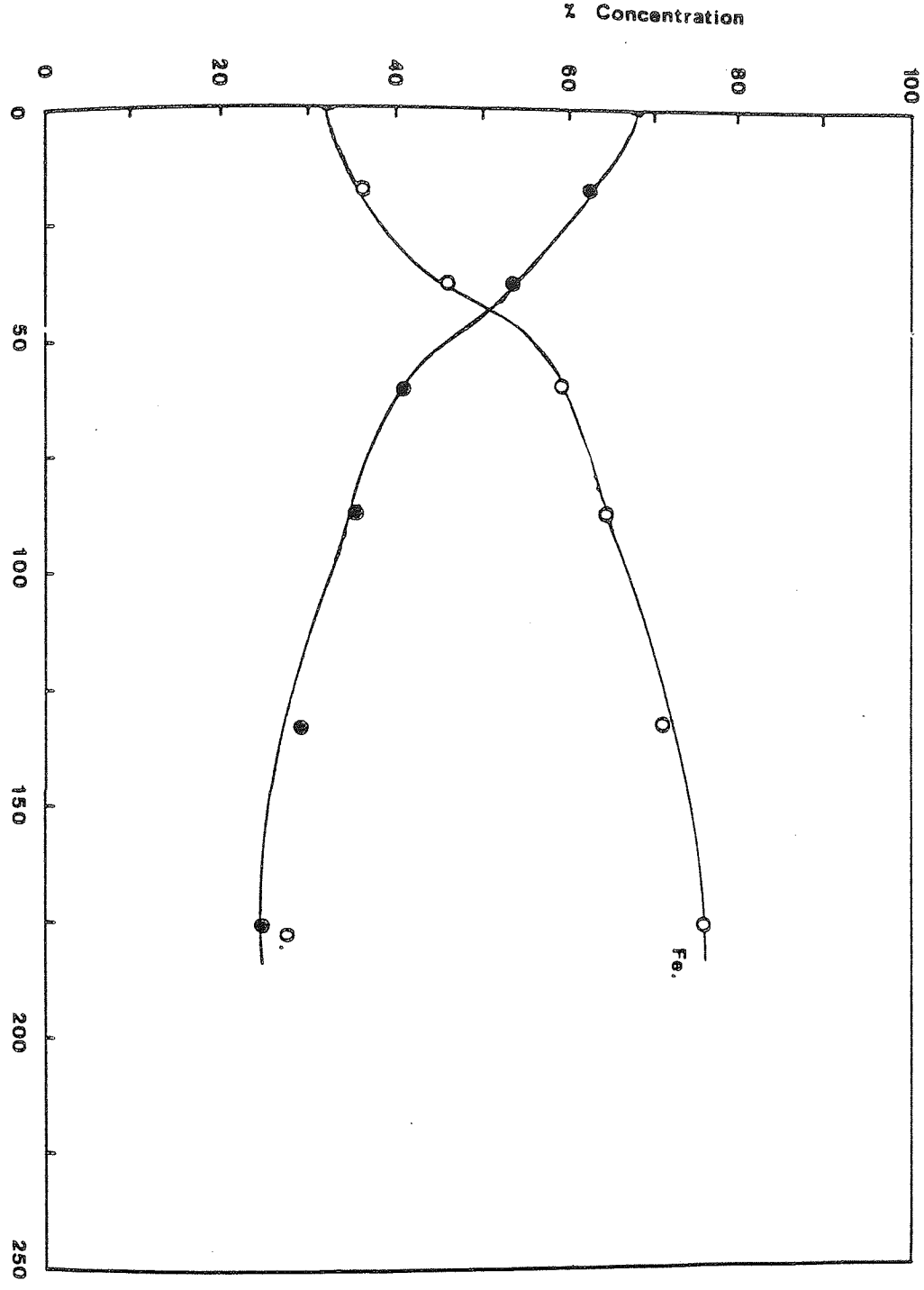

Figure 3.45

Auger electron depth profile of a pin worn at 98.2 N at a speed of 0.66 ms^{-1} in Technical White Oil with 0.1% stearic acid

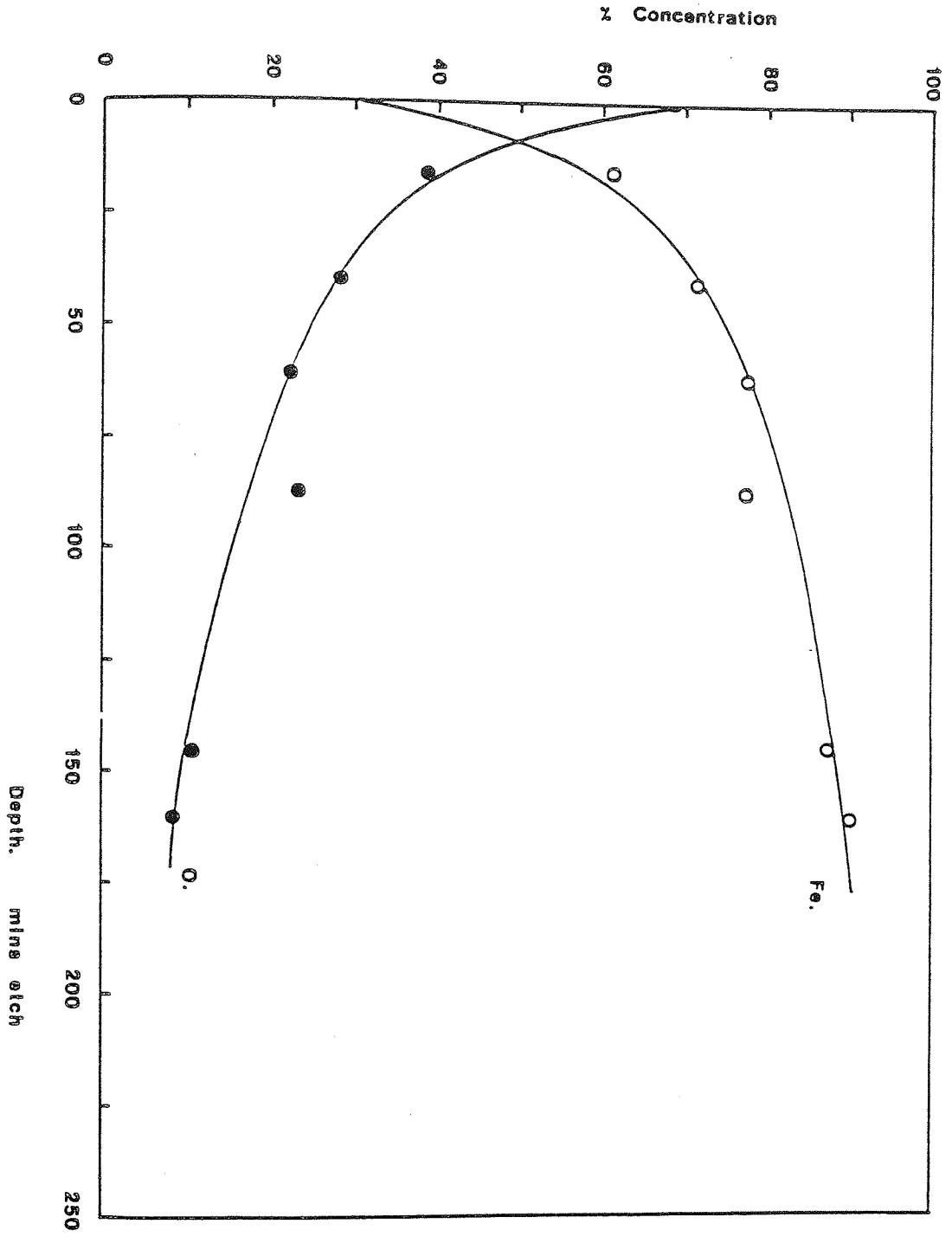

Figure 3.46.

Auger electron depth profile of a pin worn at 49.1 N at a speed of 0.02 ms^{-1} in Technical White Oil with 0.1% stearic acid

In the case of the carbon peaks, the highest binding energy corresponds to the carbon-carbon bond, the middle to carbon single bond oxygen; and the lower carbon double bond oxygen. The accompanying oxygen variation shows for highest binding energy the oxygen-oxygen bond, then a small peak corresponding to a non-stoichimetric surface oxygen or water molecule, the next lowest corresponds to oxygen single bond carbon and the lowest to oxygen double bond carbon. The binding energies here are $\pm$ 0.5 eV and within experimental error agree with published figures for these transitions [111, 112].

Figure 3.47 shows the collected spectra for a worn pin surface run in flooded conditions in Technical White Oil at 98.2 N load and a speed of 0.04 ms^{-1}. Figures 3.48 and 3.49 are from pins run in Technical White Oil with 0.1% stearic acid additive. Figures 3.48 at 98.2 N and 0.04 ms^{-1} and figure 3.49 at 122.7 N and 0.06 ms^{-1}. In each of these two figures a marked increase in C-O and C=O bonds is apparent.

Stearic acid is known to form iron-stearate soap films on steel surfaces, and further cohesive forces cause acid molecules present in the oil to increase the film thickness. The stearic acid molecule is 30 $\mathring{A}$ in length and up to five monolayers are typically found on the surface after wear (90). This then can leave a film, of up to 150 $\mathring{A}$ on the pin surface, although film thicknesses of several thousand angstroms have been measured [113, 114].

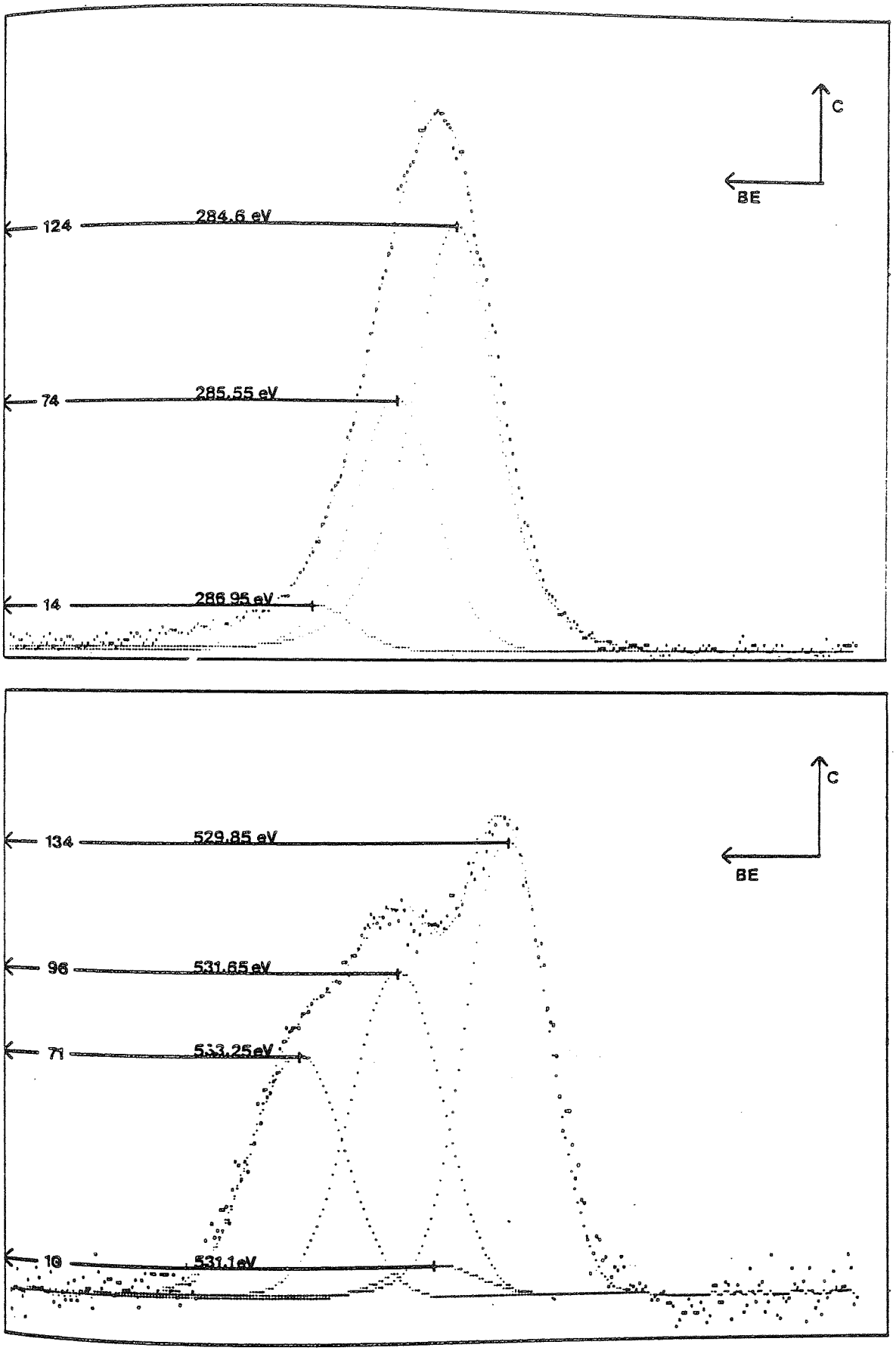

Figure 3.47

X-ray photoelectron spectra for upper C_{1s} and lower O_{1s} transitions, for a pin surface run at 98.2 N load at a speed of 0.04 ms^{-1} in Technical White Oil.

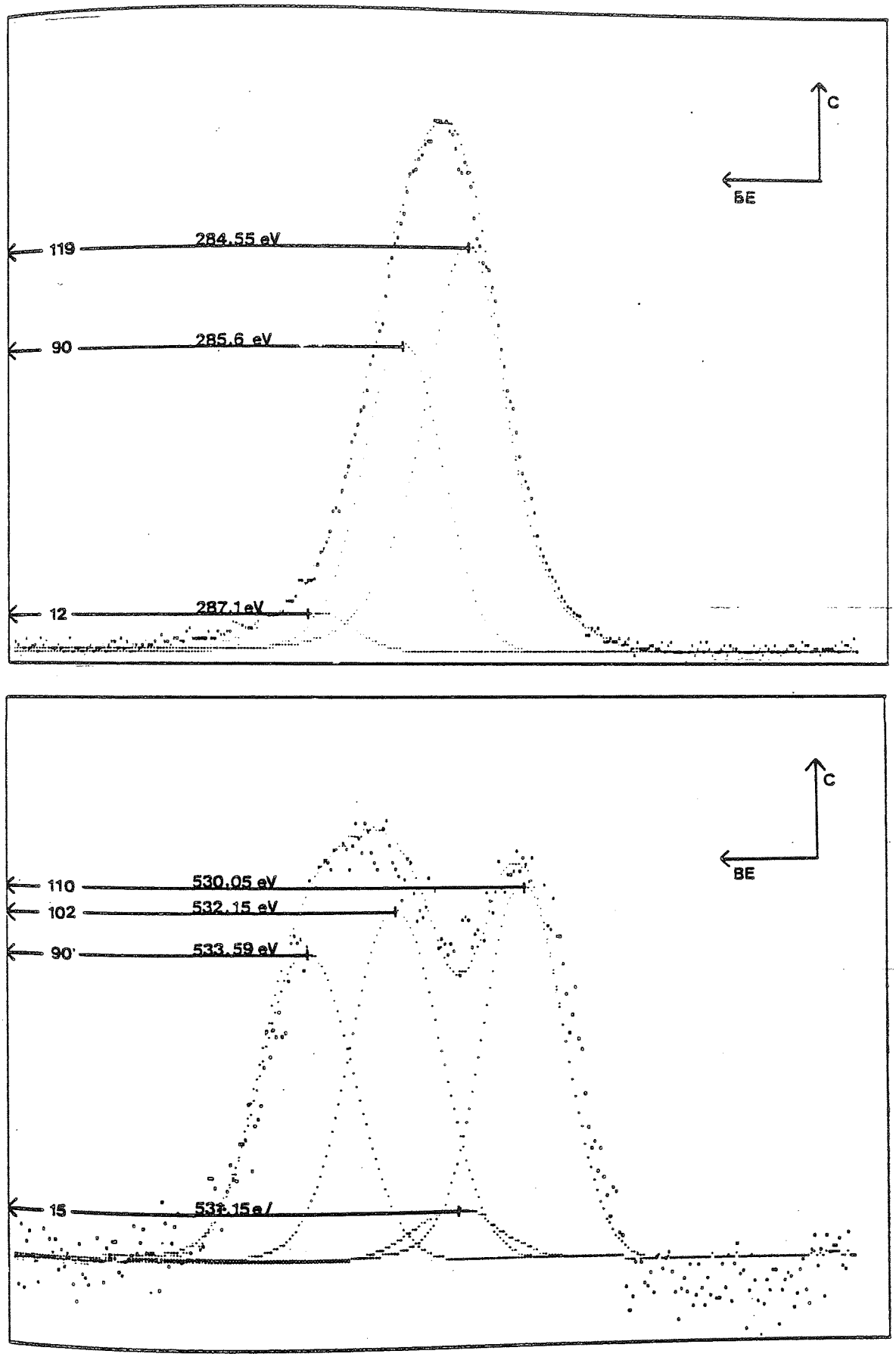

Figure 3.48

X-ray photoelectron spectra for upper C_{1s} and lower O_{1s} transitions, for a pin run at 98.2 N load at a speed of 0.04 ms^{-1} in Technical White Oil with 0.1% stearic acid.

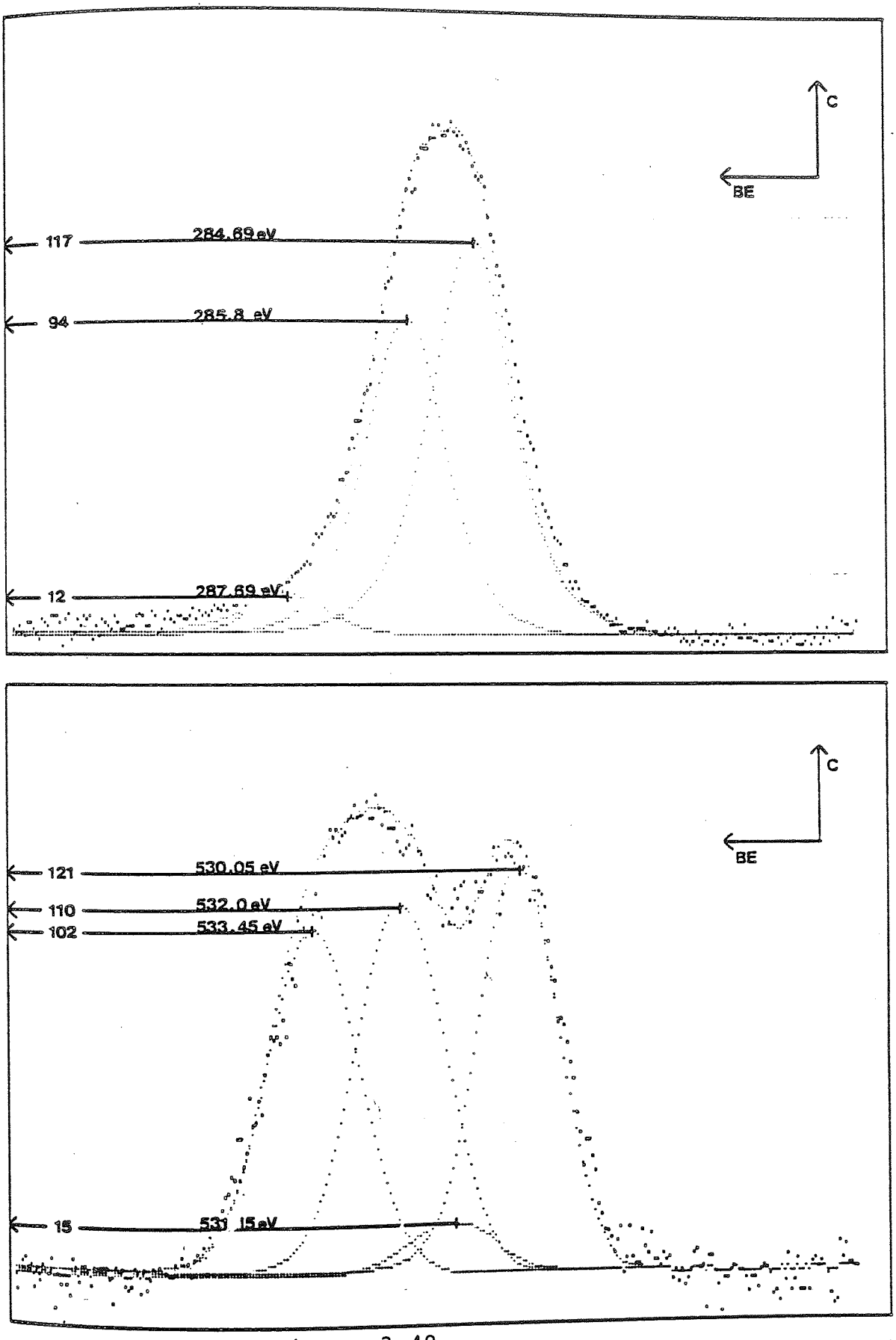

Figure 3.49

X-ray photoelectron spectra for upper C_{1s} and lower O_{1s} transntions, for a pin run at 122.7 N load at a speed of 0.06 ms^{-1} in Technical White Oil with stearic acid.

In figures 3.47 to 3.49 the C-C bond is obviously the most dominant as both oil and acid are formed of primarily long carbon chains. An increase is apparent, though in the C-O bond in figures 3.48 and 3.49, this is undoubtedly due to the presence of the acid molecules on the pin surface. This is seen also in figures 3.48 and 3.49 by the increase in the O=C and O-C peaks.

CHAPTER FOUR

THEORETICAL CONSIDERATIONS

4.1 Development of a Wear Model

The Auger electron depth profiles presented in figures 3.22 and 3.23 show that there is a gradation of oxygen with depth into the oxide which is characteristic of an agglomerate oxide layer; as opposed to the constant concentration of oxygen with depth followed by a sharp decrease at the plateaux substrate boundary seen in diffusion controlled oxide plateaux formation (44). Scanning electron micrographs seen in figures 3.8 - 3.13 clearly show the agglomerate nature of the oxide and show it to rest over existing surface features, indicating that the oxide formed elsewhere, became detached and transferred to form an agglomerate layer in the observed position.

The Auger depth profiles provide a history of the build up of the plateaux, but there are two possible explanations for the observations. It is postulated that the plateaux are formed by sintering of wear particles, it may then be assumed that either the particles consist initially mainly of metal debris with the amount of oxide increasing with sliding distance, or that the ratio of

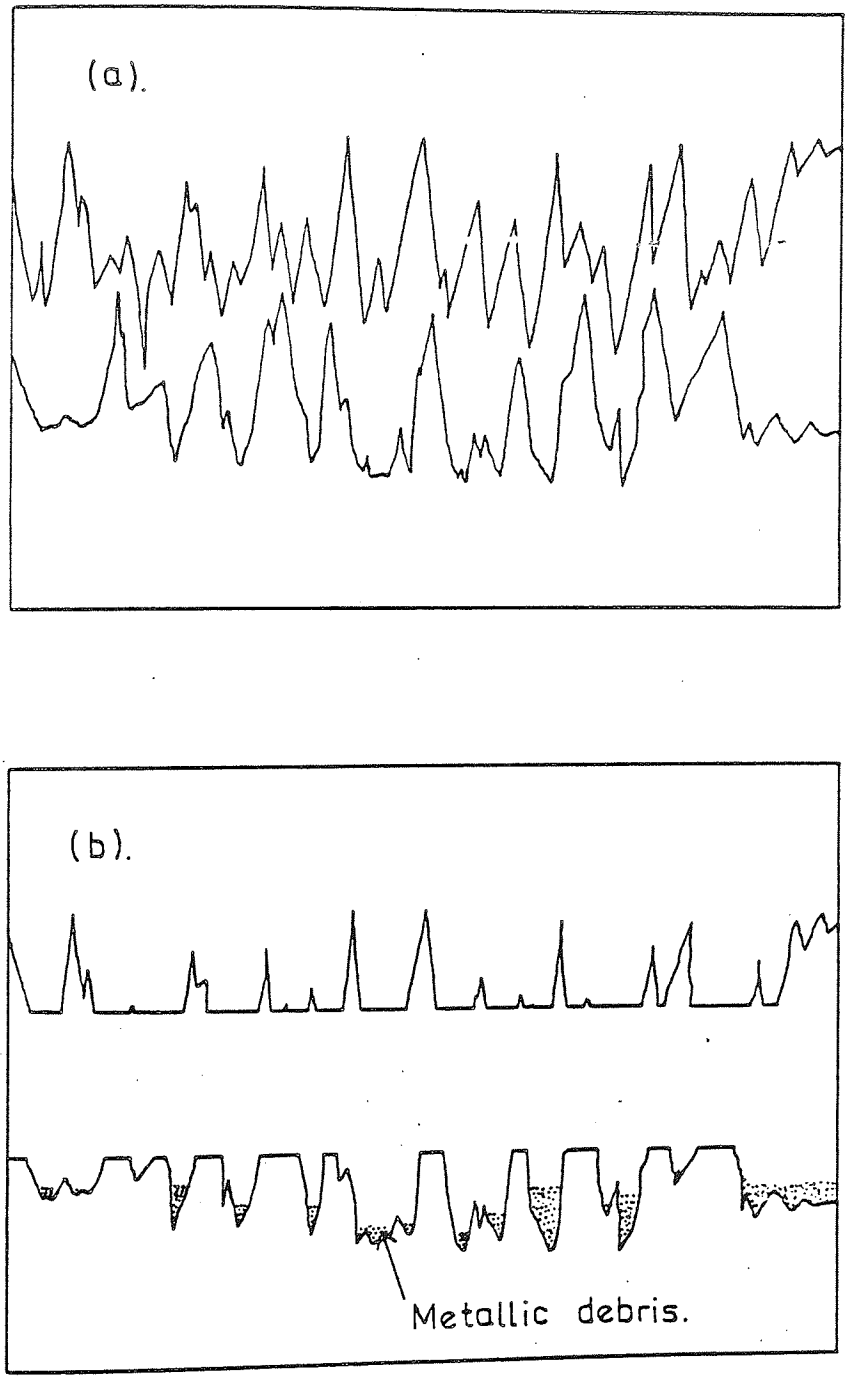

Figure 4.1

(a) The unworn microtopography of opposing surfaces and

(b) the same surfaces after a few passes showing the collection of metallic debris

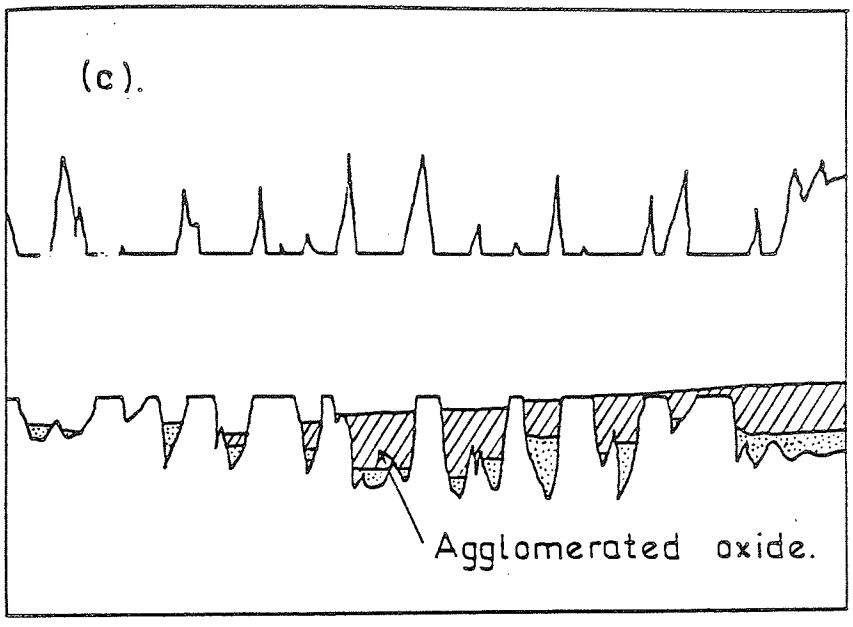

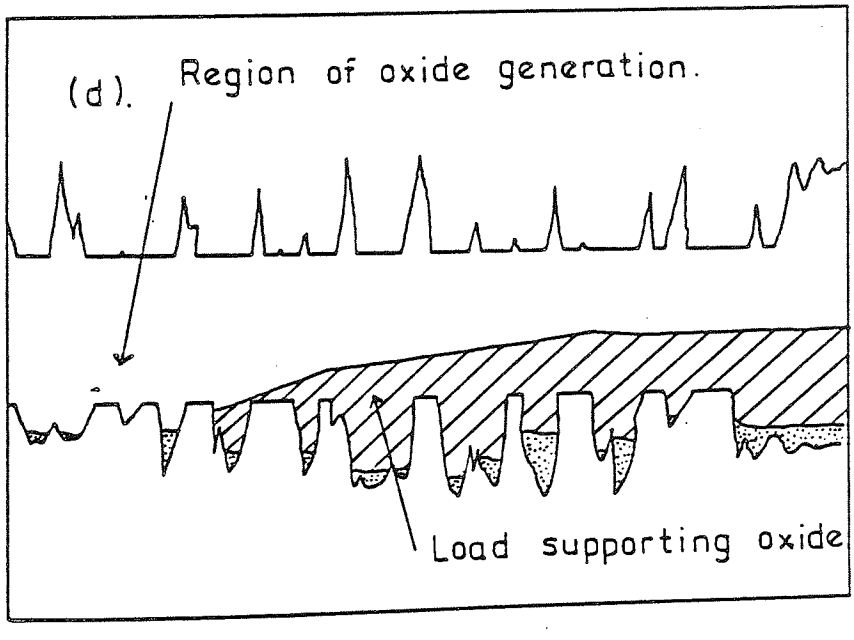

Figure 4.1

(c) after continued rubbing oxide particles collect over the metal debris and

(d) eventually further agglomeration causes this oxide to become load bearing

oxide to metal particles included in the agglomerate remains constant during formation of the plateaux, but that further oxidation takes place during and after build up to some critical thickness prior to final removal.

At the onset of rubbing a sequence of events similar to those shown in figures 4.1a - d are imagined. The initial high rough microtopography of the surface, figure 4.1a, will be quickly smoothed as the surfaces plastically deform and fracture to conform with one another. Metal debris so produced will be comminuted and collect in the remaining valleys of the surfaces, figure 4.1b. This will occur within a few passes and is consistent with the small running-in times and minimal metallic debris observed experimentally. The surfaces then oxidise rapidly with most asperity contacts; the oxidation occurring at an intermediate temperature between the contact and general surface temperature, as proposed by Stott et al[72], until the next of subsequent encounters whereby this oxide layer is removed. These oxide flakes then collect in the valleys over the metallic debris, figure 4.1C, until continued oxidation-scrape-reoxidation causes the agglomerate layer to thicken above the level of the local asperities and so become load bearing, figure 4.1d. Oxidation continues at the surface of this layer, and elsewhere due to the removal, further oxidation, and reagglomeration of parts of this plateaux.

The oxide coverage increases in the early stages of sliding in a way similar to that described by Wilson et al[73] with oxide coverage increasing laterally over the surface until some equilibrium ratio of load bearing plateaux to oxide generating regions is established. However, contrary to the report of those authors no restriction on the vertical growth of oxide plateaux has been observed in this work, and the evidence of scanning electron microscopy, figures 3.8 - 3.13 and Auger electron spectroscopy, figures 3.22 and 3.23, indicate a great difference in thicknesses of oxide plateaux. In the initial stages of sliding the lateral growth of load bearing agglomerate oxide plateau does, however, explain the decrease in wear rate from the wear-in values to the equilibrium level. Assuming that the rate determining factor in these experiments is thin film logarithmic oxide growth on asperities contacting in regions not covered by oxide plateaux, then the growth of these plateaux in the initial high wear stages of running-in reduces the areas available for oxide generation, and ultimately leads to the dynamic equilibrium between the generation, agglomeration and final removal of oxide as debris.

Oxidational growth under these conditions may be described by a direct logarithmic growth law, such that the thickness X attained in time t is given by:

$$X = C \text{ Ln } (At + K) \qquad (4.1)$$

where A and C are logarithmic rate constants and K = 1 if X = 0 at t = 0.

If it is assumed that the oxide thickness X is produced in a short time before being removed at the next encounter, then $At \ll 1$ and the equation reduces to:

$$X = C\ A\ t \qquad (4.2)$$

This form of the equation should not be confused with linear growth rate kinetics and the growth constants, A and C, appropriate to logarithmic growth must be used. These growth rate constants may be described by Arrhenius equations such that:

$$A = A_L^1 \exp - \left(\frac{Q_L^1}{RT_o}\right) \qquad (4.3)$$

and

$$C = A^{11}_L \exp - \left(\frac{Q^{11}_L}{RT_o}\right) \qquad (4.4)$$

where A_L^1 and A^{11}_L are Arrhenius constants with dimensions of time^{-1} and length respectively. Q_L^1 and Q^{11}_L are activation energies and T_o the oxidational temperatures and R the universal gas constant.

Mills[115] conducted a series of experiments on the static oxidation or iron and low alloy steels and from his data it is possible to evaluate the quantities Q_L^I and Q^{II}_L. Sullivan et al[46] have argued that activation energies calculated from static oxidation data may be applied to tribological data, but that Arrhenius constants will be very different. Thus using the values of Q_L^I = 43 KJ mol^{-1} and Q^{II}_L = 30 KJ mol^{-1} obtained from the data of Mills, equation (2) becomes:

$$X = A_L \exp - \left(\frac{73,000}{RT_o}\right). t \qquad (4.5)$$

where $A_L = A_L^I \cdot A^{II}_L$

If it is assumed that the mean asperity radius is "a", then the volume of oxide debris, V, produced at each asperity per unit distance of sliding is:

$$V = A_L \exp - \left(\frac{73,000}{RT_o}\right). \pi a^2. U^{-1} \qquad (4.6)$$

where U is the linear velocity.

As stated, it is assumed in this model that this volume is removed at the next of subsequent encounters and that the majority of debris so produced is agglomerated to form oxide plateaux. These plateaux grow to critical

thickness and are then removed to form large wear particles. Thus the plateaux do not generate the wear debris, but merely act as an intermediate stage in the debris removal process. The plateaux do, however, act as load bearing areas and reduce the area of debris generation. Thus the debris generating area may be regarded as a fraction β of the real area of contact. Careful study of a large number of scanning electron micrographs of worn pin surfaces indicates that when equilibrium conditions have been established about half of the area of contact is covered by load bearing plateaux, which is in agreement with similar analyses in other studies[60], and so a value of $\beta = \frac{1}{2}$ is appropriate.

Here an argument has been developed for oxide growth at asperity contacts, but it must not be assumed that each enounter will lead to oxide growth. Some metal to metal contacts will lead to severe adhesive wear and the production of metallic debris.

If it is assumed that in the areas not covered by plateaux, α is the fractional coverage of oxide and further assume that both oxide-oxide contacts and oxide-metal contacts will lead to oxide production and removal and that only metal-metal contacts lead to the production of metallic debris, then the total volume of material removed per unit distance of sliding, V may be written as:

$$V = A_L \exp - \left(\frac{73,000}{RT_o}\right) \frac{\beta N \pi a^2}{U} \alpha^2 +$$

$$A_L \exp - \left(\frac{73,000}{RT_o}\right) \frac{\beta N \pi a^2}{U} 2\alpha (1 - \alpha)$$

$$+ K_s (1 - \alpha)^2 \beta N \pi a^2 \qquad (4.7)$$

where

α^2 : probability of oxide-oxide contact

$2\alpha (1-\alpha)$: probability of oxide-metal contact

$(1-\alpha)^2$: probability of metal-metal contact

K_s : Archard wear factor for severe metallic wear

N : total number of asperity contacts

$N\pi a^2$ may be written as W/Pm where

W : applied load

P_m : flow pressure of the substrate.

And hence equation (4.7) may be rewritten as:

$$V = A_L \exp - \left(\frac{73,000}{RT_o}\right) \cdot \frac{W}{2UP_m} \cdot \alpha(2-\alpha)$$

$$+ K_s (1-\alpha)^2 \frac{W}{2P_m}$$

This quantity is equal to the wear rate, W, under equilibrium conditions:

$$W = \{A_L \exp - (\frac{73,000}{RT_o}) \cdot \frac{\alpha(2-\alpha)}{U} + K_s (1-\alpha)^2 \} \frac{W}{2P_m} \quad (4.8)$$

The quantity in brackets is the Archard wear factor for this wear process.

At very low speeds the first term in equation (4.8) dominates and this is supported by the experimental evidence of X-ray powder diffraction data, figures 3.17a - 3.20a, which shows in each case the debris to consist mainly of oxide. On this basis the lowest speed for each load has been taken and a value of A_L calculated assuming that all contacts produce oxide debris. The values of A_L so calculated are given in Table 4.1 and are used in equation (4.8) to calculate wear rates for the whole speed range at a given load.

It is not possible to measure the value of α, but if it is assumed that equal volumes of metallic and oxide debris are produced and further since mild wear rates are $\sim 10^{-2}$ times severe wear rates, then

Table 4.1

Calculated values of A_L with load

LOAD N	A_L ms^{-1}
4.9	2.83×10^7
9.8	1.22×10^7
19.6	7.98×10^6
49.1	4.12×10^6

$$(1-\alpha)^2 = 10^{-2}$$

$$\alpha = 0.9$$

In practice the volumes of metallic debris were always less than that of oxide and hence α will lie between 0.9 and 1. For the purpose of these calculations, however, the lower value has been adopted.

The value of the Archard severe wear factor, K_s, was obtained from estimates of experimental severe wear rates above the T_1 transition and was fixed at 6.7×10^{-3}.

The flow pressure P_m was calculated from the experimentally determined hardness of the substrate, 280 HV, and thus the appropriate value of P_m is 2.75×10^9 Nm^{-2}.

There is still controversy over the temperature responsible for the tribological oxide growth, although by the criteria suggested by Stott et al[72] one would expect that for the conditions of these experiments, that is low load and speed combinations and little frictional heating, that general surface temperatures and out of contact oxidation would predominate. Despite this contact temperatures were calculated by a method similar to that described by Rowson and Quinn[102] the outline of which will be presented in the following section, 4.2.

Meanwhile, Tables 4.2, 4.3, 4.4 and 4.5 present the sliding speed and experimental wear rate along with the estimated contact temperature and the theoretical wear rate calculated from equation (4.8) using the contact temperature as T_o .

The results presented in these tables for loads of 4.9, 9.8, 19.6 and 49.1N are graphically presented in figures 4.2 - 4.5, and show theoretical and experimental wear rates as a function of sliding speed. It can be seen from each of these curves that at the higher speeds the theoretical wear rates are orders of magnitude higher than the experimental wear rates. This is due to the rapid increase in contact temperature at these speeds. In contrast to this at the lower speeds where the contact temperatures are close to the general surface temperatures good agreement is seen between theoretical and experimental curves and, indeed, when the general surface temperatures are used throughout instead of the contact temperatures the theoretical curves follow the experimental curves closely even at higher speeds. Tables 4.6 - 4.9 show the sliding speed and experimental wear rate along with the general surface temperatures and the theoretical wear rate calculated using these temperatures from equation (4.8). This data is shown graphically for loads of 4.9, 9.8, 19.6 and 49.1N loads in figures 4.6 - 4.9 respectively.

Table 4.2

Theoretical and experimental wear rates with contact temperature and speed for a 4.9 N load.

sliding speed ms^{-1}	Exp. wear rate $m^3 m^{-1}$	contact temp °C	Theo. wear rate $m^3 m^{-1}$
0.005	7.71×10^{-13}	25.48	8.99×10^{-13}
0.006	2.89×10^{-13}	23.69	6.45×10^{-13}
0.008	4.95×10^{-13}	25.12	5.63×10^{-13}
0.016	2.88×10^{-13}	28.85	4.24×10^{-13}
0.056	1.12×10^{-13}	45.16	5.22×10^{-13}
0.105	5.03×10^{-14}	52.6	5.23×10^{-13}
0.216	6.99×10^{-14}	102.9	8.37×10^{-12}
0.355	6.84×10^{-14}	160.8	1.14×10^{-10}
0.615	1.82×10^{-13}	271.3	4.01×10^{-9}
1.05	2.0×10^{-13}	297.2	4.89×10^{-9}

Table 4.3

Theoretical and experimental wear rates with contact temperature and speed for a 9.8 N load.

sliding speed ms^{-1}	Exp. wear rate $m^3 m^{-1}$	contact temp °C	Theo. wear rate $m^3 m^{-1}$
0.003	1.01×10^{-12}	23.61	1.12×10^{-12}
0.005	8.51×10^{-13}	24.85	7.99×10^{-13}
0.0075	6.3×10^{-13}	27.57	7.11×10^{-13}
0.01	3.84×10^{-13}	23.82	4.27×10^{-13}
0.019	5.19×10^{-13}	31.66	4.65×10^{-13}
0.027	3.62×10^{-13}	32.37	3.79×10^{-13}
0.039	3.08×10^{-13}	36.87	3.93×10^{-13}
0.06	2.64×10^{-13}	47.79	5.86×10^{-13}
0.103	2.16×10^{-13}	48.7	4.13×10^{-13}
0.295	2.47×10^{-13}	138.8	4.03×10^{-11}
0.502	4.51×10^{-13}	135.2	1.97×10^{-11}
0.991	9.44×10^{-12}	459.8	1.36×10^{-7}

Table 4.4

Theoretical and experimental wear rates with contact temperature and speed for a 19.6 N load.

sliding speed ms^{-1}	Exp. wear rate $m^3 m^{-1}$	contact temp °C	Theo. wear rate $m^3 m^{-1}$
0.003	1.57×10^{-12}	25.22	1.77×10^{-12}
0.006	1.29×10^{-12}	29.73	1.42×10^{-12}
0.01	1.53×10^{-12}	28.62	8.8×10^{-13}
0.015	8.47×10^{-13}	30.23	7.38×10^{-13}
0.021	6.64×10^{-13}	36.75	8.95×10^{-13}
0.029	6.51×10^{-13}	36.62	7.08×10^{-13}
0.051	5.18×10^{-13}	47.7	9.49×10^{-13}
0.062	3.74×10^{-13}	55.88	1.39×10^{-12}

Table 4.5

Theoretical and experimental wear rates with contact temperature and speed for a 49.1 N load.

sliding speed ms^{-1} $\times 10^{-3}$	Exp. wear rate $m^3 m^{-1}$	contact temp °C	Theo. wear rate $m^3 m^{-1}$
2.85	2.51×10^{-12}	27.35	3.17×10^{-12}
3.78	1.95×10^{-12}	27.9	2.64×10^{-12}
5.14	2.12×10^{-12}	26.41	1.9×10^{-12}
6.85	1.77×10^{-12}	33.11	2.45×10^{-12}
7.01	2.50×10^{-12}	27.01	1.61×10^{-12}
9.55	6.23×10^{-11}	41.47	1.45×10^{-12}

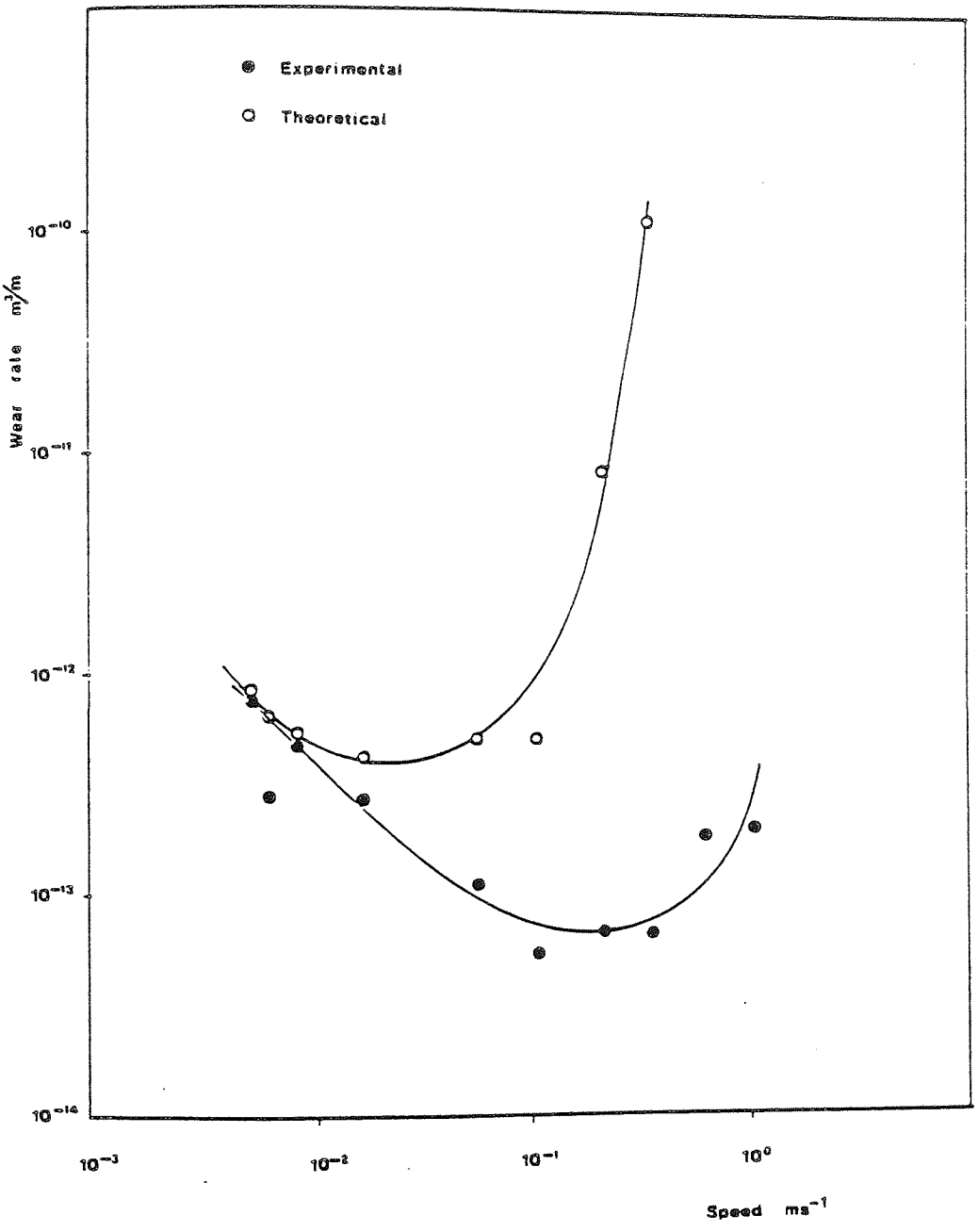

Figure 4.2

Theoretical and experimental wear rates versus speed for 4.9 N load, using contact temperature as T_o.

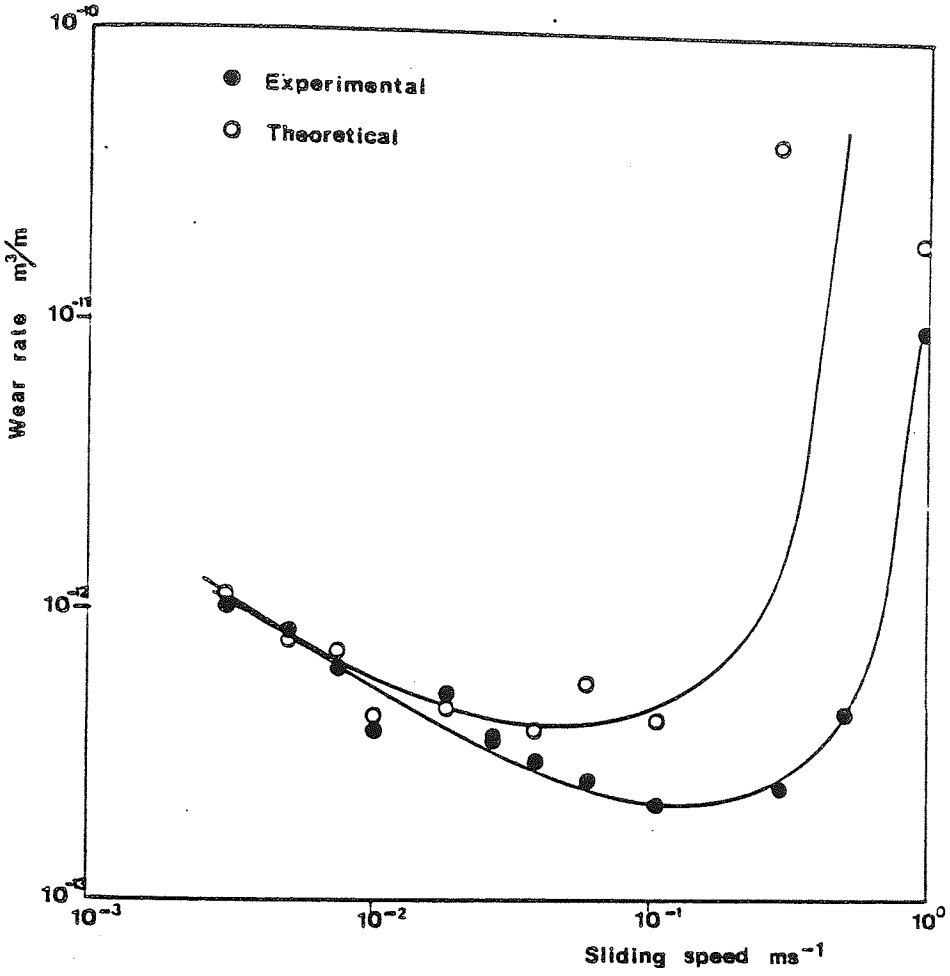

Figure 4.3

Theoretical and experimental wear rates versus speed for 9.8 N load, using contact temperature as T_o.

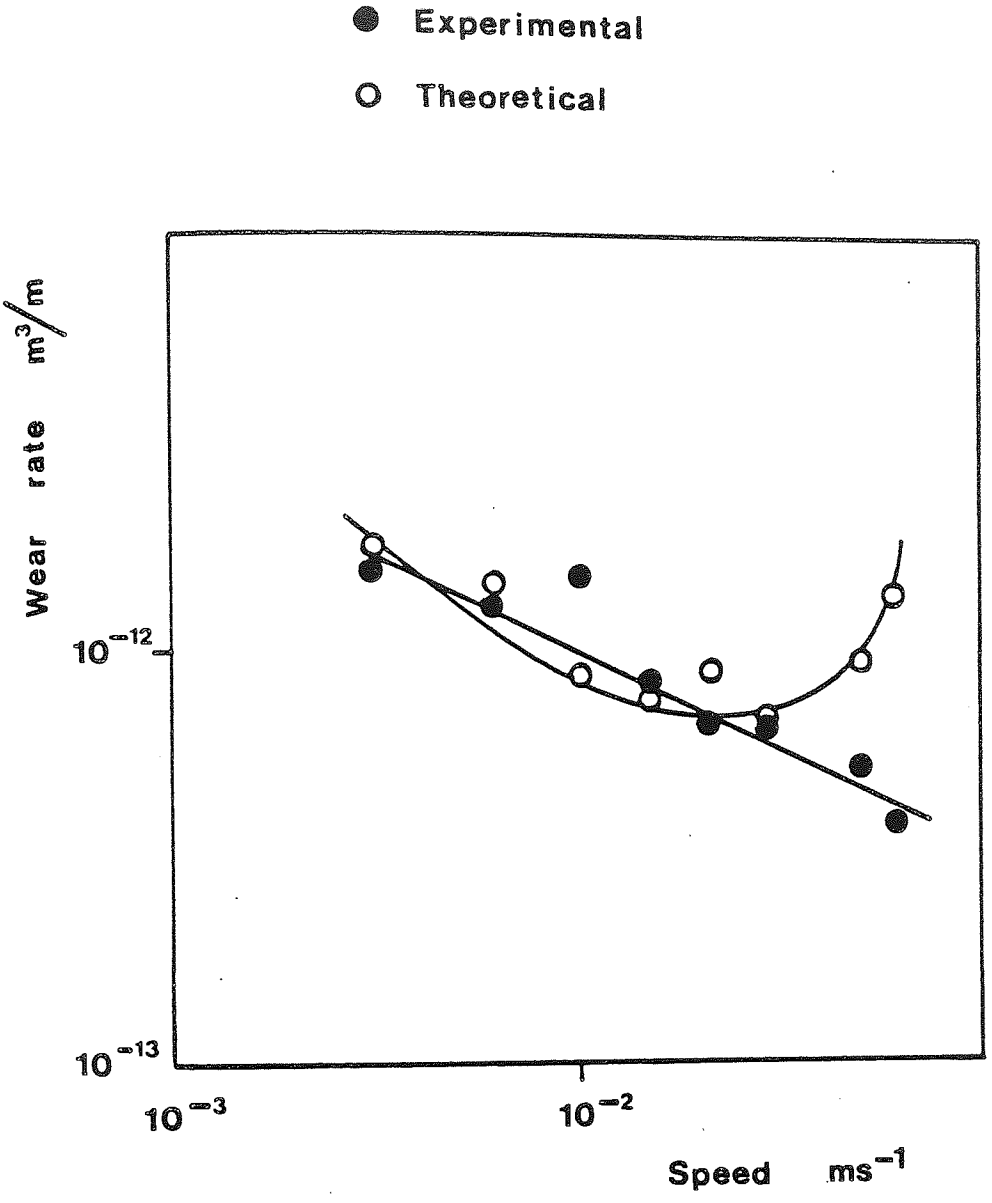

Figure 4.4

Theoretical and experimental wear rates versus speed for 19.6N load, using contact temperature as T_o.

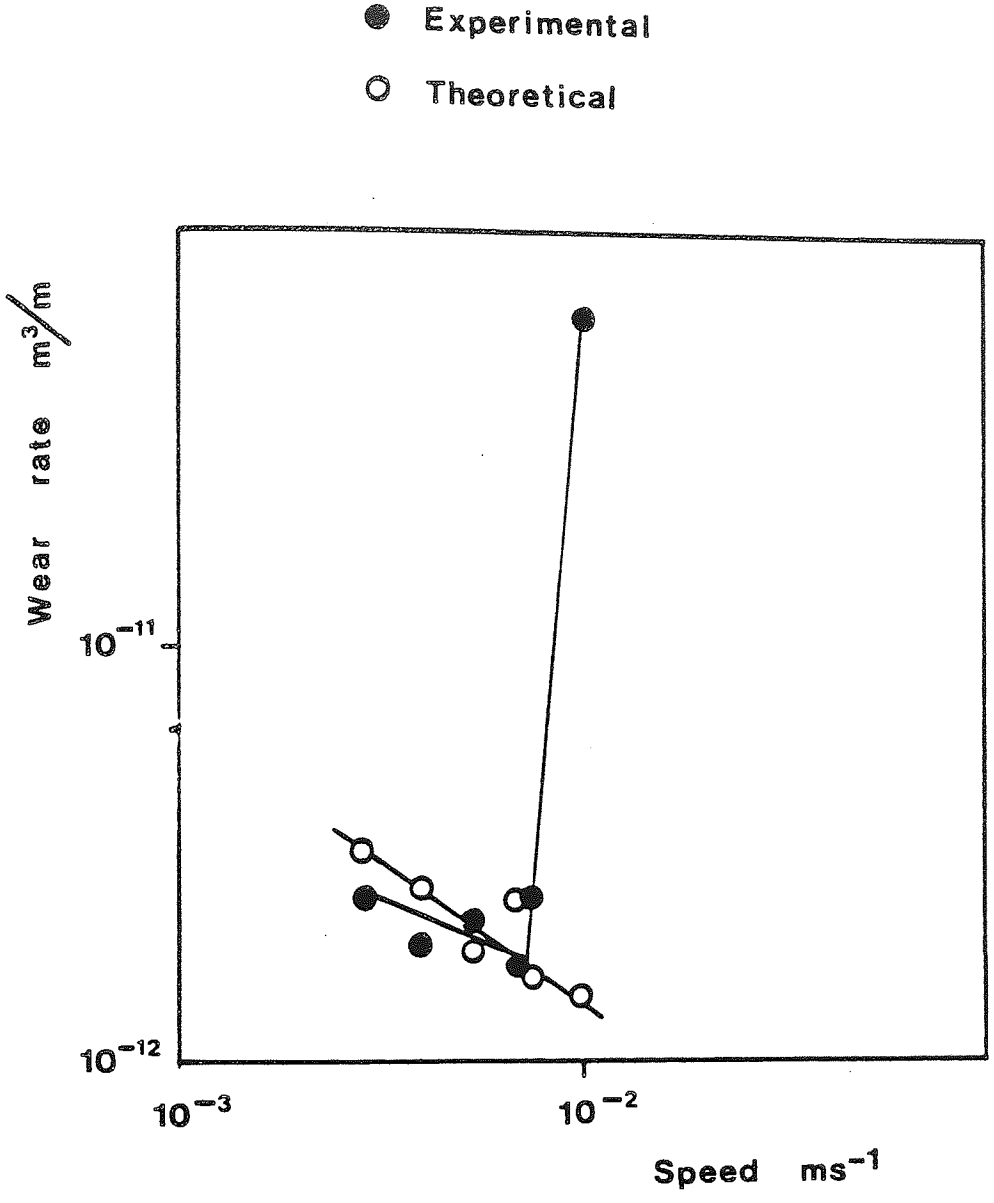

Figure 4.5

Theoretical and experimental wear rate versus speed for 49.1 N load, using contact temperature as T_o .

Table 4.6

Theoretical and experimental wear rates with general surface temperature and speed for 4.9 N load.

sliding speed ms^{-1}	Exp. wear rate $m^3 m^{-1}$	general surface temp °C	Theo. wear rate $m^3 m^{-1}$
0.005	7.71×10^{-13}	23.82	7.71×10^{-13}
0.006	2.89×10^{-13}	21.92	5.5×10^{-13}
0.008	4.95×10^{-13}	22.9	4.65×10^{-13}
0.016	2.88×10^{-13}	23.3	2.71×10^{-13}
0.056	1.12×10^{-13}	24.5	1.28×10^{-13}
0.105	5.03×10^{-14}	25.9	1.01×10^{-13}
0.216	6.99×10^{-14}	28.29	8.54×10^{-14}
0.355	6.84×10^{-14}	30.18	7.84×10^{-14}
0.615	1.82×10^{-13}	35.78	7.80×10^{-14}
1.05	2.0×10^{-13}	32.83	6.79×10^{-14}

Table 4.7

Theoretical and experimental wear rates with general surface temperature and speed for a 9.8 N load.

sliding speed ms^{-1}	Exp. wear rate $m^3 m^{-1}$	general surface temp °C	Theo. wear rate $m^3 m^{-1}$
0.003	1.01×10^{-12}	22.44	1.01×10^{-12}
0.005	8.51×10^{-13}	22.89	6.77×10^{-13}
0.0075	6.3×10^{-13}	24.28	5.47×10^{-13}
0.01	3.84×10^{-13}	21.86	3.71×10^{-13}
0.019	5.19×10^{-13}	23.96	2.82×10^{-13}
0.027	3.62×10^{-13}	24.52	2.41×10^{-13}
0.039	3.08×10^{-13}	25.09	2.08×10^{-13}
0.06	2.64×10^{-13}	25.33	1.78×10^{-13}
0.103	2.16×10^{-13}	24.05	1.49×10^{-13}
0.295	2.47×10^{-13}	29.01	1.37×10^{-13}
0.502	4.51×10^{-13}	28.51	1.29×10^{-13}
0.991	9.44×10^{-12}	65.47	2.37×10^{-13}

Table 4.8

Theoretical and experimental wear rates with general surface temperature and speed for a 19.6 N load.

sliding speed ms^{-1}	Exp. wear rate $m^3 m^{-1}$	general surface temp °C	Theo. wear rate $m^3 m^{-1}$
0.003	1.57×10^{-12}	23.78	1.57×10^{-12}
0.006	1.29×10^{-12}	26.62	1.11×10^{-12}
0.01	1.53×10^{-12}	24.18	6.54×10^{-13}
0.015	8.47×10^{-13}	24.12	5.14×10^{-13}
0.021	6.64×10^{-13}	25.64	4.67×10^{-13}
0.029	6.51×10^{-13}	24.4	3.85×10^{-13}
0.051	5.18×10^{-13}	25.47	3.31×10^{-13}
0.062	3.74×10^{-13}	28.1	3.37×10^{-13}

Table 4.9

Theoretical and experimental wear rate with general surface temperature and speed for a 49.1 N load.

sliding speed ms^{-1} $\times 10^{-3}$	Exp. wear rate $m^3 m^{-1}$	general surface temp °C	Theo. wear rate $m^3 m^{-1}$
2.85	2.51×10^{-12}	24.74	2.59×10^{-12}
3.78	1.95×10^{-12}	24.25	1.65×10^{-12}
5.14	2.12×10^{-12}	23.55	1.57×10^{-12}
6.85	1.77×10^{-12}	27.54	1.68×10^{-12}
7.01	2.50×10^{-12}	23.7	1.32×10^{-12}
9.55	6.23×10^{-11}	24.32	1.16×10^{-12}

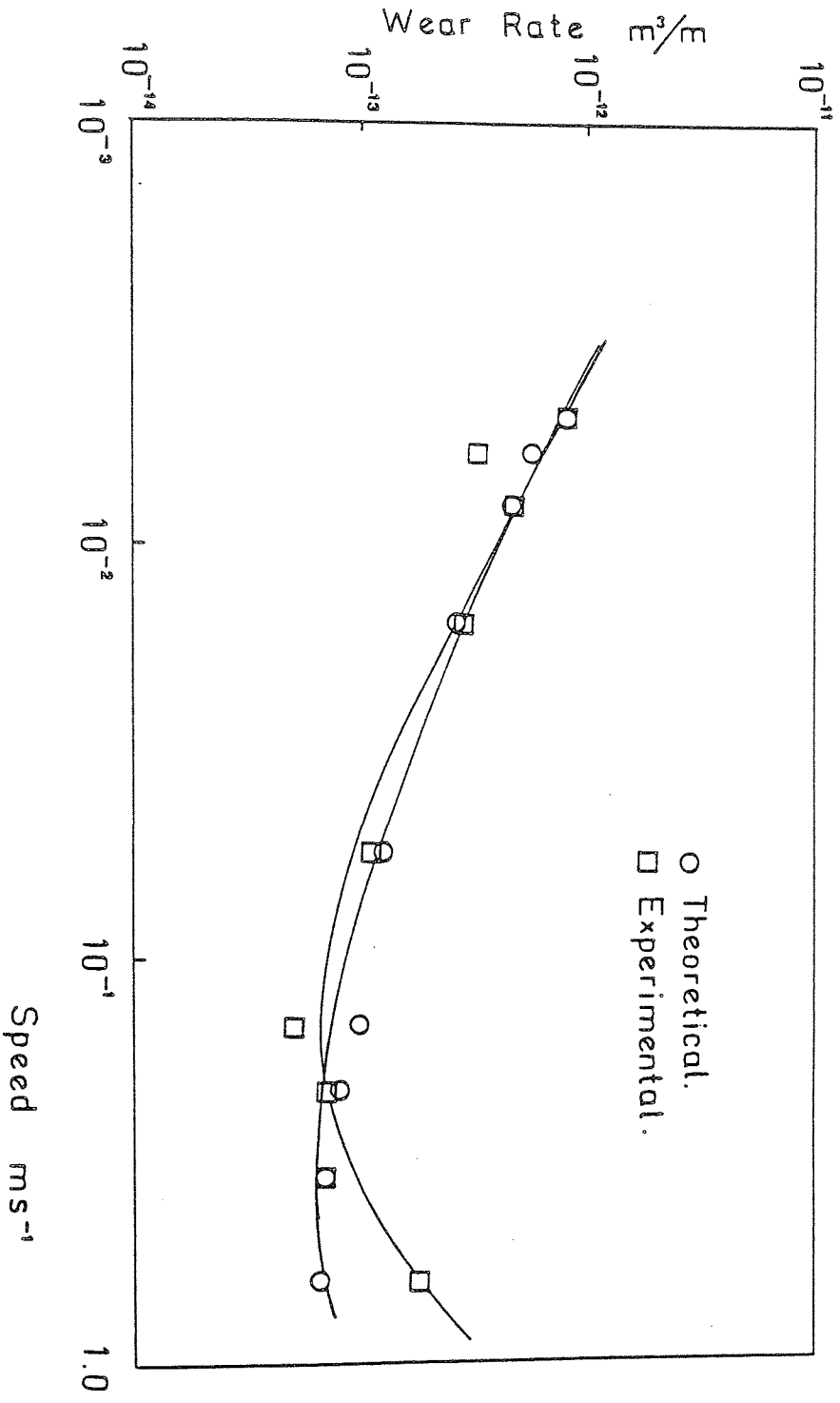

Figure 4.6

Theoretical and experimental wear rates versus speed for 49.1 N load, using general surface temperatures as T_o .

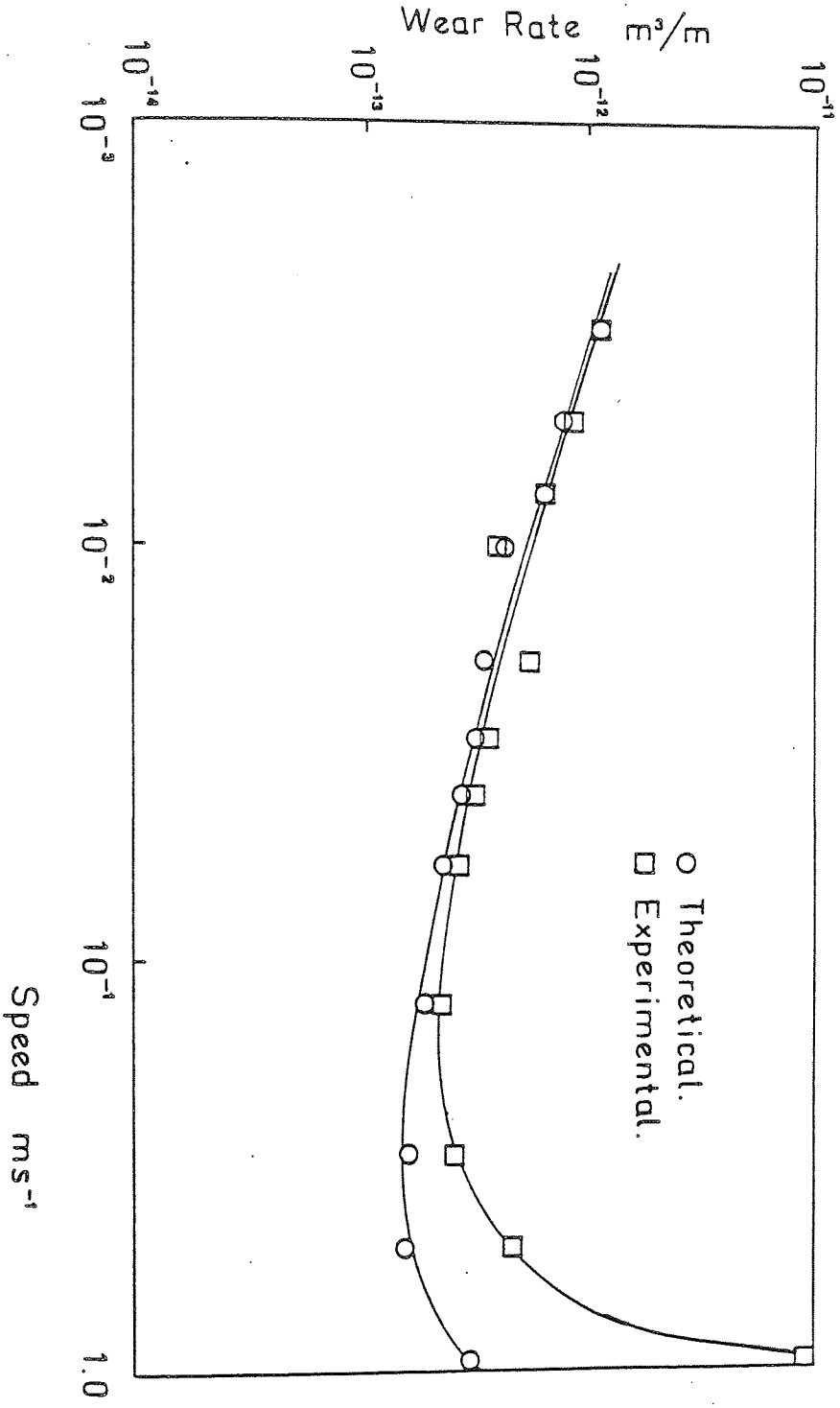

Figure 4.7

Theoretical and experimental wear rates versus speed for 9.8 N load, using general surface temperature as T_o .

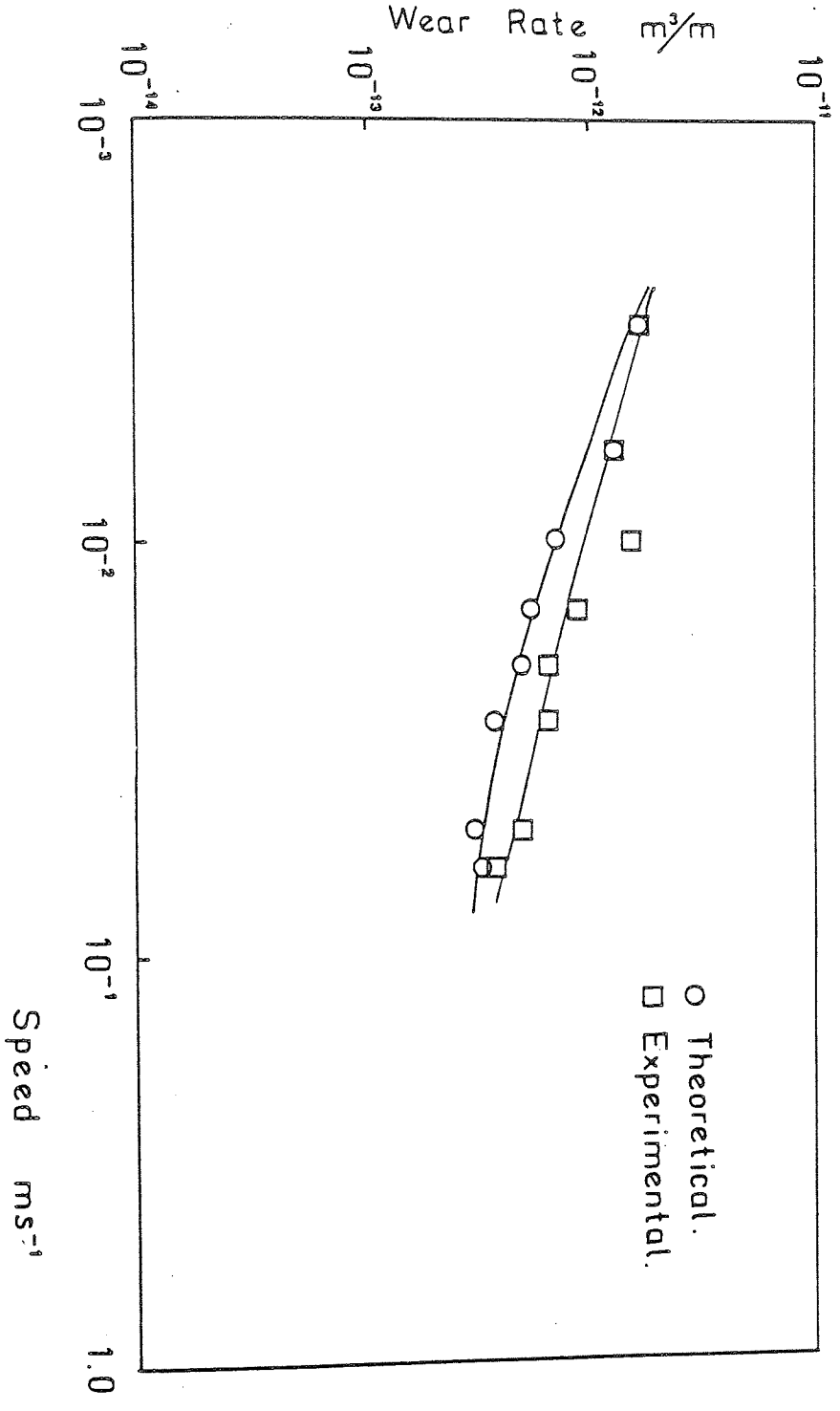

Figure 4.8

Theoretical and experimental wear rates versus speed for 19.6 N load, using general surface temperature T_o .

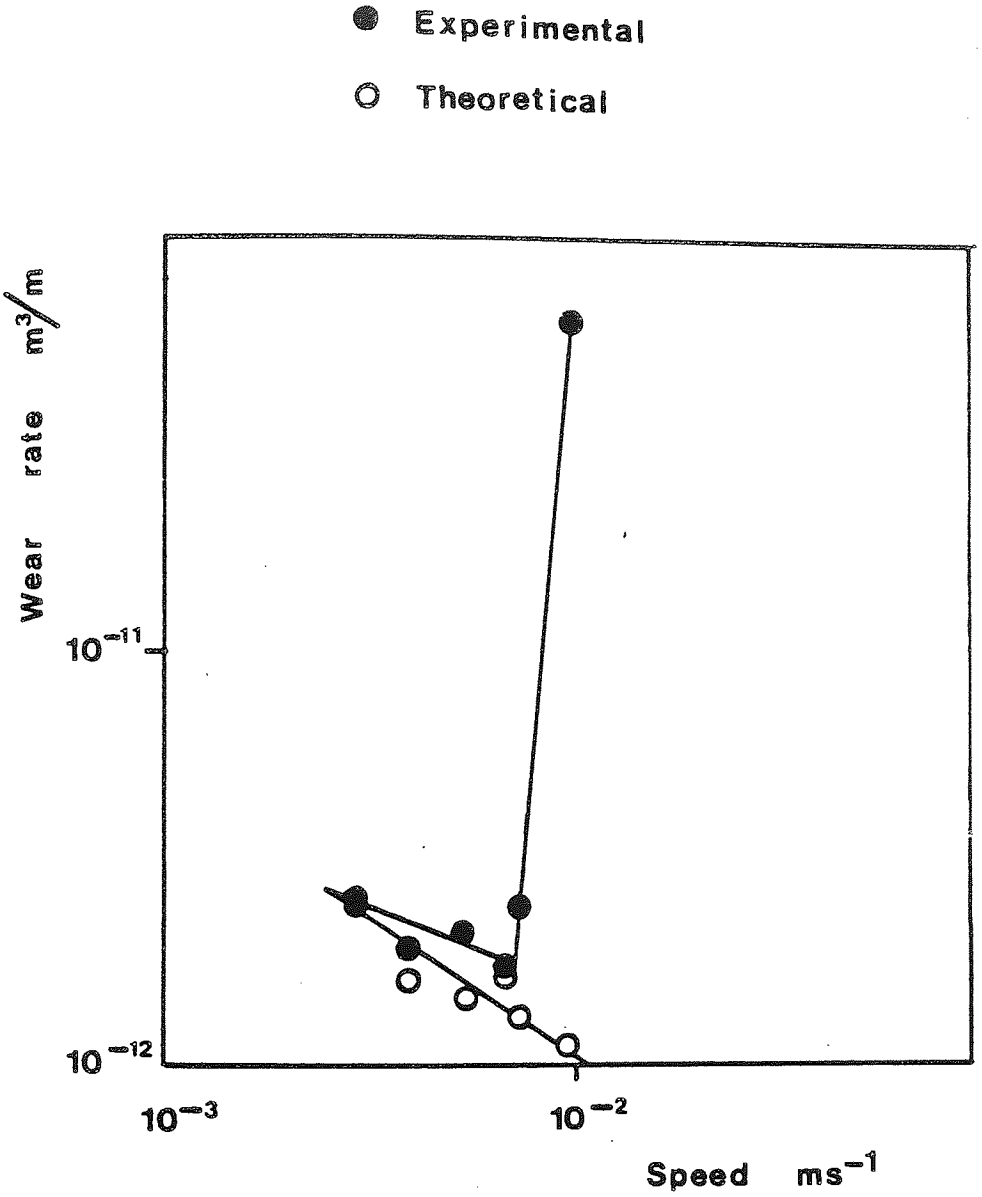

Figure 4.9

Theoretical and experimental wear rates versus speed for 49.1 N load, using general surface temperature as T_o .

One further series of wear rates were determined and are shown in figure 4.10. These are for a 14.7 N load and the theoretical curve here was calculated from equation (4.8) using the value of A_L as the average of the 9.8 and 19.6N loads and equal to 1.01×10^{7} ms^{-1} .

The theoretical results presented here indicate that the assertion of Stott et al[72] is correct and that general surface temperatures and out of contact oxidation predominate. In the case of the 49.1 N load in figures 4.5 and 4.9 where general surface temperatures and contact temperatures are similar, there is little difference in the theoretical curves, however, in other cases where speeds become quite high before the T_1 transition. Figures 4.2, 4.3 and, 4.6 and 4.7 for example, the contact temperatures cause the theoretical curve to increase dramatically above the experimental wear rates. In these cases the difference between contact and general surface temperature is clear and the better theoretical estimation is provided by the latter.

4.2 Estimation of Asperity Contact Temperatures

Contact temperatures have been estimated using a simplified version of the theory presented by Rowson and Quinn[102] and the outline of this will be given here, as

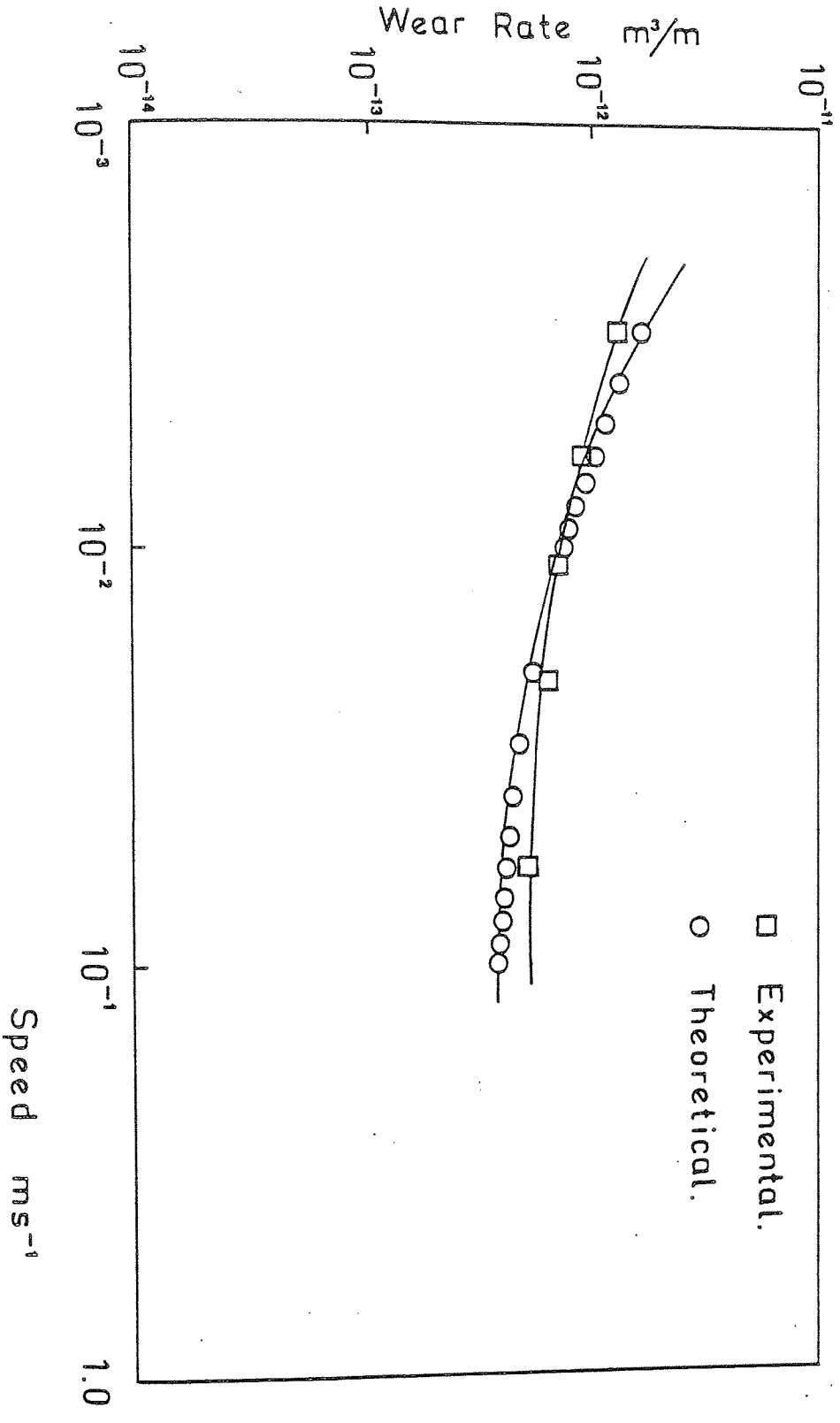

Figure 4.10

Theoretical and experimental wear rate versus speed for a load of 14.7 N using general surface temperature as T_o .

a completely rigorous handling can be found elsewhere[102,109].

The equation developed by Rowson and Quinn is based upon the oxidational wear theory of Quinn[68] and is as follows:

$$T_c = T_s + \frac{H_1}{4aNK_s} + \frac{H_1\xi}{\pi Na^2K_o} \qquad (4.9)$$

where H_1 is the heat flow into the pin, K_o is the thermal conductivity of oxide and all other parameters have been previously defined.

Using this equation in terms of the model developed in the previous section allows a number of simplifying assumptions to be made. Firstly we assume that oxidation takes place between two clean metal asperities which are then scraped on the next of subsequent encounters to remove any oxide before further oxidation takes place. Under these conditions the oxide thickness, ξ, is zero prior to each contact leading to oxidation, and the last term in equation (4.9) is thus zero. Further, to calculate the minimum possible contact temperature the Archard single contact model[49] has been adopted and thus N = 1. Using the equality $\pi a^2 = W/P_m$ we define $a = \frac{W}{\sqrt{\pi P_m}}$ and equation (4.9) becomes:

$$T_c = T_s + \frac{H_1}{\frac{W}{\sqrt{\pi P_m}}} K_s$$

Lastly the fact that load bearing area actively promoting oxidation is a fraction $\beta = \frac{1}{2}$ of the total load bearing area must be considered, so finally an approximate maximum value of the contact temperature is found using:

$$T_c = T_s + \frac{H_1}{4\sqrt{\frac{W}{2\pi P_m}}} K_s$$

The heat flow into the pin, H_1, is found from the axial heat flow equation in section 2.15:

$$[H_A]_x = - K_s \pi R_t^2 \frac{dT_x}{dx}$$

and at the limit where $x = 0$ and $T_x = T_s$

$$[H_A]_{x = 0} = H_1 = \frac{-K_s \pi R_t}{Z} (B_3 - B_4) \qquad (4.10)$$

where all constants have been previously defined, and the constants B_3 and B_4 are found from equations 2.13 and 2.14.

Although this approximate form of the Rowson and Quinn expression gives the maximum value of the contact temperature it can be seen from tables 4.2 - 4.5 that at the higher speeds the temperatures calculated produce theoretical wear rate orders of magnitude above those observed and contradict the experimental observation that only α-Fe_2O_3 was found in the wear debris, as can be seen in figures 3.17 - 3.20.

A more critical attempt to calculate contact temperatures has not yet been performed as the general surface temperatures have been found to be the important rate determining parameter in this work, however, such an attempt would probably have to resort to the iterative techniques used by previous workers[45,69].

CHAPTER FIVE

DISCUSSION

5.1 Introduction

This chapter will provide a discussion of the results and theoretical data presented in the preceding chapters. Experimental results from the various physical methods of analysis will be considered for both the unlubricated and lubricated data with respect to prior investigations, and conclusions drawn on the friction and wear behaviour of the system in each case studied.

Oxidational wear mechanisms relevant to the unlubricated and lubricated wear results will be considered, along with a critical appraisal of the theory presented in Chapter 4.

Finally, a direct comparison of the results and wearing mechanisms found in this study for unlubricated and lubricated sliding will be made. Experimental data from each system will be analysed with respect to the corresponding data from the other with any differences or similarities being pointed out and expanded on.

5.2 Discussion of Unlubricated Results

The two most apparent features of the equilibrium wear behaviour shown in figure 3.2 are the increase in wear rate with load and the decrease in wear rate with increase in speed. The former is to be expected and leads directly from the Archard wear law. It is simply due to increased real area of contact at higher loads. The latter feature has been observed before by Earles and Hayler[116] and Earles and Powell[63,117], who explained this decrease in terms of increased speed leading to higher frictionally generated surface temperatures and thus better oxide coverage, increased surface protection and reduced wear rates. A similar argument has been put forward for the reduction in wear rate with increase in speed above the T_2 transition[44,118]. In this case, at equilibrium, increased oxide production at higher temperatures is paralleled by increased oxide removal, to maintain equilibrium, as debris at higher speeds. This is at variance with the observations of this study, where, as is seen clearly in the micro-densitometer traces of figures 3.17 to 3.20, there is a progressive increase in the metallic component of the debris with speed for a given load. This is the opposite to what would be expected if increased oxidation were occurring. As will be discussed later, this effect is indicative of a difference in wear mechanisms below T_1 and above T_2.

The upper graph in Figure 3.1 showing the change in wear rate with time, from the start of the test to equilibrium, shows the process to take about 30 minutes which is typical of wear-in times seen in other studies[109]. However, in some cases, at lower loads and speeds, the wear-in time was seen to be somewhat less, with oxidised debris appearing in small amounts almost immediately. This effect seems to be due to the moderate wearing conditions combined with this particular sliding geometry. Unfortunately the small amounts of debris produced in these experiments did not allow sampling of the wear products at various stages during running-in. However the initial contact must undoubtedly be metallic, and the equilibrium contact via an oxide film; such an analysis would be expected to show a gradual change from predominently metal to mainly oxide as the equilibrium was established. This change would be seen around 20 to 40 minutes into the test for the specimens exampled in Figure 3.1

A further result apparent from the wear rate curves of Figure 3.2 is the shift of the T_1 transition to higher speeds for lower loads. The transition itself is also seen to become less abrupt. This effect is caused by an increase in load leading to an increase in the number and thus frequency of contacts. The rate of growth of oxide in this case, for the region approaching the T_1 transition, increases less rapidly and severe metallic wear ensues.

For a given transition speed the abruptness and severity of the transition will depend upon the level of oxide coverage necessary to sustain an equilibrium mild wear mode, this level of coverage is determined by the equilibrium wear, and thus generation, rate of oxide which must be higher for higher loads. Exceeding this transition speed at higher loads leads to a larger number of adhesive metallic contacts and an abrupt transition. At lower loads the number and frequency of these contacts is reduced in the transition region causing a less abrupt change between mild and severe equilibrium wear modes.

The friction coefficients presented in Figure 3.5 are seen to vary little over the range of load and speed investigated in this work. While the wear rates are seen to change over an order of magnitude, the corresponding changes in friction coefficient are in the range of 0.4 - 0.6. These values are typical of those seen in oxidational wear and indicate that the remarkable protection afforded by the oxide is consistent over a large range of sliding conditions. The mechanisms of friction governing the magnitude of the friction coefficient are likely to be due largely to the effect of oxide particles prior to agglomeration, or as evidenced on the photomicrographs, regions of oxide production where, according to the theory presented in Chapter 4, it is postulated that predominantly metallic and metallic-oxide contact is occurring.

The initial variation in friction coefficient seen in Figure 3.4 has been observed by Blau[119] in his study of frictional break-in behaviour and he explains the cause and severity of the friction changes as due to a number of competing parameters such as oxide growth, surface composition changes caused by diffusional processes, the effects of component temperature rises due to sliding friction, mechanical disruption of surface oxide films with increasing metallic contact and contact geometry changes. Blau predicts[119,120] that the final equilibrium friction will depend upon the sum of these parameters, the dominant component of which is decided by load and speed and sliding geometry. Blau[121] also found that storage time after polishing affected the magnitude of the initial friction break-in due to the growth of static oxides, this view is in agreement with the observations of other workers[73] although this phenomenon was not studied in this work. The observed reduction in friction coefficient with increase in load has been reported previously[122] especially in the region under present study[63]. This has been considered due to surface modifications due to oxide coverage[121] but has not been successfully quantified.

It can be seen clearly in Figures 3.6 and 3.7 that below 10^{-1} ms^{-1} the increase in general surface temperature due to frictional heating approximates to an equilibrium around 2°C above ambient. It is also a well documented

view that at low speeds or where external temperature is high, then out of contact or general surface temperatures dominate the oxidation process[56, 57, 60]. This view is supported here, where below $10^{-1}ms^{-1}$ frictional heating is effective only by maintaining the surfaces at a constant level above ambient. This level will be determined primarily by the external temperature and the thermal properties of the wearing pair.

Considering the asperity contact which takes place in this region we see that the time of contact is long which provides an adequate time for frictional heat to conduct away from the surface, preventing any sharp rises in temperature. In this case the oxide which grows as a result of this contact will do so immediately after the contact at a temperature little greater than the general surface temperature. At higher loads and speeds the time between contacts is reduced, so although the oxide grows at a higher temperature the time for growth is greatly reduced, thus leading to an increased number of contacts resulting in metallic debris. This effect is not compensated for by the relatively meagre temperature rises. In Chapter 4 the wear rate was found to depend upon the rate determining factor of oxide production; we see here a reduction in oxide production combined with a higher probability of metal production. These effects confirm the experimental evidence provided by the wear rate curves of Figure 3.2, showing reduced wear rates at higher speeds, and the powder diffraction data of the debris, figures 3.17

to 3.20, showing increasing metallic debris at higher speeds. The increased oxidational temperatures at higher speeds and loads, assuming an oxidation-scrape-oxidation model are seen to be ineffective due to reduced time of oxidation.

For these reasons, and results based upon the comparison of surface and contact temperatures with theoretical and experimental data, the contact temperatures, figures 4.2 - 4.5, have been rejected in favour of the general surface temperatures, figures 4.6 - 4.10, in calculations of wear rates using equation (4.8). This correlation may be seen clearly, if all other parameters remain constant, as the general surface temperatures used in equation (4.8), as opposed to the contact temperatures, provide a much superior theoretical set of curves. In every case, by comparing the temperature data given in tables 4.2 - 4.9 we see that for a given load, at low speeds the contact temperatures are similar to the general surface temperatures. However at only slightly higher speeds the contact temperatures deviate more and more from the general surface temperatures. Correspondingly, the theoretical curves shown in figures 4.2 - 4.10 show fair agreement for all temperatures at low speeds, but enormous variation with experimental points at higher speeds for the contact temperatures. The 49.1 N load being an exception, where it can be seen that contact temperatures and general surface temperatures are similar for the whole speed range; this is thought to be

exclusively due to the low sliding speeds. The results of this temperature analysis is in complete agreement with previous workers data[56,57,60].

The oxides depicted in the scanning electron micrographs of figures 3.8 - 3.13 display all the major features seen in this study. Oxide thicknesses seen here are in general similar to those found in other studies[44,109] of between 2 and 5 μm. However for the 19.6 N load, shown in figure 3.13c, and 0.05 ms^{-1} the plateaux thickness is clearly around 10 μm. A major difference, however, in this oxide formation is the structure, seen clearly in figures 3.10b, c; 3.11c and 3.12c. These photomicrographs show particularly well the grainy agglomerate nature of this oxide providing evidence toward the mechanism of its formation. These oxides may be directly contrasted with those from a diffusion controlled mechanism which show the oxide plateau edge to be a uniform homogeneous layer from the base to the surface of the oxide[44,109].

Further to this, the photomicrographs seen in figures 3.8a, c and 3.9a, b and particularly 3.9c show that the oxide plateaux rest over existing roughened surface features, indicating that the oxide formed elsewhere, became detached and transferred to form an agglomerate layer in the observed position. This characteristic, a roughened surface underlying a smooth compacted oxide, seen also in figure 3.13c supports the hypothesis of an

agglomerate mechanism of the oxide production. Although the oxide generating region would become smooth, the region over which the agglomerate plateaux form is protected and remains in a roughened condition. On break up of this plateaux the resulting 3-body abrasion caused by trapped debris could roughen the previously smooth oxide generating area prior to the formation of an agglomerate over that region. The break up of an agglomerate plateaux is seen in figure 3.8a where large flakes of oxide are seen to be breaking away from the surface. In theory these oxide flakes may either be removed as debris or be recompacted at another site on the surface. The photomicrograph of figure 3.10b appears to show the result of just such a redeposition, where one oxide plateau seems compacted onto another.

Based upon the evidence of these photomicrographs we deduce that in this study the large oxide plateaux are formed of agglomerates of small oxide flakes, and their thickness is not limited by the oxide formation mechanism. As was found in the study of wear above the T_2 transition[44] thicker oxide plateaux are formed at higher speeds, however in this case it is not due to increased frictional heating leading to increased oxidation, although this effect may facilitate the sintering of the agglomerate plateaux providing more stability. A possible explanation lies in the consideration of the wear model developed in Chapter 4 and in equation (4.8). The prediction is that the rate of production of oxide in terms of volume produced

per unit distance of sliding is inversely proportional to the linear sliding velocity which thus explains the decrease in wear rate with increase in speed seen in figure 3.2. It is probable that the higher rate of oxide production and removal at the lower speeds favours thinner less stable plateaux which are more easily penetrated by opposing asperities and thus more easily removed aiding the wear process. Conversely at higher speeds oxide production and removal are observed to be lower, this may allow time for thicker more stable oxides to form and be maintained.

The oxide plateaux have been found to rest over a work-hardened layer as would be expected and is in support of many other studies[31,33,35]. This layer was investigated for selected pins and a range of hardnesses were found between 300 and 340 VPN, seen in figure 3.14. These values are somewhat lower than the previously determined minimum value found by Welsh[35] and Athwal[109], necessary to support an oxide layer. This is probably due to the fact that extensive surface transformation and work-hardening occur during the severe running-in stage of wear[33,36] and that this is not as protracted or indeed as severe in this work as in other studies[31]. This may indicate that below the T_1 transition the work hardened layer forms quickly and only to the degree necessary to support the agglomerate oxides. The existence of the layer is however in agreement with Welsh[35].

The contact resistance results found in this study are in basic agreement with those from previous investigations[103]. The trace shown in figure 3.15 shows the rapid increase from low contact resistance and low metallic contact. The equilibrium value of ~ $10^6\Omega$ is typical of the contact resistance through an extensive oxide layer. The continuity of the trace with time shows how stable the generated oxide films are, although, as may be seen in figure 3.1b, periodic rapid drops in resistance occur where a metallic contact shorts the oxide layer.

The breadth of the trace gives some indication of the variation of resistance around the disc but no real conclusions may be drawn from this as the trace can be narrowed using a suitable filter over the input device. The comparison of this trace with that from the lubricated results, section 5.4, is much more revealing.

The experimentally observed brown/red oxide produced in these tests was expected to be α - Fe_2O_3 and this was confirmed for all loads and speeds on inspection of the powder X-ray data shown in figures 3.17 to 3.20 from debris collected on completion of each test. The absence of the oxide Fe_3O_4 indicated strongly that temperatures responsible for oxide production did not exceed 250°C[44], an important point in favour of using the general surface temperatures as the oxidational temperature. For every sample examined the debris consisted of α - Fe_2O_3 with varying amounts of α - Fe.

Another important fact emerges when considering the densitometer traces. In each case the debris is predominantly oxide at the lower speeds with the metallic component increasing with increasing speed for a given load. When this is compared with the wear rates seen in Figure 3.2 we see that it is the lowest speed which exhibits the highest wear rate and the highest oxide content in the debris, ignoring the transition effects of the higher speeds. This implies that it is an increase in oxide production which causes an increase in the wear rate, and thus that it is the production of oxide and metal debris, in areas not covered by plateaux, which is the rate determining factor. Oxide plateaux formation and removal, and attainment of critical thickness, is an intermediate stage in debris production, although plateaux growth of course reduces those areas available for the oxide production in the initial stages of wear. The increasing metallic component in the debris at higher speeds is caused by adhesive asperity contacts causing more severe metallic wear and thus debris; the removal of such large particles and consequent severity of the wear increases the wear rate toward the T_1 transition.

Figure 3.21 further shows a progressive increase in the metallic component of the debris with load for a given speed, while Figures 3.17 - 3.20 show similar increases but for a given load and increases in speed. If we consider briefly the wear model proposed in Chapter 4 we see that there is an explanation readily available:

$$w = \{A_L \exp - (\frac{73000}{RT_o})\ \alpha\frac{2-d}{U}$$

$$+ K_s\ (1-\alpha)^2\ \}\ \frac{W}{2P_m} \qquad (4.8)$$

where each symbol has its previously defined meaning and value.

In this equation the metallic component is seen to remain constant with speed, whereas the oxidational component is seen to reduce. The oxidational temperature, T_o, is known to vary only a little below 10^{-1} ms^{-1} and so on increasing the speed for a given load the metallic proportion of the wear rate is seen to increase relative to the oxidational component. This is reflected in the debris and is responsible for the observed increase in the α-Fe peak of the powder X-ray spectra.

Physically, on increasing the load or speed, as has just been explained, the number and frequency of contacts also increases. At the higher speeds a thicker load bearing plateau exists affording more surface protection; however, the amount of metallic debris is thought to be independent of speed but proportional to the number of contacts, it is thus reasonable to assume that some minimum

Typical values are for a 9.8 N load, ξ = 2 μm, a = 2 μm, T_o = 93.7^{0}C and the theoretical wear rate is 3.31 x 10^{-31} m m^{-1}. T_o in these examples are iterated contact temperatures relevant to the other parameters.

Another result of this series is for ξ = 5 μm, a = 1 μm, T_o =1139°C and W_{Theory} 3.3 x 10^{-21} m m^{-1}; ξ = 5 μm, a = 9 μm, T_o = 102.2^{0}C and W_{Theory} = 1.6 x 10^{-40} m m^{-1}. It becomes clear on examining these results and many hundreds of similar sets that the wear rates found at sensible temperatures are too small to consider by roughly 15 orders of magnitude, and that to obtain reasonable wear rates the temperatures are excessively high. It is known that such temperatures are not generated in these experiments from examination of oxide type.

Because the theory is based upon a homogeneous diffusion grown oxide it was rejected as inappropriate to the experimental evidence and a new model sought. This new model was the mathematical form of the Earles and Powell theory[63] developed by Tenwick and Earles[65] and is given as equation (1.3) in section 1.5.1. This model was found to fail where this work is concerned because the constants adopted by those authors, KP_o and Q, were the Arrhenius constant and activation energy for parabolic oxidation, and as such predicted wear rates far too low. The theory presented in Chapter 4 is similar in form to that of

Tenwick and Earles but uses logarithmic growth constants providing the higher rates of oxidation at the lower speeds, necessary to explain the observed wear rates.

This failure to make quantitative wear predictions from previous work indicated that a new approach was necessary. The work of Yoshimoto and Tsukizoe[61] made a good prediction of the shape and magnitude of the Welsh curve below the T_1 transition, but their expression for wear rate, equation (1.2) section 1.5.1, was unsupported by experimental evidence. This approach, combined with the observations of Stott et al[70,71,74], which agree in many areas with this work, provided the guidelines to develop a quantitative wear model to predict wear rates over a range of loads and speeds.

An attempt at such a wear model is presented, with all relevant arguments in Chapter 4 of this work. The theoretical curves presented, along with the corresponding experimental curves, are shown in figures 4.6 to 4.10; restricting our discussion for the moment to the general surface temperature solutions to equation (4.8). In each curve, prior to the T_1 transition, remarkable agreement is found between theoretical and experimental data. The theoretical curves are seen to break down at speeds corresponding to the onset of the T_1 transition, but this is only to be expected as conditions in this region no longer comply with the assumed surface model. In this region the model would have to be modified to include

abrasive and ploughing terms more appropriate to the severe wear mode dominant above the T_1 transition. As would be expected the severe wear term incorporated into equation (4.8) is seen to dominate the oxidational term at higher speeds, as the increased metallic proportion of the debris seen in the powder X-ray results, figures 3.17 - 3.20, would suggest.

The use of equation (4.8) relies very much on the adoption of an appropriate Arrhenius constant. The values calculated in this work, shown in Table 4.1, are of the correct order of magnitude expected of such constants[69], within certain limitations, for oxidational wear under tribological conditions. The limitations include reproducibility of results, materials in use and of course the mechanism of oxidation. These major points introduce serious uncertainty in any prediction of wear rates and it is realised that the Arrhenius constants used in this work could vary by orders of magnitude from any actual values. Nevertheless, the furthest deviation from a mean value is 30%. The values given in Table 4.1 could then be altered to some mean value and the corresponding theoretical curves changed similarly. This would then introduce a constant Arrhenius constant but otherwise serve little purpose when the uncertainty in those constants would be greater than those in Table 4.1. Addressing this directly, that the Arrhenius constants decrease with increasing load, then also introduces discrepancy. An increase in load increases the surface disruption and thus entropy of the system,

which could possibly lead to an increase in Arrhenius constant such as is seen between static and tribological values. This variation remains unaccounted for.

In consideration of this model it should be made clear that the system geometry has a profound effect on the wear mechanism. In this case the agglomeration process is aided as any oxide flake when detached is trapped between the surfaces in a vertical pin, horizontal disc geometry. This flake could remain thus for many revolutions of this disc before either being lost as debris or compacted into an oxide plateau. Conversely a horizontal pin and vertical disc is unlikely to trap a particle so, and it would be expected to drop free within a revolution of the disc. The speed through centrifugal force will also have an effect. Such a geometry is not conducive to agglomeration and thick oxides are liable to form by another mechanism[51,109]. The case of the vertical pin and horizontal disc under lubricated conditions presents an interesting situation where the geometry favours agglomeration but where the lubricant acts to remove the debris. This will be discussed in more detail in the next section.

Considering the results discussed in this section for 52100 steel sliding upon itself it is possible to draw certain conclusions. The wear behaviour below the T_1 transition consists of a reduction in wear rate with increase in speed for any given load, and in all cases the oxide α-Fe_2O_3 is found with metal particles in the debris

indicating the moderate temperatures existing between the surfaces. Scanning electron micrograph examination of the surface reveals oxide plateaux to be agglomerates of smaller oxide particles, and this is substantiated by the Auger electron oxygen depth profiles which show a gradation of oxygen with depth, expected from such agglomerate plateaux. The constitution of those plateaux and the magnitude of the wear rates at low speeds has led to the deduction that a thin film logarithmic rate law must govern the oxidation process, which indicates that an oxidation-scrape-oxidation mechanism is responsible for the production of the oxide flakes prior to agglomeration into thicker, load bearing, oxide plateaux. Based upon this logarithmic rate law a theoretical expression can be derived which makes accurate estimates of experimental wear rates below the T_1 transition. Based upon previous work, and analysis conducted here, the use of general surface temperatures as the oxidational temperature is thought to be justified.

5.3 Discussion of Lubricated Results

The lubricated wear behaviour shown against sliding speed in figures 3.24 and 3.25 and against friction coefficient in figure 3.26 is dependent entirely upon the form of contact achieved due to lubricant-surface interaction. Hence, in the case of the Technical White Oil the lubricant contains very few polar molecules which could physi- or chemisorb onto the rubbing surfaces, such that in the comparative tests with the stearic acid additive, all such adsorption was due to the acid. It has, however, been reported that white oils themselves become oxidised and polarised via a free-radical chain reaction[82], however, although this will have occurred to some extent in these experiments, causing some boundary film formation, the effect must be negligible as no boundary film action is observed. Effects of boundary additives in concentrations of 12 ppm have been investigated[93-97], indicating that in these tests free-radical alteration of the White Oil occurs to a degree approximately resulting in no boundary action. The primary functions of the lubricant in this case, then, is to produce a fluid separation of the surfaces which redistributes loading stresses through itself and thus over a greater area of the opposing surface; to act as a coolant, removing heat generated at hot-spots into the main reservior of oil outside the contact areas and to remove any wear debris that is

generated and which might otherwise remain as a third body between the sliding pair.

Load and speed combinations have been chosen which provide substantial amounts of asperity contact between the surfaces. This contact leads to oxidation of the surfaces via dissolved oxygen in the lubricant; these oxide layers can be seen clearly in the surface photomicrographs of figures 3.32, 3.33 and 3.34. Figure 3.32 is showing an extensive, uniform oxide coverage which was found to extend over that, and all other worn pin surfaces. To gain further information about the oxide formation, it was necessary to break up the oxide surface. The resulting broken surface is shown typically in figures 3.33 and 3.34. Shown particularly well, in figure 3.33c, is a fragment of oxide caught edge on; it may be seen here that the oxide layer was about 0.2 μm thick and is of uniform texture from base to top. Oxide thicknesses are seen to vary over the photomicrographs, between 0.1 and 0.2 μm , seemingly independent of the presence of the stearic acid, which evidence is supported by the Auger electron spectra 3.35 - 3.46. These homogeneous oxides shown in figures 3.33 and 3.34 may be directly contrasted with those from other studies[44,109] where, although an order of magnitude thinner, these oxides are seen to possess similar physical characteristics, that is, smoothness and homogeneity. It has been postulated that such oxides are formed via a parabolic diffusion controlled growth law[44,98], and it is reasonable to assume a similar mechanism governs the

formation and growth of the oxides seen in this study. The difference in thickness in oxide between the two studies is undoubtedly due to the presence of lubricant in this study moderating the rate of growth oxide. This will not alter the deductions made concerning the wear mechanism as the presence of oxygen dissolved in lubricants and its importance in oxidational wear is well documented[88,92].

Returning to the Auger electron depth profiles for the tests in Technical White Oil alone, we see particularly in figures 3.36, 3.38 and 3.40 a slight plateau region in the oxygen concentration which is suggestive of a thin homogeneous layer, of the correct order of thickness as seen in the photomicrographs, existing on the worn pin surface. Such plateaux have been observed previously[109] and are evidence of homogeneous diffusion controlled oxide growth which further supports the view that such oxidation is responsible for the oxides observed in this study.

It is postulated, then, that wear takes place via this oxide film, with oxide plateaux growing through asperity contacts due to a homogeneous diffusion controlled rate law, to a critical thickness where instability at the plateaux-substrate boundary leads to its final removal as debris into the oil[98].

Increasing the sliding speed causes more hydrodynamic lift and so reduces the surface asperity contact. Reduced asperity contact will lead to reduced wear. A relationship should then be apparent between wear rate and friction coefficient, which is of course also related to the amount of asperity contact. This is seen in figures 3.24 and 3.26 where wear rate decreases with increasing speed and where there is a direct relationship, as expected, between wear rate and friction coefficient. This is further illustrated in figure 3.27, where the relationship between wear rate, load and speed is shown based on Cameron's[96] estimation of fluid film thickness. Figure 3.27 shows, with a 75% correlation coefficient, that wear rate is directly proportional to the number of asperity contacts as determined by the fluid film thickness, h. Decreasing the sliding speed reduces hydrodynamic lift, increasing asperity contact, friction coefficient and wear. The wear rate varies in figure 3.26 with friction coefficient by the relation:

$$\log(w) = 6\mu - 15 \qquad (5.1)$$

with an 85% correlation coefficient, showing that for small changes in friction coefficient in this region, large changes in wear follow. This is due entirely to changes in load and speed causing changes in the fluid film thickness, which in turn determines the amount of asperity contact and thus wear.

The variation of wear rate with the function $W^{3/2}U^{-1/2}$ in figure 3.27 is supported by the curves in figure 3.24 which clearly show an increasing wear rate with load. Although the exact form of the constant of proportionality is not given in equation 3.2, as a full solution to the Reynold's equation was not undertaken for this geometry, the fact of the variation is enough to support the previous discussion.

This is to be contrasted with the case of Technical White Oil with 0.1% stearic acid, a polar molecule and well documented boundary lubricant[123]. The addition of the acid caused a marked change in the wear behaviour of the sliding pair, as seen in figure 3.25 which is the corresponding variation to that seen in figure 3.24. From examination of the X-ray photoelectron spectra of figures 3.47 - 3.49; figures 3.48 and 3.49 for White Oil with acid compared with 3.47 for White Oil alone, the existence of a surface film in the presence of the acid is noted. The notable decrease in the wear rates of 49.1 and 98.2 N loads is thought to be due to this surface film which is postulated to be iron-stearate. This is deduced primarily from the oxygen curves, of figures 3.48 and 3.49. where a clear increase in the single bond and double bond oxygen can be seen, compared with those bonds in figure 3.47 with no stearic acid additive.

For this iron-stearate soap film to form it is necessary that an oxide layer be present[7,8].

That such oxides are present is shown clearly in photomicrographs of figure 3.34, where oxide layers are seen to be similar in construction and thickness to those tests conducted without the acid, figure 3.33. Further proof is provided by reference to the Auger electron depth profiles of figures 3.43 - 3.46 which show the existence of an oxide layer of similar formation and thickness to those observed without the acid. It is thus likely that the formation of this oxide occurs by the same mechanism as that observed without the acid additive. At the outset of rubbing it is postulated, then, that the oxide grows according to a diffusion controlled growth law observed in other studies[44] but that after the initial oxidation of asperity surfaces, a soap film can form rapidly on the oxide which prevents further metallic contact[98], resulting in increased surface protection and reduced wear rates.

At equilibrium, it is seen then, that wear takes place via an oxidational wear process, similar to a White Oil alone, but dependent in this case on the physical and chemical properties of the boundary layer. This is the case because the iron-stearate film is acting as a barrier preventing direct asperity contact, and thus for contact and wear to occur that film must be removed. Hence the

increase in speed leads to a rapid drop in friction coefficient. This decrease is not readily apparent in figure 3.29. The explanation is probably that the Stribeck curve shown in figure 1.1 has been flattened out into that seen in figure 3.29 by this formation of a gelatinous deposit which could interfere with the hydrodynamic characteristic of the Stribeck curve. As stated above, this deposit is seen to build up on the leading edge of the pin in the lubricant and is possibly formed of discrete particles of oxide, removed from the wearing couple and covered in soap molecules, if these then become entrapped between the wearing surfaces, they could become indistinguishable from opposing asperities and generate boundary lubrication friction values, as depicted in figure 5.1, even at higher speeds.

It is immediately apparent that the oxide formed in this case is much more uniform and allows little serious metallic breakdown of the sort typical of figures 3.15 and 3.16. The overall variation is very uniform after the initial rise to equilibrium. No difference was found between contact resistance traces in tests conducted with and without the acid. This is not surprising where, as is seen in figures 3.33 and 3.34 there is no discernable difference in the oxide formation and thickness.

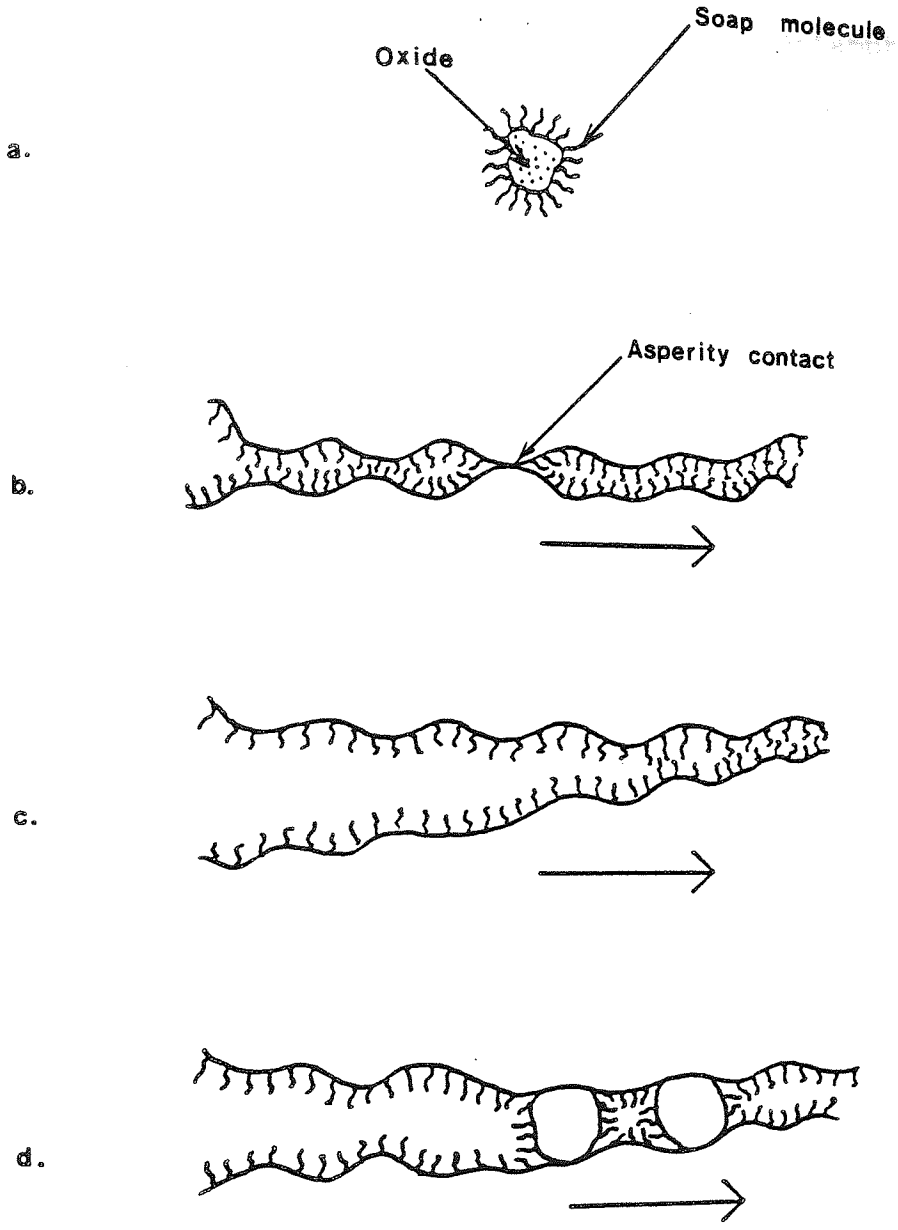

Figure 5.1

a) Representation of oxide debris covered with iron stearate molecules,

b) Low speed boundary contact

c) Higher speed showing hydrodynamic wedge and

d) Higher speed but showing debris interference with hydrodynamic separation of the surfaces. The large arrows indicate movement of the lower surface.

Many difficulties have been encountered in attempts to calculate theoretical wear rates. Sullivan's[98] wear theory, given quantitatively in equation (1.5), has been the primary focus of these attempts, however there were several experimental and theoretical set-backs which have confounded realistic approximations to experimental wear rates. The first, and foremost, has been an inability to make consistent temperature measurements. No lubricated temperatures have been presented in the experimental results section due to their extreme variability. The problem stems from the thermocouple spot-welded onto the pin near to the wearing interface; and temperature measured here is very dependent upon the oil film which is formed or which actively flows over the contact. This film is of course dependent upon the velocity of the disc; when it is low it allows a thick film to flow past the joint, and when it is high it drags an appreciable oil film up the leading edge of the pin, while leaving the trailing edge relatively free from oil. The temperature calculations presented in Chapter 2 do not take into consideration any of these conditions; that is preferential heat loss in differing parts of the pin, heat transfer coefficients between pin and oil, oil and air, and especially between the pin and the gelatinous debris deposit which sometimes forms substantially over the joint on the pin's leading edge.

These effects are under consideration, and appropriate modification to the heat flow equations being undertaken by other workers, but this, at the present time, unfortunately leaves the lubricated general surface, contact and oxidational temperatures unknown.

Due to this initial problem, guesses of the surface temperature have been made on evidence of oxide type. It has been impossible to collect sufficient quantities of oxide to make a positive identification by powder X-ray diffraction, however the bright red nature of the oxide indicates a predominance of α-Fe_2O_3 which presents an upper limit of around 250°C[118], assuming no Fe_3O_4 is produced, although some of this oxide is probably present, especially at the higher loads. Knowledge of this temperature, however, still leaves variables such as asperity radius "a" and oxide thickness "ξ" in doubt, although estimates can be made. It is thought that a computer search iterative solution would be more rigorous, such as that developed by Quinn et al[51,52] and Sullivan et al[69], but this has not been attempted here.

The lubricated evidence presented in Chapter 3 and discussed here points towards an oxidational wear mechanism. The oxide is seen to form via a diffusion controllled growth law, forming homogeneous oxide plateaux between 0.1 and 0.2 μm in thickness over the whole wearing surface. The oxide was observed to be red/brown in colour

and thus predominantly α-Fe_2O_3 . Wear rates were seen to fall on addition of stearic acid to the White Oil, and this is thought to be due to an iron-stearate soap film as seen by other workers[84,98].

5.4 Comparison of Unlubricated and Lubricated Resuults

When comparing these two systems, the most striking difference is the wear mechanism governing oxide production and removal. In the unlubricated case we have postulated oxide growth to occur via a logarithmic rate law which controls the growth of thin film oxides which are subsequently scraped off and agglomerated into thick compacted oxide plateaux, as evidenced by the electron photomicrographs of figures 3.8 - 3.13 and the Auger electron depth profiles of figures 3.22 and 3.23. These may be directly compared with the lubricated worn pin surfaces examined in the photomicrographs of figures 3.32 - 3.34, and Auger depth profiles of figures 3,35 - 3.46; of which evidence has been used to deduce a parabolic rate law governing the growth of thick, diffusion controlled, oxide plateaux. The e plateaux grow uniformly to a critical thickness where they are then removed probably by a fatigue mechanism. The unlubricated oxide plateaux are seen to be between 2 and 10 μm in thickness whereas lubricated worn pin surfaces are covered by oxide plateaux between 0.1

and 0.2 μm in thickness. The lubricated worn pin surfaces also exhibit 100% oxide coverage unlike the unlubricated pins which have variable coverage dependent upon the state of agglomeration at the time of examination.

Although, of course, both geometries favour debris entrapment, being vertical pin on horizontal disc, this is only seen to occur in the unlubricated tests. Clearly this is due to the action of the lubricant washing away loose debris particles thus preventing agglomeration and any 3-body abrasion which might have adverse effects on the growth of homogeneous plateaux. This result illustrates the crucial importance of sliding geometry and environment on the mechanism and thus severity of wear.

The 0.1 - 0.2 μm oxide plateaux covering the whole lubricated worn pin surface provided a superior protective coverage, as can be seen by comparison of the contact resistance traces of figures 3.16 and 3.31. For the lubricated case the fluctuations to lower resistance, figure 3.31, are seen to be much smaller than those in figure 3.16. This indicates that although the unlubricated oxide plateaux are much thicker, their intermittent removal and incomplete coverage of the surface led to more electrical and metallic contact. The equilibrium contact resistance for both systems was similar, however, and varied around $10^6\Omega$ as expected from oxide covered surfaces.

CHAPTER SIX

Conclusions and Further Work

For the unlubricated unidirectional sliding of AISI 52100 on 52100 steel conducted below the Welsh T_1 transition under geometric conditions such that debris was allowed to remain on the wearing surface, wear rates were found to increase with increase in load and decrease with increase in speed. The T_1 transition speed was found to decrease with increase in load.

The protective load bearing plateaux formed during unlubricated sliding consisted of agglomerates of particles of wear debris, the composition of which varied from mainly metallic particles at the boundary between plateaux and substrate to mainly oxide (α-Fe_2O_3) at the outer plateaux surface. Plateaux thickness increased with sliding speed and decreased with applied load and were in general between 2 and 10 μm in thickness, and in all cases rested on a work-hardened surface.

A wear model based upon logarithmic oxidation produces theoretical values of wear rate for unlubricated sliding which are close to those experimentally determined.

General surface temperatures were found to be the functional oxidational temperatures responsible for oxide growth, based upon examination of oxide type, and by comparison of theoretical wear rates calculated using general surface temperatures with those for the corresponding contact temperatures.

Wear rates increase with increase in load and decrease with increase in speed. Without the stearic acid, wear rates were found to be directly related to load, speed and fluid film thickness and friction coefficients. Addition of stearic acid to the White Oil causes a marked reduction in wear rate.

Friction coefficients, without the acid, were found to increase with decrease in speed. On addition of stearic acid, over this load and speed range, friction coefficents were markedly reduced below the generally accepted boundary values of between 0.1 and 0.3, however, boundary action was still seen to occur as evidenced by the production of oxidised debris.

Reductions in friction and wear on addition of stearic acid to the White Oil are probably due to the formation of an iron-stearate soap film on the oxidised surfaces of the wearing pair.

The red/brown oxide α-Fe_2O_3 was formed predominantly during all lubricated wear tests.

Sliding geometry is a major factor in determining the mechanism of wear between two bodies and in this case is exemplified by the ready formation of agglomerate oxide plateaux in a geometry conducive to debris entrapment. Further, the importance of environment is shown where the presence of lubricants to wash away debris may result in the predominance of another wearing mechanism.

The conclusions drawn here may be expanded upon if further work were to be conducted in the following areas. Firstly an extension of the original Welsh curves shown in figure 3.2 for more loads, and for lower speeds. Higher loads should result in a reduced mild wear region below the T_1 transition and would provide valuable data on the behaviour of that transition at very low speeds. A series of tests into speeds in the range below 10^{-3} ms^{-1} would provide very interesting information on the trend of increasing wear rates with decreasing speed. The limits of both decrease in speed and increase in load would be very instructive in terms of the restrictions on the wear model proposed in Chapter IV. Using a wider range of loads should narrow down the variation seen in the Arrhenius constant used in equation (4.8). Further experiments would help define this quantity better and perhaps make it a universally accepted constant for this form of wear.

A second important region requiring further work is the development of an adequate temperature measurement and heat flow analysis for the lubricated wear system, permitting, then, an investigation into the effect of temperature on lubricated wear. Along with this a more accurate measurement of lubricated wear rate particularly in the presence of stearic acid, is needed.

Finally, a direct comparison of wear mechanisms and oxide formation should be performed using a horizontal pin and vertical disc for the same material and more importantly the same load and speed combinations used in this work. This will allow more precise deductions to be made on the effect of sliding geometry on the mechanisms of wear.

REFERENCES

1. Fink M., Wear Oxidation - a new component of wear, Trans. Am. Soc. Steel Treating, 18 (1930) 1026-1034

2. Rosenberg S J and Jordan L., J. Res. Nat. Bur. Stand., Washington, 13 (1934) 267-289

3. Lancaster J K., The formation of surface films and the transition between mild and severe wear., Proc. Roy. Soc. (London), A273, (1963), 466-483

4. Welsh N C., The dry wear of steels, Part 1 - the general pattern of behaviour, Phil. Trans. Roy. Soc., 257A (1964), 31-50

5. Welsh N C., Frictional heating and its influence on the wear of steels, J. Appl. Phys, 28 (9), (1957), 960-968

6. Sullivan J L., Boundary lubrication and oxidational wear, J. Phys. D., 19 (1986) 1999-2011

7. Prutton C F., Frey D R., Turnbull D and Dloughy G., Corrosion of metals by organic acids in hydrocarbon solvents, Ind. Eng. Chem. 37 (1945) 90-100

8. Tingle E D., Influence of water on the lubrication of metals, Nature, 160 (1947) 710-711

9. Archard J F and Hirst W., The wear of metals under unlubricated conditions, Proc. Roy. Soc., A236 (1956) 397-410

10. Burwell J T and Strang C D., On the empiracal law of adhesive wear, J. Appl. Phys., 23 (1952) 18-31

11. Burwell J T., Survey of possible wear mechanisms, Wear, (1957) 119-133

12. Quinn T F J., Review of oxidational wear Part I: The origins of oxidational wear, Tribology International, 16 No. 5, (1983) 257-271

13. Bowden F P and Tabor D., The friction and lubrication of solids, Clarendon Press, Oxford, Part I (1954), Part II (1964)

14. Rabinowicz E., Friction and wear of materials, John Wiley and sons, (1965) New York

15. Rabinowicz E and Tabor D., Metallic transfer between sliding metals, Proc. Roy. Soc. (London) A208 (1951) 455-474

16. Tao F F., A study of oxidative phenomena in corrosive wear, ASLE Trans., 12 (1969) 97-105

17. Avient B W E., Goddard J and Wilman M., An experimental study of friction and wear during abrasion of metal, Proc. Roy. Soc., A258 (1960) 159-169

18. Rabinowicz E., Dunn L A and Russel P G., A study of abrasive wear under three body conditions, Wear, 4 (1961) 345-355

19. Sarkar A D., Friction and Wear, Academic Press Inc. (London) Limited (1980).

20. Barnett R S., Fretting and fretting corrosion, Lubrication, 41 (1955) 85-97

21. Wright K H R., An investigation of fretting corrosion, Proc. Instn. Mechan. Engrs. 1B (1952/53) 556-563

22. Rabinowicz E., A quantitative study of the wear process, Proc. Phys. Soc., B66 (1953) 929-936

23. Holm R., Electric contacts handbook, Springer-Verlag (1958), Berlin.

24. Kerridge M., Metal transfer and the wear process, Proc. Phys. Soc. (London) B68 (1955) 400-407

25. Kerridge M and Lancaster J K., The stages in the process of severe metallic wear, Proc. Roy. Soc. (London), A236 (1956) 250-264

26. Archard J F and Hirst W., The wear of metals, Sci. Lub., November (1959), 300-309

27. Mailander R and Dies K., Contributions to the study of wear phenomena, Archiv. F. Eisenhuttenuesen, 16 (1942) 385-398

28. Siebel E and Kobitzsch R., Verschleisscheinugen bie gletender trocker Reibung, VKI verlag (Berlin), (1941).

29. Dies K., Processes taking place during wear in conditions of pure sliding and dry friction, Reibung and Versheiss, No. 7DI Verlag (Berlin), (1939).

30. Archard J F., Single contacts and multiple encounters, J. Appl. Phys., 32 (1961) 1420-1425

31. Hirst W and Lancaster J K., Surface film formation and metallic wear, J Appl. Phys., 27 (1956) 1057-1065

32. Moore A J W and Tegart W J McG., Effect of included oxide films on the structure of the Beilby layer, Proc. Roy. Soc. A212 (1952) 458-459

33. Eyre T S and Baxter A., The formation of white layers at rubbing surfaces, Metals and materials, 6 (1972) 435-439

34. Lancaster J K., The influence of temperature upon metallic wear, Proc. Phys. Soc. (London), A257 (1965) 31-70

35. Welsh N C., The dry wear of steels, Parts I and II, Philos. Trans. Roy. Soc. (London), A257 (1963) 31-70

36. Farrel R M and Eyre T S., The relationship between load and sliding distance in the initiation of mild wear in steel, Wear, 15 (1970), 359-372

37. Childs T H C., The sliding wear mechanisms of metals- mainly steels, Tribology International, 13 (1980) 285-293

38. Furey M J., Surface temperatures in sliding contact, ASLE Trans., 7 (1964) 133-156

39. Meinders M A., Wilcox D F and Winer W O., Infra-red temperature measurement of a reciprocating seal test, Proc. Leeds-Lyon Symposium, (1982) 321-328

40. Quinn T F J and Winer W O., Thermal aspects of oxidational wear, Wear 102 (1982) 321-328

41. Earles S W E., Hayler M G and Powell D G., A comparison of surface temperature theories and experimental results for high speed dry sliding, Trans ASLE, 14 (1971) 135-143

42. Powell D G and Earles S W E., An assessment of surface sliding temperature predictions in the high speed sliding of unlubricated SAE 1113 steel surfaces, Trans ASLE, 15 (1972) 103-112

43. Quinn T F J., The division of heat and surface temperatures at sliding steel surfaces and their relation to oxidational wear, Trans ASLE, 21 (1978) 78-86

44. Sullivan J L and Athwal S S., Mild wear of low alloy steel at temperatures up to 500 C, Tribology International 16 (1983) 123-131

45. Blok H., Determination of surface temperatures under extreme pressure lubricating conditions, Proc. World Congr. Petrol. (Paris), 2 (1937) 471-492

46. Blok H., Theoretical study of temperature rise at surfaces of actual contact under oiliness lubricating conditions, Inst. Mechn. Engrs., (Proc. General Discussion on Lubrication and Lubricants), 2 (1937) 222-243

47. Jaeger J C., Moving sources of heat and the temperature at sliding contacts, Proc. Roy. Soc. (New South Wales), 56 (1942) 203-224

48. Holm R., Calculation of the temperature development in a contact heated in the contact surface, and the application to the problem of the temperature rise in sliding contact, J. Appl. Phys., 19 (1948) 361-369

49. Archard J F., The temperature of rubbing surfaces, Wear 2 (1959) 438-448

50. Grosberg P and Molgaard J., Aspects of the wear of spinning travellers: the division of heat at rubbing surfaces, Proc. Instn. Mech. Engrs., 181 (3L), (1966-67) 16-24

51. Quinn T F J., Rowson D M and Sullivan J L., Application of the oxidational theory of mild wear to the sliding wear of low alloy steel, Wear, 65 (1980) 1-20

52. Quinn T F J., Sullivan J L and Rowson D M., New developments in the oxidational theory of mild wear of steels, Proc. ASME Conf. on Wear, Dearbon, Michigan, April (1979) 210-222

53. Sullivan J L., Quinn T F J and Rowson D M., Developments in the oxidational theory of mild wear, Tribology International 13 (1980) 153-158

54. Tao F F., A study of oxidational phenomena in corrosive wear, ASLE Trans., 12 (1969) 97-105

55. Molgaard J and Srivastava V K., The activation energy of oxidational wear, Wear, 41 (1977) 263-270

56. Molgaard J and Srivastava V K., Apparatus for the study of unlubricated surfaces, Wear, 33 (1975) 179-188

7. Stott F H., Glascott J and Wood G C., Models for the generation of oxides during sliding wear, Proc. Roy. Soc. A402 (1985) 167-186

8. Stott F H., Lin D S and Wood G C., The structure and mechanism of formation of the "glaze" oxide layers produced on nickel-based alloys during wear at high temperatures, Corrosion Science, 13 (1973) 449-469

9. Glascott J., Wood G C and Stott F H., The influence of experimental variables on the development and maintenance of wear protective oxides during sliding of high temperature iron-base alloys, Proc. Instn. Mech. Engrs., 199 No. C1 (1985) 35-41

0. Sullivan J L and Granville N W., Reciprocating sliding wear of steel in carbon dioxide at elevated temperatures, Tribology International, 17 (1984) 63-71

1. Yoshimoto G and Tsukizoe T., On the mechanism of wear between metal surfaces, Wear, 1 (1957) 472-490

2. Uhlig M H., I. Appl. Mech. 21 (1954) 401-411

3. Earles S W E and Powell D G., Variation in friction and wear between unlubricated steel surfaces, Proc. Instn. Mechn. Engrs. 182 (3N), (1968) 167-179

4. Earles S W E and Powell D G., Stability of self-generated oxide films on unlubricated EN1A steel surfaces, Proc. Instn. Mechn. Engrs. 181 (pt30), (1966-67) 171-188

5. Tenwick N and Earles S W E., A simplified theory of oxidative wear, Wear, 18, (1971) 381-393

6. Earles S W E and Powell D G., Surface temperature and its relation to periodic changes in sliding condition between unlubricated steel surfaces, Trans ASLE, 11 (1968) 109-120

7. Quinn T F J., The division of heat and surface temperatures at sliding steel surfaces and their relation to oxidational wear, Trans ASLE, 21 (1978) 78-86

8. Quinn T F J., The role of oxidation in the mild wear of steel, B. J. Appl. Phy., 13 (1962) 33-37

69. Sullivan J L., Ouinn T F J and Rowson D M., Developments in the oxidational theory of mild wear, Tribology International 13 (1980) 153-158

70. Stott F H and Wood G C., The influence of oxides on the friction and wear of alloys, Tribology International, 11 (1978) 211-218

71. Stott F H., Lin D S and Wood G C., The structure and mechanism of formation of the glaze oxide produced on nickel-based alloys during wear at high temperatures, Cor. Sci. 13, (1973) 449-469

72. Stott F H., Glascott J and Wood G C., Factors affecting the progressive development of wear protective oxides on iron-based alloys during sliding at elevated temperatures, Wear, 97 (1984) 93-106

73. Wilson J E., Stott F H and Wood G C., The development of wear protective oxides and their influence on sliding friction, Proc. Roy. Soc. (London) A369 (1980) 557-574

74. Stott F H., Glascott J and Wood G C., Models for the generation of oxides during sliding wear, Proc. Roy. Soc. A402 (1985) 167-186

75. Crook A N., The lubrication of rollers, I, II, III, Phil. Trans. A250, 387; A254 223-251

76. Klauss E E and Beiser H E., Effect on some physical and chemical properties of lubricants on boundary lubrication, ASLE Trans, Vol 7., (1964) 1-10

77. Fein R S and Kreuz H L., Chemistry of boundary lubrication of steel by hydrocarbons, ASLE Trans, Vol 12., (1969) 140-150

78. Bose A C., Klaus E E and Tewksbury E J., Evaluation of some wear products produced by some chemical reactions in boundary lubrication, ASLE Trans, Vol 9., (1976) 287-292

79. Appledoorn J K., Goldman I B and Tao F F., Corrosive wear by atmospheric oxygen and moisture, ASLE Trans, Vol 8., (1965) 29-38

80. Godfrey D., Fretting wear of steels in lubricating oil, Paper 16 AGARD Conf. Proceedings, No. 161, (1974) 83-101

81. Bjerk R O., Oxygen- an extreme pressure agent, ASLE Trans, Vol 16., (1973) 97-106

Newly R A., Spikes H A and Macpherson P B., Oxidative wear in lubricated contact, J. Lubrication Tech, Vol 102, (1980) 539-544

Denison., Ind. Eng. Chem., 36 (1944) 477-482

Prutton C F., Frey D R., Turnball D and Dloughy G., Corrosion of metals by organic acids in hydrocarbon solvents, Ind. Eng. Chem., 37 (1945) 90-100

Hsu S M and Klauss E E., Some chemical effects in boundary lubrication, Part I, Base-oil /metal interaction, Trans ASLE Vol 22, (1977) 135-145

Bowden F P and Young J E., Friction of clean metals and the influence of adsorbed films, Proc. Roy. Soc. A208 (1951) 311-325

Hirst W and Lancaster J K., The influence of oxide and lubricant films on the friction and surface damage of metals, Proc. Roy. Soc. A223 (1954) 324-338

Feng I M and Chalk H., Effects of some gases and liquids in lubricating fluids on lubrication and surface damage, Wear, 4 (1961) 257-268

Godfrey D., Boundary lubrication, Proc. Int. Symposium on lubrication and wear, Houston (1963) 283-299

Godfrey D., Boundary lubrication, Interdisciplinary approach to friction and wear, NASA SP-181, (1968) 335-384

Nakayama K and Okamoto J., Effect of dissolved oxygen on friction and wear of copper under boundary lubrication, Trans ASLE, 23 (1980) 53-60

Begelinger A and deGee A J W., On the mechanism of lubricant film failure in sliding steel concentrated contacts, Trans ASME. Luch. Tech., 98 (1976) 575-579

Poole W and Sullivan J L., The wear of aluminium bronze on steel in the presence of aviation fuel, Trans ASLE, 22 (1979) 154-161

Poole W and Sullivan J L., The effects of the addition of corrosion inhibitors on the wear of aluminium bronze on steel in kerosene, Proc. Eurotrib. 77 (1977) 189-196

Poole W and Sullivan J L., The role of aluminium segregation on the wear of aluminium bronze on steel under conditions of boundary lubrication, Trans ASLE, 23 (1980) 401-408

Sullivan J L and Wong L F., Wear of aluminium bronze on steel under conditions of boundary lubrication, Tribology International, 18 (1985) 275-281

Sullivan J L and Wong L F., The influence of surface films on the protection of metal surfaces under boundary lubrication, Surface and Interface analysis, 9 (1986) 493-499

Sullivan J L., Boundary lubrication and oxidational wear, J. Phys. D. 19 (1986) 1999-2011

Kingsbury E P., The heat of absorption of a boundary lubricant, ASLE Buffalo, (1959) 321-330

Kingsbury E P., Some aspects of the thermal desorption of a boundary lubricant, J. Appl. Phys. 29 (1958) No. 6, 888-891

Frenkel J., Z. Phys. 26 (1924) 117-138

Rowson D M and Quinn T F J., Frictional heating and the oxidational wear theory, J. Phys. D., 13 (1980) 209-219

Stott F H., Glascott J and Wood G C., The use of contact resistance measurement to study oxide films developed during high temperature slidind, J. Appl. Phys. 18 (1985) 541-556

C.I.L. Electronics Ltd., TA880 Manual 1984.

Palmberg P W and Rhodin T N., J. Appl. Phys., 39 (1968) 2425-2431

Pains L E et al., Handbook of Auger Electron Microscopy, second edition, Physical Electronics Industries, Minnesota, 1978

Briggs D and Seah M P., Practical surface analysis by Auger and X-ray photoelectron spectroscopy, John Wiley and Sons, 1983

Seah M P., Surf. Sci., 32, 703 (1972) 501-505

Athwal S S., Ph.D. Thesis, The University of Aston (1983), Birmingham

110. Cameron A., Basic lubrication theory, Ellis Horwood series in Engineering science, John Wiley and Sons, 1981, pp 76

111. Dilks A., X-ray photoelectron spectroscopy for the investigation of polymeric materials.

112. Clark D T and Dilks A., ESCA applied to polymers. RF. Glow discharge modification of polymers in pure oxygen and helium-oxygen mixtures, J. Polymer Science, Vol 17 (1979) 957-976

113. Fuks G I., The properties of solutions of organic acids in liquid hydrocarbons at solid surfaces, in B. V. Deryagin (ed)., Research in surface forces, Vol 1, (1960)

114. Fuks G I., The polymolecular component of the lubricating boundary layer, in B. V. Deryagin (ed)., Research in surface forces, Vol 2, (1964)

115. Mills P., Ph. D. Thesis, The University of Aston (1984) Birmingham

116. Earles S W E and Hayler M G., Wear characteristics of some metals in relation to surface temperature, Wear, 20 (1972) 51-72

117. Powell D G and Earles S W E., Wear of unlubricated steel surfaces in sliding contact, Trans ASLE, 11 (1968) 101-117

118. Quinn T F J, Sullivan J L and Rowson D M., Origins and developments of oxidational wear at low ambient temperatures, Wear, 94 (1984) 175-191

119. Blau P J., Interpretations of the friction and wear break-in behaviour of metals in sliding contact, Wear, 71 (1981) 29-43

120. Blau P J., Mechanisms for transitional friction and wear behaviour of sliding metals, Wear, 72 (1981) 55-66

121. Blau P J., An investigation of the unlubricated friction and wear break-in behaviour of a dual phase steel, Wear, 72 (1981) 67-80

122. Dunkley P M and Quinn T F J., The effect of evaluated temperatures and speed upon the wear of mild steel, Trans ASLE 19 (3), (1978) 221-237

123. Allen C M and Draughs E., Boundary layer lubrication : monolayer or multilayer, Wear, 14 (1969) 363-384

A Study of Mild Oxidational Wear for Conditions of Low Load and Speed

J L Sullivan and S G Hodgson

Paper Published in Wear 121
(1988) 95-106

Wear, *121* (1988) 95 - 106

A STUDY OF MILD OXIDATIONAL WEAR FOR CONDITIONS OF LOW LOAD AND SPEED

J. L. SULLIVAN and S. G. HODGSON

University of Aston in Birmingham, Department of Mathematics and Physics, Gosta Green, Birmingham B4 7Et (U.K.)

(Received August 12, 1987; accepted August 12, 1987)

Summary

A vertical pin on a horizontal disc wear test machine has been used to conduct a series of experiments on 52 100 steel in air under dry sliding conditions. The experiments were performed under conditions of low load and speed, corresponding to the mild wear region below the Welsh T_1 transition. The investigation involved loads from 5 to 50 N and a range of speeds from 10^{-3} to 1.0 m s^{-1}; the resulting pins and wear debris were analysed using a number of techniques including scanning electron microscopy (SEM), powder X-ray diffraction, Vickers' microhardness testing and Auger electron spectroscopy (AES).

Wear rates were found to decrease with increasing speed up to the T_1 transition, and to increase with increasing load, while the T_1 transition speed decreased with increase in load. The protective load-bearing plateaux consisted of agglomerate wear debris composed of the rhombohedral oxide α-Fe_2O_3, with varying proportions of metal debris. SEM and AES results show oxide thickness increasing with speed from about 2 to 10 μm, reflecting the increase in thickness of the work-hardened subsurface layer with load and speed.

1. Introduction

Lancaster [1] and Welsh [2, 3] were the first to demonstrate clearly that under dry sliding conditions large changes in wear rate can result from small changes in applied load and/or sliding speed. Welsh produced a series of curves, the general pattern of which now bears his name, from which three transitions, T_1, T_2 and T_3, were defined. These transitions were originally defined in terms of applied load at a fixed sliding speed but subsequent work has shown that sliding speed at a fixed load is an equally valid definition. Below the T_1 and above the T_2 transition the equilibrium wear mode is oxidational mild wear. Above T_3 a further different mild wear mechanism predominates. The severe wear region between the T_1 and the T_2 transition

0043-1648/88/$3.50

Wear, *121* (1988) 95 - 106

A STUDY OF MILD OXIDATIONAL WEAR FOR CONDITIONS OF LOW LOAD AND SPEED

J. L. SULLIVAN and S. G. HODGSON

University of Aston in Birmingham, Department of Mathematics and Physics, Gosta Green, Birmingham B4 7Et (U.K.)

(Received August 12, 1987; accepted August 12, 1987)

Summary

decreased with [illegible]

[illegible] of agglomerate wear debris composed of the rhombohedral oxide α-

Pg 253 - 263
removed

The Generation of Agglomerate Oxide Plateaux under conditions of low load and speed

S G Hodgson and J L Sullivan

Paper presented at 14th Leeds-Lyon Symposium, Lyon. September 1987.

To be published in proceedings of Leeds-Lyon Symposium, July 1988

SYNOPSIS

Pages Removed